1-1-2003

Investigation of the damaging effects of exposure to deicing chemicals on Portland cement materials

Daniel Erik Nelsen
Iowa State University

Investigation of the damaging effects of exposure to deicing chemicals on Portland cement materials

by

Daniel Erik Nelsen

A thesis submitted to the graduate faculty
in partial fulfillment of the requirements for the degree of

MASTER OF SCIENCE

Major: Civil Engineering (Civil Engineering Materials)

Program of Study Committee:
Dr. Kejin Wang (Major Professor)
Dr. Brian Coree
Dr. Wilfrid Nixon
Dr. Paul Spry

Iowa State University
Ames, Iowa
2003

Graduate College
Iowa State University

This is to certify that the master's thesis of

Daniel Erik Nelsen

has met the thesis requirements of Iowa State University

Signatures have been redacted for privacy

TABLE OF CONTENTS

CHAPTER 1. INTRODUCTION

Every year in the United States, millions of dollars are spent repairing damage to Portland cement concrete (PCC) pavements associated with deicing salts. Considerable effort has been taken to determine the mechanisms of salt damage and to assess relative aggressiveness of different deicing chemicals to concrete. The ultimate goal of such work is to maximize the durability and longevity of pavements while using the most cost-effective deicing agents. Fundamental to this objective is an understanding of the mechanisms of damage caused by salt exposure and winter environments.

Theories concerning the mechanisms of damage to PCC caused by exposure to deicing salts in winter environments have been proposed for many decades. The changes in concrete behavior with temperature and humidity variation are complex, and when reactive deicing chemicals join the system, complexities increase further. Concrete damage is linked to a variety of causes, including freeze/thaw damage, corrosion of steel reinforcement, chemical reaction between salts and concrete constituents, crystallization pressures, hydraulic and osmotic pressures, leaching of cement material, and chemical precipitation in void spaces resulting in decreased durability. These processes are all interrelated, increasing or decreasing the rate and magnitude of damage to PCC materials.

Two other important sources of variation stem from differences in concrete compositions and mixing conditions. Factors such as aggregate mineralogy and constitution, water-to-cementitious-material ratio, curing temperature, and curing humidity alter the behavior of PCC materials stressed by deicing salts and winter environments. In researching damage to PCC, the aforementioned influences must be considered accordingly. Because of the multifarious nature of this problem, an encompassing solution to describing and predicting deicer and winter damage to PCC materials has yet not been found.

The purpose of this research was to analyze the effects on Portland cement materials of exposure to one of five deicing compounds typically employed by the Iowa Department of Transportation (IaDOT). These five chemicals are as follows: sodium chloride (NaCl), calcium chloride ($CaCl_2$), $CaCl_2$ with a corrosion inhibiting additive, potassium acetate (K Acetate), and Geomelt. Sodium chloride and calcium chloride are commonly used in deicing applications throughout the world. Corrosion inhibitors are frequently employed with

deicing salts, and the $CaCl_2$ solution with the corrosion inhibitor was chosen to determine what, if any, effect this additive had on concrete performance. Potassium acetate is used primarily in airport deicing, because of its effectiveness and its non-corrosiveness. The cost of potassium acetate is probably prohibitive for large scale use on highways and interstates, however. Geomelt, a new organic-based deicer produced from agricultural waste, has not yet been investigated for interactions with concrete. The IaDOT is beginning to test employ Geomelt in trial locations, and this report is intended to supplement the preliminary IaDOT study.

The laboratory testing regimen, while not a direct simulation of field conditions, was designed to provide an indication of how PCC materials may perform when exposed to the aforementioned deicing chemicals. Paste and concrete samples were prepared and exposed to deicing solutions in wet-dry or in freeze-thaw environments after seven days in optimal curing conditions. Physical deterioration was quantified through the measure of changes in sample weight, compressive strength, and visual scaling. Chemical deterioration was analyzed using a combination of ion concentration tests, x-ray diffraction, and scanning electron microscopy.

Literature describing mechanisms of frost damage and previous studies involving similar deicing agents are reviewed. The methods used in gathering data are described, subsequent results are discussed, and recommendations based on the experimental results are made. Suggestions for continued research are made as well.

CHAPTER 2. LITERATURE REVIEW

One principal reason concrete is vulnerable to frost damage is because it typically contains a large amount of adsorbed and absorbed water. This also explains much of concrete's susceptibility to damage from deicing chemicals. Water may exist in capillaries, as adsorbed water, as interlayer water, or as chemically combined water (Mehta, 1993). The behavior of water with fluctuating temperatures can produce internal pressures that may damage concrete. Additionally, the movement of water into concrete aids the influx of deicing chemicals, which in turn may react with concrete constituents and alter the air void system via precipitation. Previous studies of these water-related mechanisms as well as interactions with deicing chemicals are described in this section.

2.1 Mechanisms of Frost Damage

Modern understanding of the effects of frost action on concrete combines the ideas of three main theories relating the behavior of pore fluids in winter environments to concrete damage: the hydraulic pressure theory, the osmotic pressure theory, and a third theory emphasizing variations in vapor pressure between liquid and solid phases, and between fluids of varying salinities. This last theory was first proposed by G.G. Litvan in 1972 and will henceforth be referred to as 'Litvan's theory'.

2.1.1 Hydraulic pressure theory

Water can be adsorbed and held in concrete in three ways: a) in voids within hydrated tobermorite gel, b) around aggregate particles and within the capillary system of cement paste, and c) within the larger entrained air bubbles (Mehta, 1993). The pore size of voids in the tobermorite gel is extremely small, averaging approximately 15 to 20Å in diameter (Cordon, 1966). This is only eight times the diameter of a single water molecule (Powers, 1945). Water adsorbed on gel pore surfaces (gel water) is bound by relatively high surface energies and subsequently does not freeze at 32°F but instead becomes supercooled to temperatures well below this point.

Capillary cavities are significantly larger, averaging 5000Å in diameter (Cordon, 1966). Water molecules adsorbed on capillary pores (capillary water) are bound by much lower surface energies than those in gel pores. Fluid is therefore free to move about the capillary system and may be evaporated or frozen, or it may carry dissolved ions in solution.

Voids formed around bubbles of entrained air are significantly large – microns to millimeters in diameter – so that surface energies are largely insignificant in determining adsorbed fluid behavior.

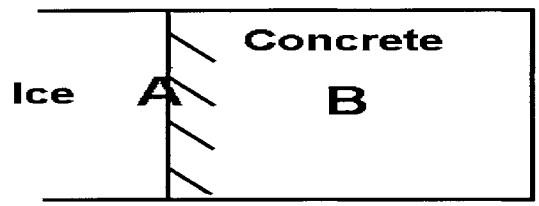

Figure 1. Freezing at the fluid/concrete interface (From Powers, 1945).

The hydraulic pressure theory (Powers, 1945) combined these insights into a working model of how differential freezing and fluid movement within the concrete may lead to pressures significant enough to cause permanent damage. As shown in Figure 1, heat will flow from concrete to water when a concrete specimen is immersed in cold water under freezing conditions. As the fluid temperature continues to decrease, fluid in the concrete surface region, A, at the periphery of the slab will freeze while fluid at the slab interior, B, is still liquid. Freezing at A seals the concrete from the ingress of additional water. As water in the capillary spaces of region A freezes, its increasing volume forces unfrozen fluid towards the unfrozen interior. This process is resisted by the limited diameter of pore and capillary channels leading to the interior. The forcing of water through these narrow channels creates hydraulic resistance. Additionally, the surface energies of pore channels offer significant resistance to fluid movement. This described example of hydraulic pressure is a function of the concrete permeability, the degree of pore saturation, and the rate of freezing (Powers, 1945).

Supercooled water. Supercooled water remains a fluid at temperature below 0°C. Some condition keeps the water from changing phase, such as volume constriction in a saturated pore. Supercooled water exerts a force on the system around it equal to the forces keeping it from changing state. For example, distilled water, in the absence of any nucleating agent, will supercool to approximately -15°C (Chatterji, 1999). Because it cannot freeze, the water is out of thermodynamic equilibrium and therefore exerts pressure forces on the

surrounding concrete matrix. The magnitude of this pressure is significant: 1.2MPa per degree to prevent ice crystal growth (Scherer, 1999). If there is insufficient pore volume to accommodate freezing of all the pore water – a condition that exists if saturation exceeds 91% - then this supercooled liquid will be forced into the interior of the concrete. Supercooling gives rise to instability that must be eliminated by fluid mass transfer (Litvan, 1976). If this necessary mass transfer cannot progress at the required rate, mechanical damage will occur.

Influence of deicing chemicals. Deicing chemicals increase the degree of saturation, which keeps voids at or near maximum fluid saturation for extended periods (Litvan, 1976). Additionally, the salts contained in deicing solutions depress the freezing point of pore water, which increases the surface energy between the pore surface and the developing pore ice nucleus. This also may ultimately lead to increased hydraulic pressure (Setzer, 1997). Damage caused by hydraulic pressure increases is worst at low salinity levels because pores near the surface and in conduits through the pore system may freeze, prohibiting escape of supercooled liquids (Litvan, 1976).

This phenomenon is most often demonstrated in studies employing NaCl solutions. In one such study, solutions of 1, 2, 3, 4, 8, and 16% NaCl were tested for comparative damage to PCC materials. The 3% solution caused the most damage (Cantor & Kneeter, 1977). The freezing point of pore fluid at this salinity is only slightly depressed at approximately -2°C (Minsk, 1998), which allows freezing and restriction of fluid movement. The saline solution will increase the level of saturation and thus the propensity for hydraulic pressure development. Additional studies have confirmed 3% NaCl solutions to be most damaging (Setzer, 1997). Analysis of sample expansion with freezing of paste specimens in solutions of varying salinities showed maximum deterioration from low salinity solutions (Litvan, 1976). A 5% NaCl solution caused paste length expansion of 0.5%. A water solution caused paste length expansion of 0.08%, and a 26% NaCl solution caused only 0.01%. These results demonstrate that low salinity deicing solutions can increase hydraulic pressure effects by increasing saturation due to salinity and by limiting mass transfer with conduit blockage via freezing and inadequate freezing point depression. This serves to exacerbate the action of all three damage-causing mechanisms.

Gel water fluctuations. Due to surface tension, gel water is often in a supercooling state at a given freezing temperature. As the supercooling water diffuses into larger capillary pores, the capillary pores will expand and gel pores will shrink. The capillary pore, with its increasing volume of water, is likely to expand. Air entrainment was developed to ameliorate this process. Air entrained bubbles serve as fluid reservoirs for gel fluid in freezing conditions (Powers, 1954). They are large enough that they almost never fill with fluid and therefore experience little or no stress from the expansion of freezing water.

When the temperature increases and ice within the concrete fluidizes, the water will flow away from saturated areas to the unsaturated gel paste in reverse of the manner described above. The paste will then re-expand with increasing water content. This fluctuation in size with repeated freezing episodes fatigues the structure of the gel paste and can lead to fracture of the concrete. As fracturing increases, permeability increases and as additional water ingresses onto these surfaces and expands upon freezing, additional damage may occur. This is an important feature of the propagation of freeze/thaw damage.

Crystal growth. Growth of ice and growth of other crystals is a major source of deterioration. The propensity for crystal growth increases with increasing saturation. As the solution becomes increasingly saturated, the hydrostatic pressure necessary to suppress crystal growth increases. For example, the pressure required to suppress crystal growth in a 20°C solution of NaCl supersaturated at twice the equilibrium solubility is approximately 30MPa (Scherer, 1999). The mechanisms propagating crystal growth pressures are similar to those responsible for hydraulic pressures: limited pore size restricting the fluid's capacity to reach equilibrium. Consequently, larger crystallization stresses develop in smaller pores (Scherer, 1999).

2.1.2 Osmotic pressure theory

In cases where a highly concentrated solution is separated from a dilute solution by a permeable barrier, an osmotic pressure develops to drive the dilute solution towards the solution of greater concentration. In the case of concrete in a deicing solution, the high salinity fluid within a large capillary pore begins to freeze, the salinity of the unfrozen water within that pore increases. The high concentration fluid draws lower salinity fluid out the gel and small capillary pores and towards the larger capillary pores. Internal pressures from

fluid movement will accumulate as soon as ice begins to form if the paste is saturated (Pigeon and Pleau, 1995).

This buildup of osmotic pressure may amplify increases in hydraulic pressure. As the capillary volume is filled with expanding ice, high salinity fluid is forced away from the capillary pores and back into adjacent areas of smaller diameter capillaries and gel pores. Gel water is drawn towards the saline fluid to balance saline concentrations and, in effect, is drawn towards the capillary pores. This pressure effectively opposes the flow of the saline fluid as it is forced away from the pore by ice crystallization and must be overcome by an increase in the hydraulic pressure driving the saline solution away from the capillary pores (Cordon, 1966).

Fluid movement resulting from osmotic pressures can establish a perpetuating flow cycle within freezing concrete that can further increase damage. Low salinity fluids are osmotically drawn to capillary pores containing high salinity fluid and an ice crystal. Within the capillary pore, the ice and saline fluid are at or near thermodynamic equilibrium. The salt concentration reduced the freezing point of the pore fluid, and as much ice has formed as is thermodynamically stable at the given salinity. As ice crystallization commences, the salinity of the unfrozen pore fluid increases, thus increasing the osmotic forces drawing additional water to that pore. As this extra water arrives, the fluid salinity decreases, allowing additional freezing. This cycle perpetuates as additional freezing continues to increase the salinity, drawing additional fluid to the capillary pore (Pigeon and Pleau, 1995) and thus increasing the propensity for concrete damage.

2.1.3 Litvan's theory

Litvan's theory describes the relative differences in vapor pressure between liquid and ice phases and between solutions of different salinity. Figure 2 shows the relative vapor pressures for these constituents at given temperature and pressure magnitudes. For example, if water at 5°C is in a saturated pore at a given pressure level and the temperature drops below 0°C, the system is no longer in equilibrium, and ice will begin to form on the pore surfaces. This is shown in Figure 2 by following line AO through decreasing temperature values. The vapor pressure of the liquid (line OD) is higher than the vapor pressure of ice (line OB). To minimize vapor pressure and achieve thermodynamic equilibrium one of two

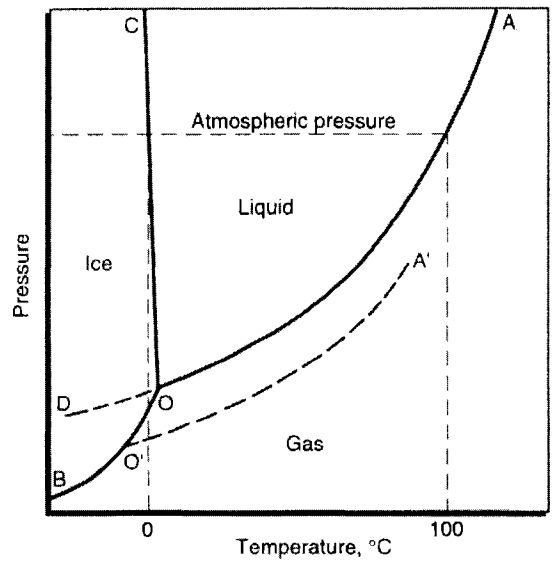

Figure 2. Vapor pressure stability diagram for water. Line AO represents pure water; A'O' represents water with dissolved substances; OD, supercooled water-water vapor equilibrium curve; OB, the ice-water vapor equilibrium curve (From Pigeon and Pleau, 1995).

things must occur. Either the fluid must change state from liquid to ice, or the vapor pressure must be reduced through desorption (Pigeon and Pleau, 1995).

The onset of freezing of the fluid within a capillary pore gives rise to unequal vapor pressures within that pore. The vapor pressure of the supercooled water is greater than that of the ice. This pressure inequality will endure until the saturation of the pore decreases through either fluid movement or evaporation (Pigeon and Pleau, 1995). Mechanical damage will occur whenever moisture transfer is prohibited out of the pore, such as when the freezing rate is too high or the distance that supercooled pore fluid must move is too large. Rapid freezing can cause large hydraulic pressure development and cracking. As water is forced out of capillary pores, it accumulates in an adjacent reservoir, whether that be an air void or a microcrack. Such accumulated adsorbed water causes microcrack propagation when it freezes. Subsequently, the higher the freezing rate, the higher the risk of mechanical damage (Pigeon and Pleau, 1995).

2.1.4 Summary – physical mechanisms of frost damage

The aforementioned mechanisms are strongly interdependent. Rates of mass transfer caused by volume constraints and changes in conditions of thermodynamic equilibrium are constantly altered by changes in temperature, saturation and salinity of pore fluids, and

pressure within pore systems. If capillary pores are saturated, any freezing will increase hydraulic stress as fluid is forced away from the capillary pores. Osmotic pressure will increase as fluid from the concrete interior is drawn towards the higher salinity fluids near the surface, and thermodynamic stresses will develop as the vapor pressure of supercooled fluid seeks an escape from the capillary volume constraints. Clearly the three mechanisms of frost-related damage overlap and many of their functions contribute to the activity of other mechanisms.

2.2 Chemical Interactions Between Deicing Chemicals and Concrete

Chlorides cause leaching of portlandite, $Ca(OH)_2$, from concrete. This occurs when chloride concentrations within PCC materials exceed 0.4 weight percent (Hoffmann, 1984). The leaching rate increases as the pH of the pore fluid decreases. Higher diffusivity values allow additional fluids to penetrate into concrete and also increase leaching. Calcium leaching is a coupled diffusion-dissolution process that leads to sharp dissolution fronts that migrate through concrete structures (Heukamp, 2001). Mineral dissolution and leaching causes degradation of concrete mechanical properties. With the penetration of dissolution fronts, mechanical properties therefore will vary with increasing depth and may, in turn, lead to localized stress concentrations and failure in weakened regions. Thus, there is loss of strength due to chemical decohesion with increased porosity and lowered density (Heukamp et al., 2001).

Chlorides also cause decomposition of C-S-H (Tobermorite) gel right after leaching of $Ca(OH)_2$ (Kurdowski et al., 1997 & Heukamp et al., 2001). Tobermorite that quickly decomposes in the presence of chloride solutions leads to the formation of a calcium-depleted C-S-H and silica gel (Kurdowski et al., 1997). Analysis of concrete specimens exposed to strong chloride solutions (Kurdowski et al., 1997) revealed a total amorphisation of tobermorite. Precipitation of calcium chloride was associated with tobermorite decalcification and the expansive growth of silica gel.

There is also evidence to suggest that chloride exposure causes formation of Friedel's salt, $3CaO \bullet Al_2O_3 \bullet CaCl_2 \bullet 10H_2O$ (Brown and Doerr, 2000 & Hoffmann, 1984). Additionally, high alkali concentrations associated with ionization of chloride deicers encourage the conversion of ettringite to monosulfate (Hoffman, 1984). The production of

Friedel's salts and monosulfate increases the expansive stress within concrete structures exposed to such deicers.

2.2.1 Sodium chloride exposure

Of the chloride deicing compounds commonly employed, NaCl is perceived as the most benign to PCC materials. Cody et al. (1996) noticed some fracturing and cracking in samples immersed in 3M NaCl solution and then dried at 90°C, but no damage was observed at lower solution concentrations or in 3M samples dried at cooler temperatures. In freeze-thaw conditions, NaCl concentrations of 3-4% cause more damage than higher salinity fluids (Cantor and Kneeter, 1977, Cody et. al., 1996, Setzer, 1997). Hoffman (1984) reported that six and twelve month exposures to NaCl solution caused a decrease in total and gel pore volumes, accompanied by an increase in the amount of capillary pores. This may be associated with portlandite leaching from larger void areas and deposition in smaller radii gel pores. Brown and Doerr (2000) suggest that NaCl and carbonates from the atmosphere may react with concrete constituents to form fronts where Na_2CO_3 and Friedel's salts are deposited.

2.2.2 Calcium chloride exposure

Calcium chloride is aggressive in promoting damage to PCC materials. $CaCl_2$ solutions are very hygroscopic and can leave concrete structures wet – even on their surface – for extended durations. This continued, building saturation increases freeze-thaw susceptibility, facilitates osmotic pressure build-up, and causes volumetric expansion. Additionally, $CaCl_2$ causes significant chemical reactions with concrete constituents.

Cody et al. (1996) analyzed results of concrete specimens immersed in $CaCl_2$ solutions of variable salinities in wet-dry and freeze-thaw conditions. Wet-dry conditions caused the most serious deterioration. Fracturing was identified immediately adjacent to coarse aggregate boundaries oriented approximately parallel to the interface, and a small number of cracks existed precisely at the paste/aggregate interface. Pore and crack surfaces were partially or completely filled with secondary mineral precipitates, which may give rise to mineral growth pressures. Cody et al. (1996) therefore concluded that damage from $CaCl_2$ is both physical and chemical in nature, and they discounted previous conjectures (Litvan, 1976) that freeze-thaw deterioration results from physical mechanisms alone. Expansive

mineral precipitates such as brucite, calcite, halite, and other complex salts exert significant growth pressures that cause or at least accelerate damage to PCC materials (Cody et al., 1996).

Chatterji (1978) suggests that chemical alteration is the primary means of $CaCl_2$ damage. PCC samples immersed in $CaCl_2$ solution at 40°C showed no damage in that study. Samples immersed in the same solution at 20°C and 5°C were significantly deteriorated. Chatterji (1978) concluded mechanisms such as thermal shock, osmotic pressure, and the acidity of $CaCl_2$ solutions are not principally responsible for concrete damage. The breakdown of PCC was instead due to chemical reactions between hydrated cement, $CaCl_2$, and possibly atmospheric CO_2, all of which occur at temperatures below 20°C. Chatterji (1978) distinguished this reaction from the formation of Friedel's salt or the leaching of $Ca(OH)_2$.

2.3 Corrosion Inhibitors

The service life of reinforced concrete structures is defined as having two phases. The first phase describes the time for chlorides to penetrate the concrete cover and break down the passive film of steel reinforcement (Hansson, et al., 1998). The duration of phase one depends on the degree of chloride binding in the concrete cover (i.e. how much Cl^- actually remains in solution to reach the steel), the chloride diffusion rate, and the chloride threshold value. The term chloride threshold value describes the chloride concentration necessary to break down the passive layer.

Phase two of the structural service life extends from the onset of corrosion to the ultimate failure of the concrete. Phase two is related to a) the rate of corrosion, b) the ability of the concrete cover to withstand internal stresses imposed by corrosion products, c) the persistent level of oxygen availability, d) the electrical resistivity of the concrete, and e) environmental factors, namely relative humidity and temperature (Hansson, et al., 1998).

Most corrosion inhibitors used in the modern concrete industry are one of two chemical types: alkali- or alkaline-nitrites and organics. The most common chemical forms of corrosion inhibition are sodium nitrite, $NaNO_2$ and calcium nitrite, $Ca(NO_2)_2$ (Tritthart, accepted for publication Nov., 2002). Of late, however, the use of organics versus the nitrite varieties is increasing (Morris and Vazquez, 2002). This may be in part due to organics' ease

of handling versus that of nitrites, which are toxic.

Inhibitors may be used as an admixture or applied surficially after concrete hardening. The effectiveness of surficially applied inhibitors depends on their ability to diffuse through the concrete cover, as well as the chloride concentration of the concrete before application.

There are six mechanisms by which a corrosion inhibitor may function:

1. Slowing the rate of chloride ingress into the concrete matrix
2. Increasing the degree of chloride bonding and physical trapping in the concrete cover
3. Increasing the chloride threshold value required to penetrate the protective film
4. Reducing the rate of dissolved oxygen ingress, thereby slowing the corrosion half-cell reaction
5. Increasing the electrical resistance of the concrete
6. Altering the chemical composition of the electrolytic cement pore solution to reduce the rate of corrosion (Hansson, et al., 1998).

Nitrite-based inhibitors act as catalysts for the formation of passive films on reinforcement surfaces. Organic-based inhibitors usually contain an aminoalcohol. A polarized region of this aminoalcohol molecule adsorbs onto the metallic surface while a nonpolar hydrophobic chain orients perpendicular to this surface. In theory, these chains repel aggressive contaminants and form a tight film barrier on the metallic exterior (Morris and Vazques, 2002). Investigation of the rate of diffusion of the aminoalcohol indicates that chloride ions diffuse through cover to reinforcement much more quickly than does the organic molecule (Tritthart, accepted for publication Nov., 2002). This suggests that organic inhibitors are unsuitable for use when intermixed with chloride deicers and that a pre-treatment of the concrete may be required if organics are to be used.

In one recent experiment (Mammoliti, et al., 1999), steel members were immersed in electrochemical cells with synthetic pore solutions (pH ~ 13.3) and deicing salts added. Four corrosion inhibitors were tested – two calcium nitrite-based and two organic-based. Results indicated that all four inhibitors were ineffective at preventing the corrosion of the steel. They all failed to increase the chloride threshold required to penetrate the protective film and

were incapable of reestablishing passivity with increasing chloride concentration. For example, samples immersed in one of the calcium nitrite-based compounds actually had higher pitting corrosion values than the control samples. This last case can most likely be attributed to a decrease in the pH of the system, which reduced the calcium nitrite effectiveness.

In another study (Trepanier, et al., 2001), all tested corrosion inhibitors again failed to prevent corrosion. Like the previously mentioned study, two calcium nitrite-based and two organic-based inhibitors were tested. All inhibitors failed to prevent corrosion and only the calcium nitrite-based compounds delayed corrosion. The organic-based compounds failed to alter the corrosion rate significantly.

These studies suggest that the effectiveness of corrosion inhibitors in concrete may be influenced by many factors and vary from case to case.

2.4 Summary

Previous work shows the damaging effects of exposure to winter environments - particularly freezing and thawing - and of exposure to deicing chemicals. The experimental work that follows was designed to expand on previous research and provide quantitative analysis on the relative damage of the five deicers (NaCl, $CaCl_2$, $CaCl_2$ with a corrosion inhibitor, K Acetate, and Geomelt) to PCC materials.

CHAPTER 3. MATERIALS AND TESTING METHODS

3.1 Scope of the Experiment

Individual experiments focused on one of two areas: physical deterioration or chemical deterioration to PCC materials. Physical deterioration was measured on paste and concrete samples exposed to one type of deicing solution under either wet-dry or freeze-thaw conditions. At regular intervals, these samples were measured to determine change in sample weight, compressive strength, and in visual scaling.

Chemical deterioration was determined by analyzing concrete samples exposed to wet-dry conditions using x-ray diffraction (XRD) and scanning electron microscopy (SEM) to identify new mineral phases, to map elemental concentrations within samples, and to obtain visual images of the concrete microstructure. Additionally, samples were collected from various depths within these concrete samples and ion concentrations of various elements were measured.

3.2 Materials

3.2.1 Paste and concrete materials

The cement used in all samples was Lafarge, Type I/II from Davenport, Iowa. The coarse aggregate used was D-57 1-inch nominal maximum aggregate size limestone (LS) from beds 19-25 of the Gilmore City LS formation from Martin Marietta's Ames Mine. The fine aggregate consisted of Cordova sand, F. M. = 2.83, supplied by the Iowa DOT. The air entraining agent (AEA) AEA 92 produced by Euclid Chemical from Cleveland, Ohio. Concrete and paste mix designs and procedures may be found in the Appendices.

3.2.2 Deicing chemicals

All deicers were originally received from suppliers mixed to full eutectic salt composition. The NaCl and both $CaCl_2$ solutions were provided by Scotwood Industries through the Iowa DOT, Ames Highway 30 Depot. The corrosion inhibitor pre-mixed in one of the $CaCl_2$ solutions was TEA, tetraethanolamine. The Potassium acetate solution was supplied courtesy of Cryotech Deicing Technology Fort Madison, Iowa. Grain Processing Corporation (GPC) of Muscatine, Iowa donated the (Na-type) Geomelt solution. Geomelt components can be found in Table 2, Appendix A-1. According to the producer, Geomelt is

should be applied mixed 1:1 with NaCl solution. Only pure Geomelt solutions were used in these experiments to determine the potential damage of this deicer.

Table 1. Salinities of deicing solutions employed in wet-dry and freeze-thaw exposures

Chemical	Wet-Dry Concentration, %	Freeze-Thaw Dilution Raio	Freeze-Thaw Concentraion, %
NaCl	26.5	1:1	13.3
$CaCl_2$ w/o	37.9	1:2	9.5
$CaCl_2$ w/	39.9	1:2	10.0
K Acetate	54.5	1:2	13.6
Geomelt	N.A.	1:3	N.A.

* See below for description of wet-dry and freeze-thaw exposure conditions.

Deicing solutions employed in wet-dry and freeze-thaw exposure tests are shown in Table 1. These concentrations were measured directly from the chemicals provided. High solution concentrations were used in wet-dry exposures to maximize the amount of potential chemical interaction between deicer and concrete or paste. Solutions had to be diluted so that they would freeze, hence the reduced salinities used for freeze-thaw testing.

3.3 Specimen Description and Test Methods

Three types of variables were considered in these experiments: the type of deicer (five types), type of cement-based material (paste and concrete), and environment of exposure (wet-dry or freeze-thaw). Mix designs and raw materials were constant for all paste and concrete samples, respectively. These paste and concrete samples were used for the tests described immediately below (See Table 2).

3.3.1 Weight loss, compressive strength, and scaling samples

(See Appendix A for paste and concrete sample preparation.) After seven days of curing, samples, sized $2in^3$ for paste and $4in^3$ for concrete, were placed in plastic storage containers according to the appropriate testing chemicals and environments. Batch sizes

were fifteen paste and twelve concrete specimens for each chemical and environment. Containers were then placed in either a refrigerator set at 4.4°C for wet-dry cycling or a freezer set at -20°C for freeze-thaw cycling. One-cycle durations for both environments were twenty-four hours total: fifteen hours in the immersed or frozen state, followed by nine hours in the dry or thawing state. To facilitate thawing, the storage tubs containing frozen samples and solution were placed in larger tubs filled with hot water. Using this technique, solutions were typically completely thawed within four hours.

It is important to emphasize that both the paste and the concrete samples were only cured for seven days in optimal curing conditions. By exposing them to deicing solutions after this short period, cement's normal maturity process is interrupted. That the cement materials are being subjected to saline solutions at such a young age should be considered when analyzing the test results and in interpolating these results to field conditions. Mature concrete may exhibit different behavior.

Weights of the freeze-thaw specimens were taken approximately every five cycles, and weights of wet-dry specimens were taken every ten cycles. Before taking a weight measurement, the specimens were first gently rinsed in a static tub of tap water to remove loose particles adhering to their surfaces. Next, the specimens were laid on paper towels to dry and, if the sample was not too friable, blotted with paper towels. Samples were rotated periodically to facilitate even drying of all faces. After twenty minutes of drying, samples were weighed to the nearest hundredth of a gram using an Ohaus balance.

Every twenty cycles, three samples were removed from the cycling process for use in additional testing. Initial weights through 20 cycles therefore reflect an average of fifteen or twelve samples, which were reduced by four every 20 cycles due to this additional compression and scaling analysis. Compression tests on both paste and concrete samples were conducted using a uniaxial compression machine. Tests were analyzed according to ASTM C 109, which indicates that strength differences between averaged data points must exceed 8.7% to be statistically significant when each datum is the average of 3 samples. Scaling values were determined according to ASTM C 672.

3.3.2 Penetration, XRD, and SEM tests

Cubic plastic molds, 3.5in^2 by 4in, were filled to within 0.5in of their top surface

with concrete. Mixing design and procedures were the same as those used above, and explained in Appendix A-3. Following the seven-day curing period, marine sealant was applied around the perimeter of each sample to restrict chemical access. Deicer solution contacted each sample on the surface layer only, thereby simulating conditions on a pavement or structural surface. (Note that ponding effects below a pavement slab are not considered). After the necessary forty-eight hour drying time required of the marine sealant, deicer solutions were poured onto sample surfaces to a depth of approximately 1/4 inch. Eleven concrete samples were made altogether: two for exposure to each chemical and one for distilled water exposure. One sample was tested per deicing chemical after 20 and 60 cycles, respectively, while the distilled water sample was tested after 20 cycles of exposure. Each cycle was twenty-four hours in total length.

Specimens taken from these samples were used in perform x-ray diffraction (XRD) analysis, scanning electron microscopy (SEM), and to determine the depth of ion penetration by Cl^-, Na^+, and K^+ ions. XRD and ion penetration tests were conducted on samples after both 20 and 60 cycles; SEM analysis on samples subject to 60-cycles of exposure. The SEM samples were small sections (approximately 0.5"x 0.5" x 0.3") cut from the corners of concrete samples. The interior surface of these samples was polished using a silicon carbide grinding bit without any lubricating solution. (Use of an aqueous lubricant or cooling solution may have removed chlorides and other phases.) These polished sections were then mounted on a small glass slide and analyzed with a Hitachi variable pressure SEM device. This SEM was operated using a 20 kV acceleration voltage at 4,000 counts per second with a 30° take-off angle and a 25mm working distance. Backscattered electrons were analyzed for imaging. Chamber pressure was maintained at 40 Pa (~0.3 torr) with helium gas. While not technically an 'environmental' SEM, which operates at minimal vacuum levels, this variable pressure SEM chamber pressure is several orders of magnitude greater than that typically employed in standard microscopy. The vacuum state of the chamber at 40 Pa should not damage the sample nor influence the results.

Elemental mapping via scanning electron microscopy (SEM) was employed to identify the phases present in void and crack spaces. The following elemental maps were assayed at the following magnifications for the given deicers: NaCl at 25x; $CaCl_2$ without

Table 2. Summary of experimental regimen

I. Analysis of Physical Deterioration.						
Sample Type	**Exposure Environment**	**Exposure to 1 of 6 Deicers**	**# of Samples per Group**	**Physical Analyses and Testing Intervals through 60 cycles:**		
				Weight Loss	**Scaling**	**Compressive Str.**
Paste	W-D (40°F)	1. Distilled H_2O 2. NaCl 3. $CaCl_2$ 4. $CaCl_2$ with Corr. Inh. 5. K Acetate 6. Geomelt	15	10 cycles	20* cycles	20* cycles
	F-T (-20°C to 20°C)		12	5 cycles	20 cycles	20 cycles
Concrete	W-D (40°F)		12	10 cycles	20 cycles	20 cycles
	F-T (-20°C to 20°C)		12	5 cycles	20 cycles	20 cycles

II. Analysis of Chemical Deterioration.							
Sample Type	**Exposure Environment**	**Exposure to 1 of 6 Deicers**	**# of Samples**	**Analysis Age, Cycles:**	**XRD**	**SEM**	**Analysis of Ion Concentration**
					(of near-surface layers only, ~3/16" depth)		
Concrete	W-D (40°F)	Distilled H_2O	1	60	x		x
		NaCl	2	20	x		
				60	x	x	x
		$CaCl_2$ without corrosion inhibitor	2	20	x		
				60	x	x	x
		$CaCl_2$ with corrosion inhibitor	2	20	x		
				60	x	x	x
		Potassium Acetate	2	20	x		
				60	x	x	x
		Geomelt	2	20	x		
				60	x	x	x

[a] Exposure regimen was continued on Paste, W-D samples through 130 cycles. Weight loss, scaling, and compressive strength were measured after 130 cycles.

inhibitor at 25x, 100x, and 300x; $CaCl_2$ with inhibitor at 25x; K Acetate at 25x and 200x; and Geomelt at 25x.

Ion penetration testing (IPT) and XRD required powdered material for analysis. The sample powder was obtained as follows. Beginning from the top surface of each sample,

seven 3/16" layers were measured and marked on the sample side. (7*3/16"=1 5/16" total depth of analysis. As results indicated (see Results section below), the total depth of analysis should have been increased.)

A drill press was set such that the maximum bit penetration matched the bottom thickness of each of these seven layers successively. At each layer depth, numerous holes 3/16" depth were drilled into the sample and the powder was collected in a pan beneath the sample. This powder was passed through a #50 sieve to increase sample homogeneity and to remove fractured concrete bits that broke off previous sampling layers. The sieved powder was then transferred to sealed plastic vials and labeled for analysis. 3/16" intervals were used because this was the minimum layer thickness at which enough powder could be obtained for subsequent analysis requirements.

Powder samples that were taken from the surficial 3/16" layers of each concrete sample were used in XRD testing. Cu K_α radiation was generated using an excitation voltage of 50 kV at 27mA. Slit-spacings of 1°, 1°, and 1° were employed with 0.05° detector slits. Two-second dwell times with 0.05° step-sizes were employed to scan from 5° to 70° 2θ. MDI JADE 6.5 software was used to analyze peak intensity data. XRD of the 20-cycle samples was conducted at the Geoscience Laboratories of the Ministry of Northern Mines and Development in Sudbury, Ontario, Canada. (Samples were sent to this lab because of perceived time and financial constraints. In hindsight, this was unnecessary.) 60-cycle samples were analyzed at the Materials Analysis Research Laboratory at Iowa State University in Ames, Iowa. The powder from the surface layer of each sample used in XRD was subsequently used in IPT.

IPT testing was conducted at the Soil and Plant Analysis Laboratory at Iowa State University in Ames, Iowa. Powder samples were analyzed for Na^+ and K^+ using a water extraction procedure followed by atomic cation absorption techniques (see Appendix A-4). Chloride concentrations were obtained via the Mercury (II) Thiocyanate Method (see Appendix A-5). These data were returned indicating a ppm concentration for each element.

CHAPTER 4. RESULTS AND DISCUSSION

Presented in the following section are results of physical and chemical deterioration analyses. Physical deterioration is listed first, followed by chemical deterioration. Discussion sections immediately follow descriptions of results.

4.1 Physical and Mechanical Evaluation of Deicer Damage

4.1.1 Results of paste under wet-dry cycling (40°F)

Weight loss observations. As shown in Figure 3, NaCl and H_2O-immersed samples experienced a slow and steady weight gain, while samples exposed to all other chemicals lost weight. The most significant weight loss occurred in Geomelt, which experienced more than 3% total weight loss after 60 cycles. K Acetate samples steadily lost weight, with a final weight loss slightly exceeding 1.25%. The two solutions of $CaCl_2$ exhibited high weight loss early in the testing period, but then both regained significant weight. The solution without the corrosion inhibitor had a higher weight loss (approximately 2.5% versus approximately 2%) than the solution with the corrosion inhibitor. $CaCl_2$ without inhibitor also regained weight at a slower rate than the $CaCl_2$ with-inhibitor solution.

Compressive strength. (Note: Compressive strength analysis based on comparison of deicing sample final cycle strength vs. final cycle strength of H_2O samples.) H_2O samples gained significant strength over the course of exposure (Figure 4). Paste samples in the two $CaCl_2$ solutions showed an initial strength gain followed by significant strength loss: a 33% loss for $CaCl_2$ without corrosion inhibitor and -38% for the solution with the corrosion inhibitor. Strength decreases in K Acetate (-25%) and NaCl (-25%) solutions were also substantial (Figure 5). Geomelt experienced the smallest strength loss, -15%.

Scaling. (Note: in Figure 6, gaps between the data bars indicate zero scaling for these chemicals.) NaCl and H_2O solutions showed no visible physical damage to the paste structure, but at 60 cycles, voids and depressions in NaCl samples were covered in white precipitate (Figure 6). K Acetate and Geomelt samples showed a small amount of visible deterioration, first observed at 60 cycles for K Acetate samples and at 130 cycles for samples in Geomelt. Deterioration in Geomelt samples did not include bits of material sloughing off; instead, tiny pores less than one millimeter in diameter formed over most sample surfaces.

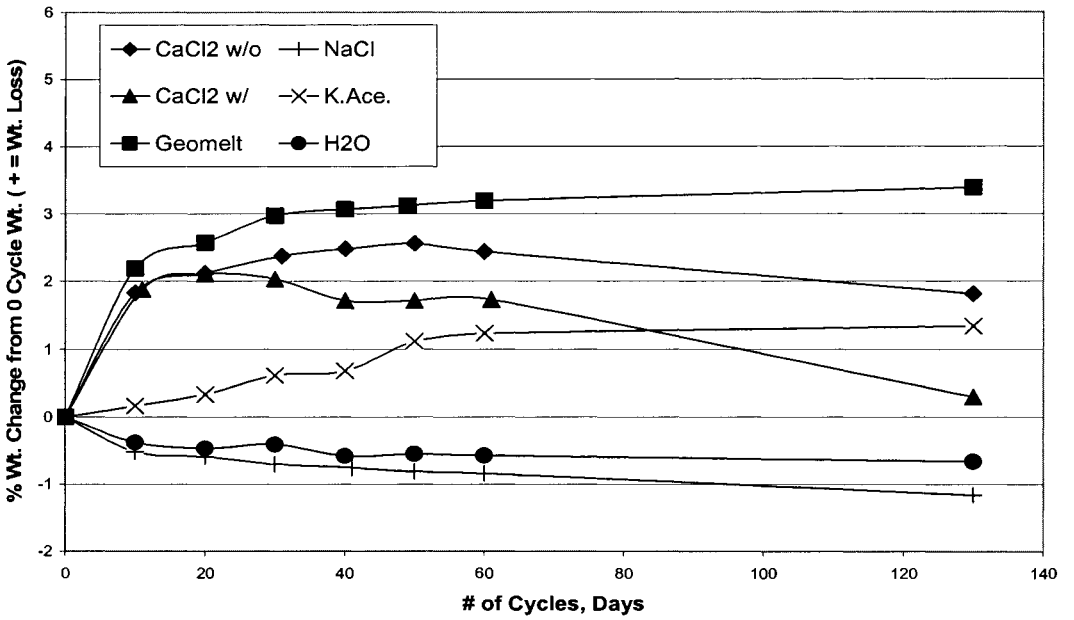

Figure 3. Weight loss of wet-dry paste samples.

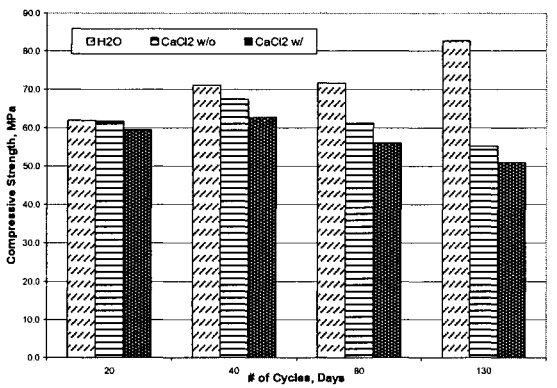

Figure 4. Paste w-d compressive strengths

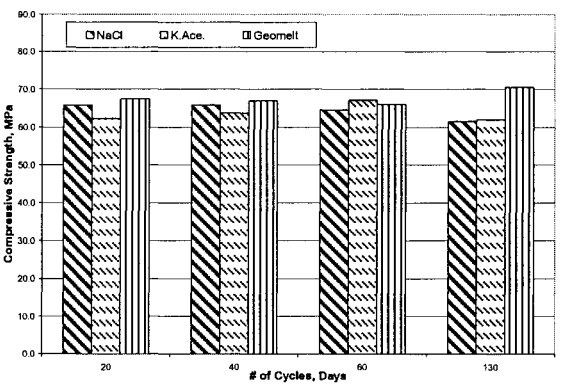

Figure 5. Paste w-d compressive strengths

Samples in the $CaCl_2$ solutions scaled much earlier, at 20 cycles. Scaling was initially more severe in the $CaCl_2$ solution without inhibitor, while visible damage was delayed in the solution with the inhibitor. However, the rate of sample scaling in the $CaCl_2$ solution with inhibitor was more accelerated once scaling began.

4.1.2 Discussion of paste under wet-dry cycling (40°F)

There are two means by which sample weight may be increased through exposure to deicer solutions: by imbibing water and by salt precipitation. In contrast, mass leaching of

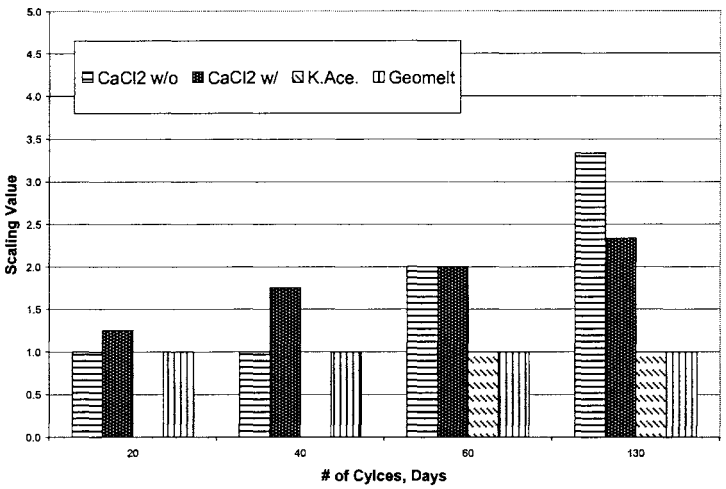

Figure 6. Paste w-d scaling values

paste or concrete constituents and physical loss of mass through scaling or other macroscopic damage will cause weight decrease. The differential rates at which these reactions occur determines relative changes in weight caused by the different deicers and shed considerable light on the damage such deicers cause to PCC materials.

Weight gain was observed in H_2O and NaCl samples (Figure 3). In immature paste and concrete samples, cement hydration reactions will continue to consume pore fluid until hydration ceases, which typically does not occur for at least 120 days. This fluid consumption, coupled with natural drying, leaves such samples in an unsaturated state. Pastes and concretes will therefore continue to absorb water and increase in weight until maximum saturation is reached, so long as they are in an environment with sufficient moisture availability. This mechanism can account for the steady weight gain observed in H_2O and NaCl samples throughout the 130-cycle testing period.

A second means of weight gain is salt precipitation on sample surfaces and in pore spaces. White precipitates were visible on exterior surfaces of NaCl samples after 60 cycles. This probably accounts for the slight additional weight gain observed in NaCl samples versus H_2O samples. That NaCl samples incurred only weight gain (with no measured weight loss or visual deterioration) suggests that exposure to NaCl is benign under these environmental conditions.

Exposure to all other chemicals did result in weight loss, however. Samples that

experienced the largest amounts of weight loss were those exposed to Geomelt solution. This weight loss may be attributed to acid attack or leaching (refer to XRD and SEM results below), as no material ever scaled off of these samples. The $CaCl_2$ samples' initial weight loss was due to macroscopic particle loss as surface layers swelled. Following their initial weight loss, the samples steadily gained weight. The surface expansion noted in both sets of $CaCl_2$ solution samples caused a substantial increase in surface area. Fluid adhesion and salt precipitation noted on these expanded surfaces account for the secondary weight gain. Because the magnitude of both the maximum and the final (130-cycle) weight loss was greater in the $CaCl_2$ solution without corrosion inhibitor than in the solution with inhibitor, it can be inferred that the corrosion inhibitor slightly impedes the rate of damage to hardened cement paste.

The increase in compressive strength of H_2O samples was expected, as the samples were immersed in solution after only seven curing days and had not yet reached maturity. Most salts accelerate hydration reactions and should accelerate strength development. Calcium chloride is used in industry as a commercial accelerator, although in concentrations much lower than those used in deicers. However, the samples exposed to deicers exhibited a significant impairment in strength development. Strength loss occurred in all samples exposed to deicers. This further reinforces why such salts should not be used with immature pavements. Samples exposed to NaCl, K Acetate, and Geomelt showed minimal strength decreases between their 20-cycle and 60-cycle strengths. However, compared to the strength development they should otherwise have experienced (as compared to H_2O sample strengths at 60 cycles), loss of potential strength in the samples was considerable (Table 3). Strength loss was slightly greater in both $CaCl_2$ sample groups. A –33% change occurred in samples exposed to $CaCl_2$ without inhibitor and a –38.5% change was observed in samples immersed in solution with the inhibitor. Although $CaCl_2$ with corrosion inhibitor caused greater strength loss in the samples than the solution without inhibitor, the difference is not statistically significant (ASTM C 109).

The fact that all samples exposed to saline solutions failed to develop strength relative to the distilled water-immersed control samples indicates that the damaging mechanisms described earlier in the Literature review were at work. Some combination of

osmotic pressure, crystal growth pressure, and/or chemical reaction stresses caused strength impairment and damage in the concrete pastes. Because some samples exposed to deicers were never frozen, significant hydraulic pressures could not develop, and the observed damages were only caused by chemical reaction or crystal growth pressures. Because the samples never froze, damage stresses cannot be attributed to hydraulic pressure development or to ice crystal growth.

4.1.3 Results of paste under freeze-thaw cycling, weight loss observations

The paste samples immersed in Geomelt experienced the most weight loss of the non-$CaCl_2$ samples with freeze-thaw cycling (Figure 7), although it was only a 2% loss versus the >3% loss observed in wet-dry testing (Figure 3). NaCl, H_2O, and K Acetate treated samples gained minimal amounts of weight (<1%). Samples exposed to plain $CaCl_2$ gained weight through 30 exposure cycles. After 30 cycles, however, drastic weight loss occurred. Final weight loss values for samples in the $CaCl_2$ solution without corrosion inhibitor exceeded 7.5%. Samples submerged in $CaCl_2$ with the corrosion inhibitor underwent two cyclical periods of weight increase followed by weight loss. These samples initially gained weight for the first 10 cycles, then lost weight through 30 cycles. Weight gain ensued through 55 cycles, followed by a sharp weight loss. Final weight loss at 60 cycles totaled 1.5%.

Compressive strength. H_2O treated samples gained a small amount of strength: 57MPa at 20 cycles to 62MPa at 60 Cycles. However, the total strength gain by samples immersed in H_2O and subject to freeze-thaw cycling was less than that for the wet-dry H_2O samples: 62MPa at 60 cycles in freeze-thaw versus 83MPa at 60 cycles in wet-dry (Figures 8 and 4, respectively). Samples exposed to Geomelt, NaCl, and K Acetate all experienced minor gains in strength (Figure 9). Both groups of samples immersed in $CaCl_2$ solutions were badly damaged, and thus lost considerable strength (Figure 8). Samples in the $CaCl_2$ solution without corrosion inhibitor lost more than 65% of their 20-cycle strength (see Table 3). $CaCl_2$ with corrosion inhibitor caused significant damage as well; 60-cycle strength was reduced by more than 50% from the 20-cycle strength.

Scaling. (See Figure 10.) All samples showed some visible deterioration after 60 freeze-thaw cycles. K Acetate samples showed the least signs of wear at 60 cycles. H_2O and Geomelt samples showed minor amounts of damage. Samples immersed in Geomelt

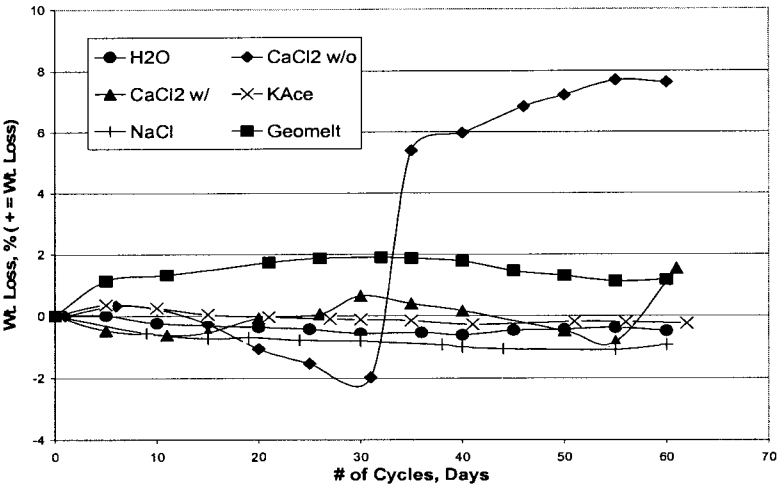

Figure 7. Weight loss of freeze-thaw paste samples

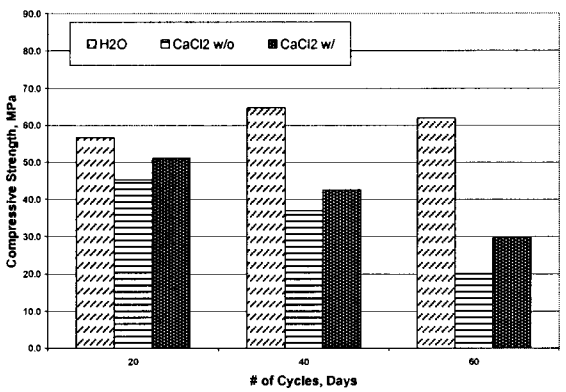

Figure 8. Paste f-t compressive strengths

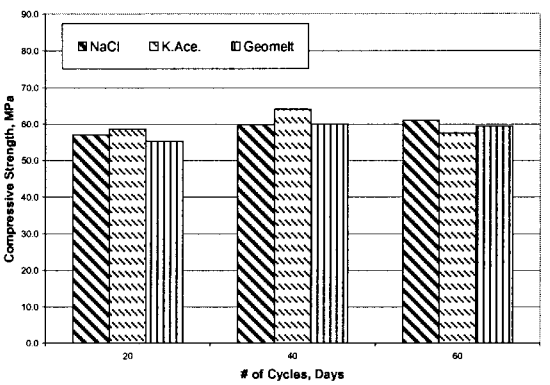

Figure 9. Paste f-t compressive strengths

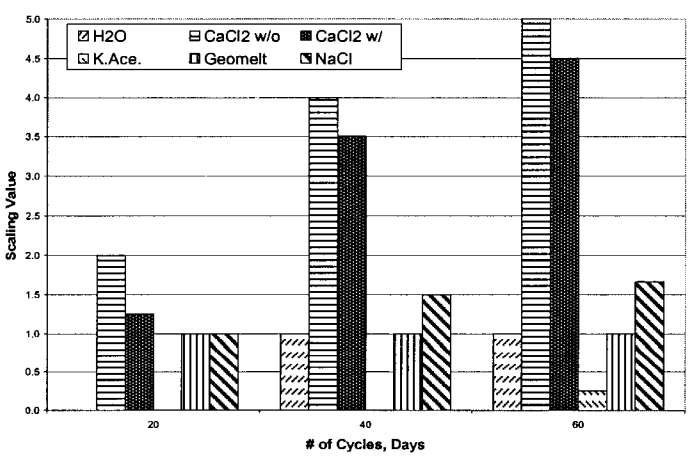

Figure 10. Paste f-t scaling values

exhibited numerous tiny pits less than 1mm in diameter and had a bleached appearance, both changes first observed after 20 cycles. NaCl samples were slightly more deteriorated, reaching a maximum average scaling value of 1.7 at 60 cycles. Samples in the two $CaCl_2$ solutions were by far the most visibly deteriorated. Both sets of samples were badly scaled and showed pealing of surface layers in wide planar sheets. The $CaCl_2$ solution without the corrosion inhibitor caused slightly worse scaling: 5.0 average maximum at 60 cycles versus 4.5 average maximum at 60 cycles for the solution with the inhibitor. Needle-like crystals formed on samples in $CaCl_2$ without inhibitor samples after only 6 cycles (Table 4). These crystals appeared on $CaCl_2$ with inhibitor-exposed samples after 15 cycles.

4.1.4 Discussion of paste under freeze-thaw cycling

Samples did not experience the same uniform weight loss pattern in freeze-thaw as they did in wet-dry cycling. In wet-dry cycling, four of the five deicing solutions caused immediate and sustained weight loss, an effect attributed to leaching. Freeze-thaw cycling had the opposite effect on sample weights. In this case, only samples exposed to Geomelt had immediate and sustained weight loss. This loss was possibly due to leaching, as no material physically scaled off sample exteriors. The Geomelt samples' weight loss in wet-dry cycling eclipsed 3%, while in freeze-thaw conditions, maximum weight loss by the samples was less than 2% of their total weight. This suggests that rates of leaching were reduced under the lower temperature conditions.

The NaCl, K Acetate, and distilled water solutions all caused slight weight gains throughout the duration of the experiments. All samples underwent a minor degree of visual deterioration by 60 cycles, so there was some mass reduction via physical loss in all samples. However, in the NaCl, K Acetate, and distilled water samples, this mass loss was offset by imbibed water and salt crystallization processes that added to overall sample weights. As a result, NaCl and K Acetate solutions seem relatively benign at freeze-thaw conditions.

The principal reason for the dramatic weight loss in samples exposed to $CaCl_2$ without inhibitor – greater than 7% of the original sample weight - is probably the precipitation and growth of needle-like crystals observed after only 10 cycles (See Table 30). Also, physical scaling was observed in these samples at 10 cycles, and it is almost certainly associated with this crystal growth. As cracking occurred in the near-surface void system

Table 3. Percent change of compressive strengths - final strength vs. initial strength

Material	Condition	Chemical	20 Cycle Strength, MPa	Final Age	Final Age Strength, MPa	% Change vs. 20 Cycle Strength	% Change vs. 60 Cycle H2O Strength
Paste	W/D	H2O	61.9	130	82.7	33.6	0.0
		NaCl	65.8	130	61.5	-6.5	-25.6
		CaCl2 w/o	61.6	130	55.3	-10.2	-33.1
		CaCl2 w/	59.5	130	50.9	-14.5	-38.5
		K.Ace.	62.3	130	61.9	-0.6	-25.2
		Geomelt	67.4	130	70.5	4.6	-14.8
Paste	F/T	H2O	56.7	60	62.0	9.3	0.0
		NaCl	57.1	60	61.1	7.0	-1.5
		CaCl2 w/o	45.4	60	20.0	-55.9	-67.7
		CaCl2 w/	51.1	61	29.7	-41.9	-52.1
		K.Ace.	58.6	62	57.6	-1.7	-7.1
		Geomelt	55.3	60	59.4	7.4	-4.2
Concrete	W/D	H2O	27.0	60	29.5	9.3	0.0
		NaCl	28.8	60	28.5	-1.0	-3.4
		CaCl2 w/o	27.3	61	27.7	1.5	-6.1
		CaCl2 w/	24.8	60	27.6	11.3	-6.4
		K.Ace.	26.4	60	27.2	3.0	-7.8
		Geomelt	29.8	60	29.6	-0.7	0.3
Concrete	F/T	H2O	22.8	60	25.5	11.8	0.0
		NaCl	20.2	61	24.2	19.8	-5.1
		CaCl2 w/o	11.8	61	7.7	-34.7	-69.8
		CaCl2 w/	25.7	60	9.7	-62.3	-62.0
		K.Ace.	22.7	60	21.2	-6.6	-16.9
		Geomelt	26.5	60	24.3	-8.3	-4.7

due to crystal growth pressures, the degree of saturation likely increased due to higher porosity of fractured media, the increased surface area available for adsorption, and the high salinity fluid osmotically drawing moisture to the sample from the solution. Increased moisture content associated with saturation makes the paste more vulnerable to hydraulic, thermodynamic, and osmotic pressures upon freezing.

Increased saturation and crystal precipitation also could account for the weight gain of $CaCl_2$ without inhibitor samples observed through 30 cycles. Weight increase occurred while the level of damage steadily increased. Entire surface planes were swollen and fractured like stacks of previously wet paper. At 30 cycles, these layers finally sloughed off, accounting for the significant weight loss observed in Figure 7. Needle-like crystals were not

observed in $CaCl_2$ samples in wet-dry conditions. This absence of crystal growth in the warmer environment supports the assertion by Chatterji (1978) that $CaCl_2$ causes the formation of complex salts stable only at reduced temperatures.

Needle-like crystals did not develop in samples exposed to $CaCl_2$ with the corrosion inhibitor until the 15-cycle point (Table 4). Significant crystallization was already visible on without-inhibitor samples after only 6 cycles. On samples immersed in $CaCl_2$ with inhibitor, an amorphous gel-like precipitate formed several cycles before the first ordered crystals appeared. While needle-like crystals were the major precipitates on $CaCl_2$ without-inhibitor samples, both crystals and the amorphous gel precipitate formed on the $CaCl_2$ with-inhibitor samples. This suggests that the corrosion inhibitor delays crystal precipitation, thus delaying the onset of damage to samples exposed to corrosion inhibitors.

Needle-shaped crystals eventually did form on $CaCl_2$ with-inhibitor samples in sufficient quantity to cause the considerable damage observed. Because the amorphous gel formed almost 10 cycles before any crystals were observed (Table 4), the onset of crystal growth pressure was delayed in the with-inhibitor $CaCl_2$ solution.

As displayed in Figure 7, $CaCl_2$ with-inhibitor samples were about to undergo significant mass loss similar to that undergone by without-inhibitor samples at 30 cycles when sample weight measurements were concluded. The sharp reduction in weight noted between 55 and 60 cycles supports this assertion, and had the testing gone on for just five more cycles, weight loss in with-inhibitor samples may have been more severe than the current data would suggest. However, due to the brevity of the testing time, the present test results are not able to conclude that employment of corrosion inhibitor prevents significant damage from $CaCl_2$ exposure but that it delays damage only slightly. (Concrete test results confirmed this conclusion; see below.)

Compressive strength loss was negligible for samples immersed in H_2O, NaCl, K Acetate, and Geomelt (Figures 8 and 9). In properly air-entrained pastes exposed to H_2O, NaCl, K Acetate, or Geomelt, hydraulic and osmotic pressures do not reach sufficient magnitude to cause damage. Compressive strength loss was severe in both $CaCl_2$-exposed samples: with-inhibitor samples lost 52% while without-inhibitor samples lost almost 68%. The greater strength loss in the $CaCl_2$ without-inhibitor versus the with-inhibitor samples is

Table 4. Visual deterioration of paste freeze-thaw samples

Chemical / # of Cycles	Distilled H_2O	NaCl	$CaCl_2$ w/o	$CaCl_2$ w/	K Acetate	Geomelt
5-10			* Significant crystallization already visible at 6 cycles. * Already scaling * Long, bladed surface crystals ~2-6 mm long.	* Some salt deposits on surfaces: amorphous gel rather than individual crystals.		
11-15			* Peeling at edges & corners like pages of a wet book. * Damage to ~3mm depth.	* Amorphous, white, slippery deposits. (11 Cycles) * Many needle-like crystals visible on some faces. (15 Cycles)		
16-20			* Significant material loss from edges & corners. * Top and bottom scaled most badly.	* Significant peeling of surface faces & edges. * Needle-shaped crystals prevalent. * Small pits 1-2mm depth, ~1mm dia.	* Small amounts of white, amorphous powdery deposits on surfaces.	
21-25			* Long, bladed crystals on and coming out of surface.			* Samples bleached a very pale brown. * Tiny pitting of surfaces; looks highly porous, like dense bone).
26-30			* Surface too fragile to touch. * 1-3mm of expansion in book-like scaled layers. * Long, needle-like crystals abundant.	* Scaling at edges, chunks and planes breaking away. * Some surfaces covered with a slick, white, amorphous gel.	* Little or no visible damage. * White, amorphous residue still visible on some surfaces.	* Bleached and light brown appearance.
31-35			* Swollen book-like layers fall off as whole units; significant weight loss. * Needle-like crystals visible on many surfaces.	* Faces peeling like pages of a book. * Significant damage at edges & faces. * Visible mix of crystals & white amorphous gel.		
36-40		* Material loss at edges. * Chunks breaking off rather than small particles individually.				
41-45						
46-50				* Surfaces & edges badly damaged: peeling and breaking away. * Needle-like crystals visible on surfaces.		* Dozens of small (<1mm dia.) holes.
51-55		*** Chunks coming out of surfaces and edges to a depth of ~3mm.** * Bits coming out from all areas, not confined to edges only.		* Swollen book-like planes continue to fall off.	* On two samples, thin parallel slices (<1mm thickness) scaled off.	
56-60					* Amorphous, white precipitate on all faces. * Texture feels like fine sand and looks like cracking paint.	

attributed to the earlier onset of crystal growth damage in the without-inhibitor sample group.

4.1.5 Results of concrete under wet-dry cycling (40°F)

Weight loss. Geomelt samples lost weight progressively through all 60 cycles (Figure 11). Total weight loss by the samples in the Geomelt solution was approximately 2%. Samples immersed in H_2O, K Acetate, and NaCl solutions exhibited minimal weight change. Both sets of samples in the $CaCl_2$ solutions gained weight. Samples in the $CaCl_2$ solution with corrosion inhibitor gained more than 2% total weight, whereas samples in the $CaCl_2$ solution without corrosion inhibitor gained more than 1% of their total weight.

Compressive strength. No statistically significant strength losses occurred in any of the samples (see Figures 12 and 13).

Scaling. Geomelt samples displayed tiny pitting, with numerous cavities less than 1 mm in diameter on some faces. A bleached white appearance was first noted in these samples after 20 cycles. Samples immersed in H_2O, NaCl, and K Acetate showed no visible deterioration. $CaCl_2$ without corrosion inhibitor initiated significant deterioration in the concrete samples, which were damaged to an average scaling rating of 3 after 60 cycles (Figure 14). These samples first exhibited structural weakness at the 20-cycle point, and this damage steadily increased. $CaCl_2$ with the corrosion inhibitor also initiated deterioration. The average 60 cycle scaling rating for these samples was 1.8. A white, amorphous residue was visible on these samples as early as 6 cycles. By 45 cycles, each physical contact when handling these samples caused mass loss.

4.1.6 Discussion of concrete under wet-dry cycling (40°F)

Although concrete mix designs were prepared based on saturated surface dry aggregate conditions, inevitably the aggregate will not all be in this condition. Much of the weight gain observed in concrete samples in wet-dry conditions may be due to aggregate absorption of water and saline fluid. As with the paste wet-dry samples, Geomelt caused the most weight loss in the concrete wet-dry. Again, this is attributed to chemical leaching because no particle scaling was observed. Weight loss reached an asymptotic maximum of about 2% weight loss, which it maintained for the remaining twenty cycles. Samples exposed to distilled H_2O, NaCl, and K Acetate had no statistically significant weight change

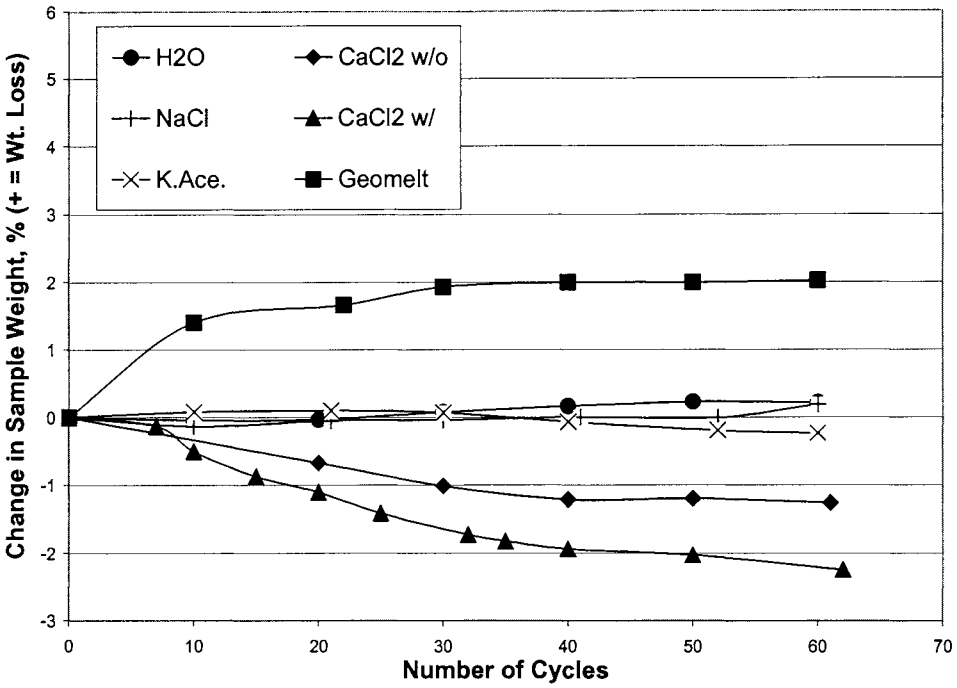

Figure 11. Weight loss of concrete wet-dry samples

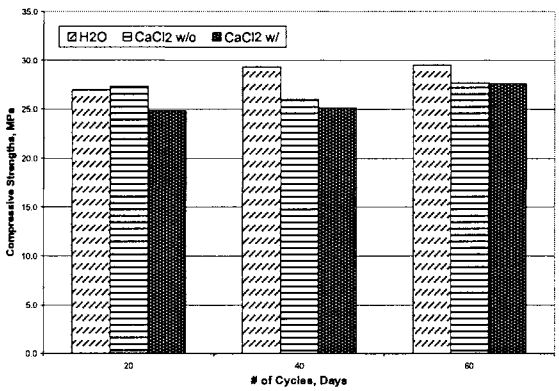

Figure 12. Concrete w-d compressive strengths

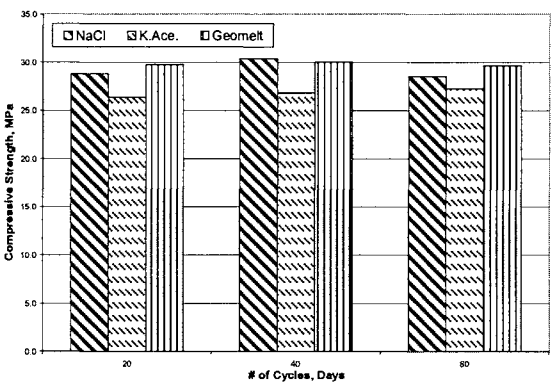

Figure 13. Concrete w-d compressive strengths

(according to ASTM C 109 standards). In paste samples at the same conditions, H_2O and NaCl samples gained weight while K Acetate samples lost more than 1% of their total weight. Reasons for these variances are unclear. Both $CaCl_2$ sample groups gained weight, despite experiencing considerable scaling. At 60 cycles, $CaCl_2$ without-inhibitor samples recorded a scaling value of 3 and with-inhibitor samples, 1.8. Scaling damage increased the

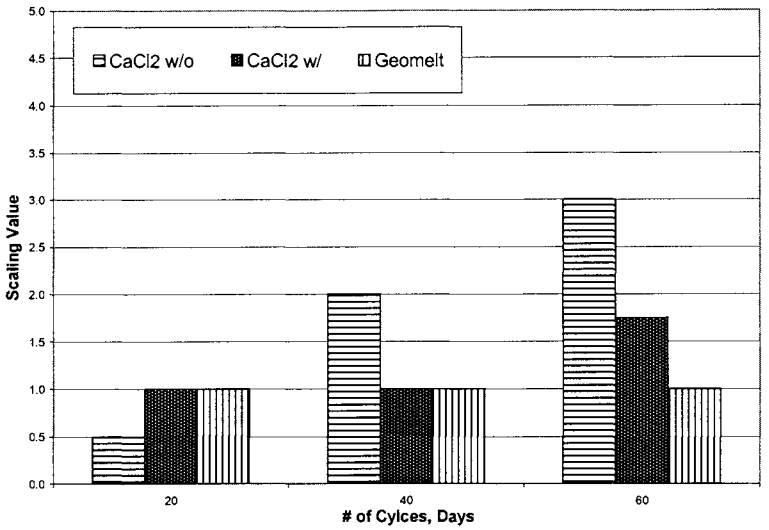

Figure 14. Concrete w-d scaling values

can account for the weight increases in the damaged samples. Measured weight gain was greater in $CaCl_2$ with-inhibitor samples than in without-inhibitor samples because more material physically came off the without-inhibitor samples, reducing the net weight gain.

No significant changes in compressive strength occurred in any of the concrete wet-dry samples. Even in the scaled samples – those exposed to the $CaCl_2$ solutions and Geomelt – the volume of affected material relative to the total sample volume was insufficient to cause strength loss. Samples exposed to all the tested chemicals held up well under wet-dry conditions. The presence of aggregate alleviated drying shrinkage by resisting volume reduction.

4.1.7 Results of concrete under freeze-thaw cycling

Weight loss. Samples immersed in Geomelt, H_2O, K Acetate, and NaCl experienced total weight gains of less than 2% after 60 cycles (Figure 15). However, significant weight losses were observed in the $CaCl_2$ samples. Weight loss in plain $CaCl_2$ treated samples began after 30 freeze-thaw cycles. Total weight loss at 60 cycles was almost 5%. $CaCl_2$ with corrosion inhibitor treated samples gained weight throughout the first 40 cycles, and then experienced precipitous weight loss. The 60-cycle average weight loss in $CaCl_2$ with corrosion inhibitor samples was nearly 8%. Once weight loss in the with-inhibitor $CaCl_2$ samples began, the rate was significantly greater than the rate of weight loss in samples

unexposed to the corrosion inhibitor.

Compressive strength. NaCl and Geomelt samples experienced no significant loss in compressive strength (Figures 16 and 17). K Acetate experienced a slight strength decline. In comparison, both sets of $CaCl_2$ samples suffered significant losses in strength. While samples immersed in $CaCl_2$ without corrosion inhibitor lost slightly more strength than the samples exposed to the $CaCl_2$ solution with corrosion inhibitor, both had strength reductions exceeding 60% (Table 3).

Scaling. H_2O and K Acetate samples exhibited no visible damage (Figure 18). NaCl and Geomelt samples displayed a minor amount of damage that was observed at 20 cycles but became no worse with additional freeze-thaw cycling. Samples immersed in $CaCl_2$ solution without a corrosion inhibitor were badly damaged. The average scaling value of these samples was 3.5 after only 20 cycles, and they reached a maximum scaling value of 5 at 60 cycles. $CaCl_2$ solution with a corrosion inhibitor also produced an average scaling value of 5 after 60 cycles. However, damage was delayed in these samples. After 20 cycles, the scaling value for samples in $CaCl_2$ with corrosion inhibitor was 1.0. After 40 cycles, the value was only 1.5, but damage accelerated rapidly thereafter, and by 60 cycles, the scaling value had increased to 5.0 (Figure 18). Needle-like crystals were on samples exposed to $CaCl_2$ without the corrosion inhibitor after 31 cycles (Table 6), but were never seen on samples exposed to $CaCl_2$ with the corrosion inhibitor.

4.1.8 Discussion of concrete under freeze-thaw cycling

The concrete samples behaved similarly to the paste samples in freeze-thaw conditions. Some weight gain in all samples can be attributed to aggregate absorption. H_2O, NaCl, and K Acetate samples all gained weight. Geomelt, which caused weight loss in the paste freeze-thaw samples, did not cause any weight loss in the freeze-thaw concrete samples. One possible explanation for this difference is that Geomelt causes leaching only of cement paste and that the volumetric percentage of paste in concrete (15-20%) is too low for a minor leaching effect to cause significant macroscopic weight change. The leaching that did occur probably offset the weight gain due to the imbibing of fluid from the Geomelt solution. Geomelt concrete wet-dry samples lost weight despite this factor because of higher leaching rates due to increased temperature and stronger Geomelt concentration.

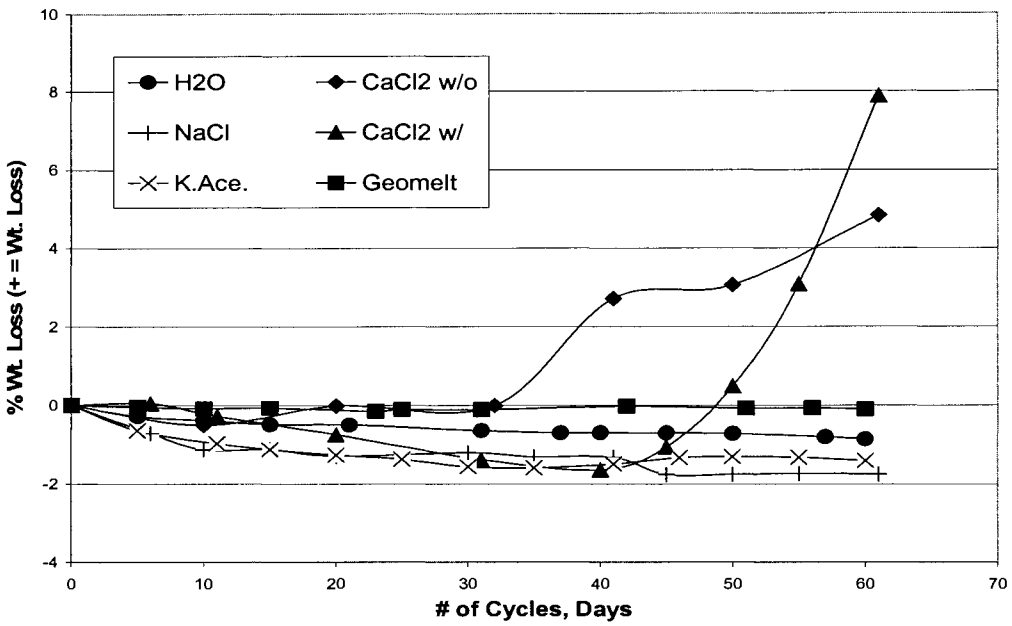

Figure 15. Weight loss of concrete freeze-thaw samples

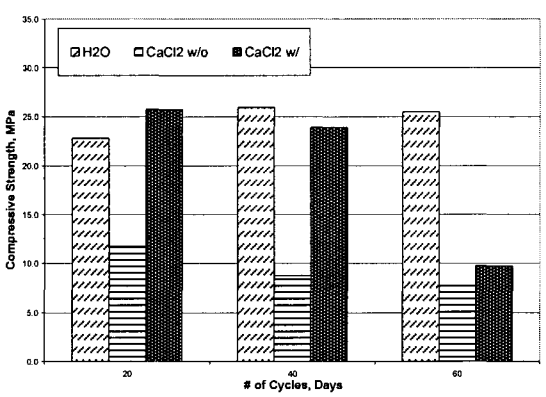

Figure 16. Concrete f-t compressive strengths

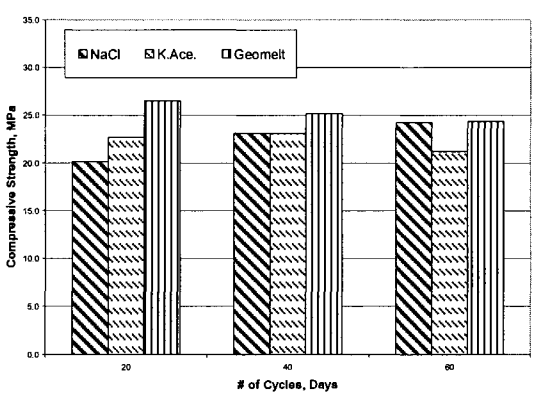

Figure 17. Concrete f-t compressive strengths

$CaCl_2$ solution without corrosion inhibitor caused severe damage to concrete samples, with significant weight loss beginning at 30 freeze-thaw cycles. Coincidentally, this was the same age at which paste freeze-thaw samples immersed in $CaCl_2$ without inhibitor began to disintegrate. Samples exposed to $CaCl_2$ with corrosion inhibitor gained weight (1.6%) during the first 40 cycles, then precipitously lost weight as considerable amounts of surface material scaled off. This initial weight gain was associated with sample damage that increased

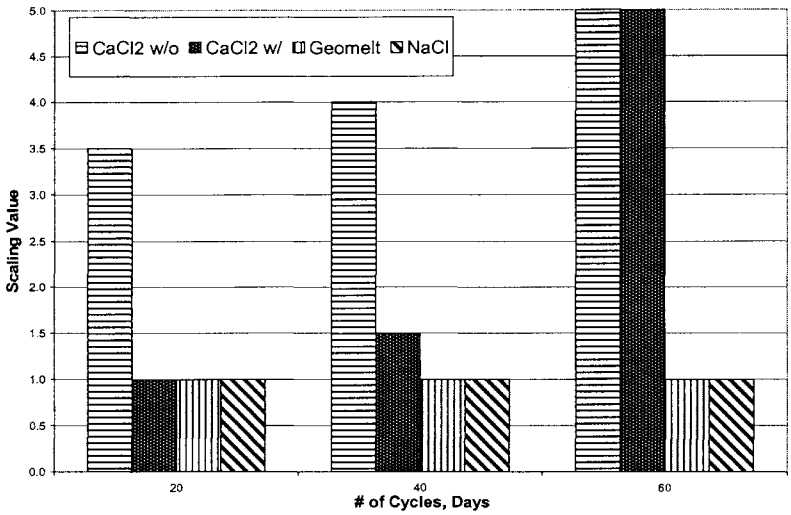

Figure 18. Concrete f-t scaling values

surface area available for fluid adsorption and salt precipitation.

Long needle-like crystals were first observed on the $CaCl_2$ without-inhibitor samples after 31 freeze-thaw cycles, but such crystals were not seen on samples with corrosion inhibitor throughout the testing period. Their presence is inferred, however, given the significant scaling and strength loss damage experienced by with-inhibitor samples beginning after 40 cycles. The significant damage that occurred in both sets of $CaCl_2$ sample groups is attributed primarily to crystal growth pressures. As these crystals grew and filled near-surface void spaces, they made the concrete more susceptible to additional damaging mechanisms like hydraulic and osmotic pressures. This combination of factors, initiated by crystal growth pressures, is responsible for the dramatic weight loss in $CaCl_2$-exposed samples.

Compressive strength change was negligible in NaCl and Geomelt samples. The NaCl samples steadily gained weight, and appeared to suffer little damage in freeze-thaw conditions. As in other environments, the leaching damage to Geomelt samples did not alter the macroscopic strength properties. In contrast, K Acetate samples experienced slight strength impairment, indicating that exposing immature concrete to this chemical may reduce concrete's ultimate performance. Both $CaCl_2$ sample groups experienced dramatic strength loss associated primarily with crystal growth pressures. The $CaCl_2$ without-inhibitor samples

Table 5. Scaling data from paste and concrete samples. Each value represents the average of four samples, based on ASTM C 672.

Sample Type	Exposure Environment	Deicing Solution	# of Exposure Cycles			
			20	40	60	130
Paste	Wet-Dry	Dist. H_2O	0.0	0.0	0.0	0.0
		NaCl	0.0	0.0	0.0	0.0
		$CaCl_2$ w/o	1.0	1.0	2.0	3.3
		$CaCl_2$ w/	1.3	1.8	2.0	2.3
		K Acetate	0.0	0.0	1.0	1.0
		Geomelt	1.0	1.0	1.0	1.0
Paste	Freeze-Thaw	Dist. H_2O	0.0	1.0	1.0	
		NaCl	1.0	1.5	1.7	
		$CaCl_2$ w/o	2.0	4.0	5.0	
		$CaCl_2$ w/	1.3	3.5	4.5	
		K Acetate	0.0	0.0	0.25	
		Geomelt	1.0	1.0	1.0	
Concrete	Wet-Dry	Dist. H_2O	0.0	0.0	0.0	
		NaCl	0.0	0.0	0.0	
		$CaCl_2$ w/o	0.5	2.0	3.0	
		$CaCl_2$ w/	1.0	1.0	1.8	
		K Acetate	0.0	0.0	0.0	
		Geomelt	1.0	1.0	1.0	
Concrete	Wet-Dry	Dist. H_2O	0.0	0.0	0.0	
		NaCl	1.0	1.0	1.0	
		$CaCl_2$ w/o	3.5	4.5	5.0	
		$CaCl_2$ w/	1.0	1.5	5.0	
		K Acetate	0.0	0.0	0.0	
		Geomelt	1.0	1.0	1.0	

Table 6. Visual deterioration of concrete freeze-thaw samples

Chemical / # of Cycles	Distilled H_2O	NaCl	$CaCl_2$ w/o	$CaCl_2$ w/	K Acetate	Geomelt
5-10	NO VISIBLE ALTERATION THROUGH 60 CYCLES.				NO COMMENTS RECORDED.	* Bleached appearance.
11-15						* Bleached appearance. * Tiny pits clearly visible.
16-20			* Very bad scaling. * CA visible over entire surface in nearly all samples. * Surface paste covering almost totally eroded.			
21-25				* Weakness at edges & corners.		
26-30						
31-35		* Amorphous precipitate on select faces. * Significant pop-outs on some faces.	* Long, needle-like crystals abundant. * Highly damaged.	* Material loss at edges & corners.		
36-40						
41-45			* Very severe scaling. * Pressure on almost any CA particle pries it and surrounding material loose.			
46-50		* Some surfaces covered with a blotchy, white layer.	* Rate of material loss has slowed now that original exterior eroded away.	* Continued weakness at edges & corners. * Some cracking 2-4mm from edges.		
51-55						
56-60		* White, amorphous, blotchy deposits on some surfaces.				

lost strength much earlier than the with-inhibitor samples did (Figure 16). At 20 cycles, $CaCl_2$ with-inhibitor sample strength averaged 25.7 MPa and without-inhibitor sample strength averaged 11.8 MPa (Table 3). Once significant scaling and weight loss commenced in the with-inhibitor samples, strength loss precipitously declined. By 60 cycles, strengths were 9.7 and 7.7 MPa, respectively. The corrosion inhibitor appears to delay concrete damage (via impairment of crystal growth), but it does not prevent or mitigate damage once it begins.

4.2 Chemical and Microstructural Evaluation of Deicer Damage

4.2.1 Ion penetration testing of concrete under wet-dry conditions Results of ion penetration tests are shown in Figures 16 through 18 for Cl^-, Na^+, and K^+ ions, respectively. These Figures indicate that significant levels of ions are penetrating into concrete specimens, where they may exacerbate chemical reactions or crystal deposition. The depth of Cl^- ion penetration exceeded the maximum sampling depth of 1.2 inch (Table 6). This is based on the maximum depth at which the saline-exposed sample concentration exceeds the ion concentration of the distilled H_2O control sample. Similar results were achieved in the Na^+ excess of 1.2 inch (Table 8). For all cases, the concentration after 60 cycles exceeded the ion concentration after 20 cycles. Cl^- ions penetrated more than 1.2 inches. This observation suggests that steel reinforcement with an embedment depth of 1.2 inches or less will be and K^+ ion analyses: Na^+ penetrated approximately 0.8 inch (Table 7), and K^+ penetrated in exposed to increased levels of Cl^- ions. High concentrations of Na^+ and K^+ ions could contribute to deleterious alkali-silica reactions. Ion penetration test results demonstrate that ions contributed by deicing solutions reach significant concentrations at depths up to and

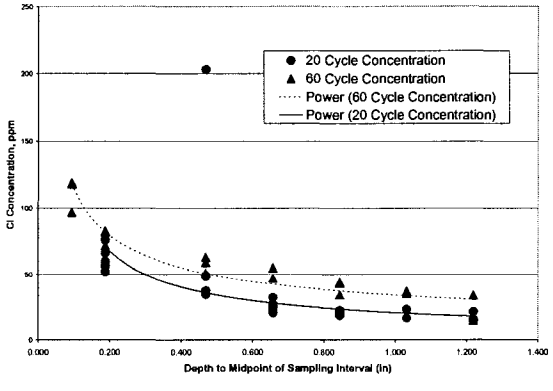

Figure 16. Na^+ ion penetration with depth

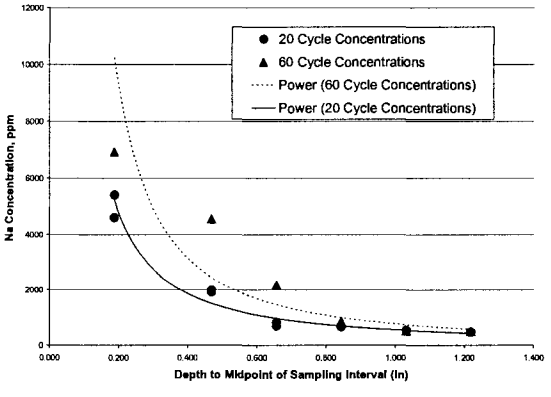

Figure 17. Cl^- ion penetration with depth

exceeding 1 inch into concrete.

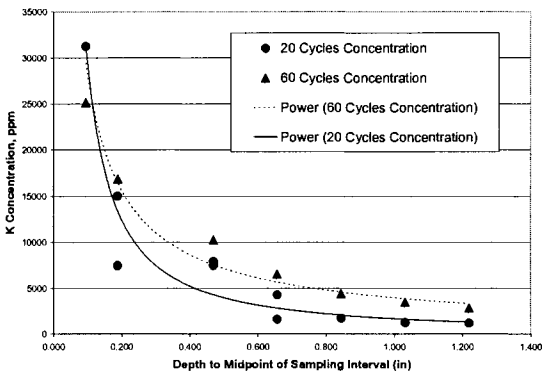

Figure 98. K^+ ion concentration with depth

Table 6. Cl^- concentrations (ppm) in 60-cycle samples exposed to chloride solutions

Depth to Interval Midheight, in	H_2O	NaCl	$CaCl_2$	$CaCl_2$ with Cl
0.094	--	97	119	118
0.188	7	72	82	83
0.469	7	59	63	51
0.657	11	47	47	55
0.844	8	34	43	44
1.032	6	23	35	37
1.219	8	14	34	34

Table 7. Na^+ concentration (ppm) at 60 cycles

Depth to Interval Midheight, in	H_2O	NaCl
0.094	112	12822
0.188	452	6925
0.469	483	4550
0.657	463	2190
0.844	675	848
1.032	710	503
1.219	695	485

Table 8. K^+ concentrations (ppm) at 60 cycles

Depth to Interval Midheight, in	H_2O	K Acetate
0.094	8346	25145
0.188	488	16850
0.469	444	10250
0.657	598	6575
0.844	418	4400
1.032	500	3475
1.219	495	2800

4.2.2 Preliminary photographic analysis of concrete

The following color photographs show concrete surface regions in cross section at 8x and 25x magnification (See Figures 19-28). Photographs were taken for 60-cycle samples exposed to all chemicals except distilled water. For all photographs, the original concrete surface exposed to deicing chemicals is towards the top of the page.

The large, bright white spots in the marked areas of Figures 20-24 are interpreted as salt precipitates. It appears that significant salts have been deposited in pore spaces in both $CaCl_2$ samples. The NaCl sample may show a minor amount of void filling, but it is not conclusive at this magnification. Dullish white areas, such as those seen in the upper-right area of the K Acetate sample, are aggregate surfaces rather than voids filled with salt precipitate. The picture of the sample exposed to Geomelt shows a thin brown layer on the upper exterior of the sample but little or no alteration to the matrix itself.

At 25x magnification, the void filling of the $CaCl_2$ samples becomes much more apparent. White streaks radiate from void spaces and follow the interfaces between paste and fine aggregate particles.

4.2.3 NaCl

Figure 20 shows the 25x resolution image of the polished sample surface. Figure 29 shows the air void system clearly. Figure 30 reveals some cracking within a small region of congested air voids. The cracks do not appear to contain precipitated salts. Figure 31 (see appendices) is an elemental map of this area. It shows high concentrations of both Na and Cl ions surrounding pore edges. According to the image in Figures 20, there is no crack network developed in this sample, and salt precipitation (i.e. halite growth) is confined to voids. Therefore, it does not appear that crystal growth pressures could have developed in this sample.

The background ionic concentrations shown in Figure 31 (Appendix B) indicate the presence of some Cl and Na ions. Figure 32 (Appendix B) is taken at 100x resolution and specifically focuses on precipitate within a pore (see Figure 30). Cl concentration increases from just over 30 counts in Figure 31 to nearly 100 counts in Figure 32. Na concentrations increase from approximately 25 counts to approximately 60 counts.

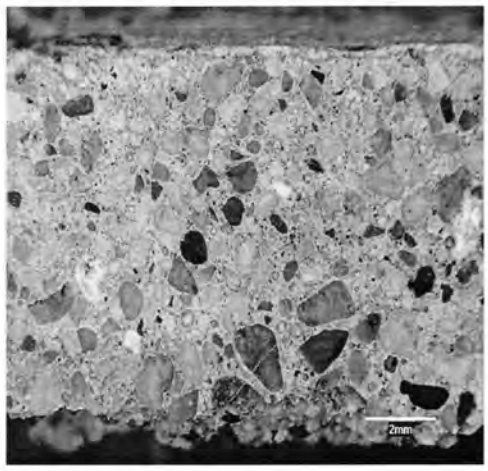

Figure 19. NaCl at 8x magnification

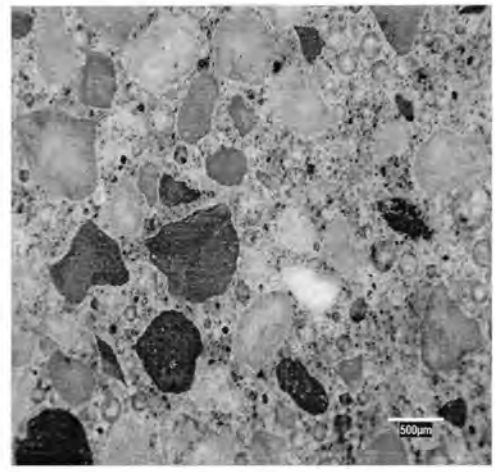

Figure 20. NaCl at 25x magnification

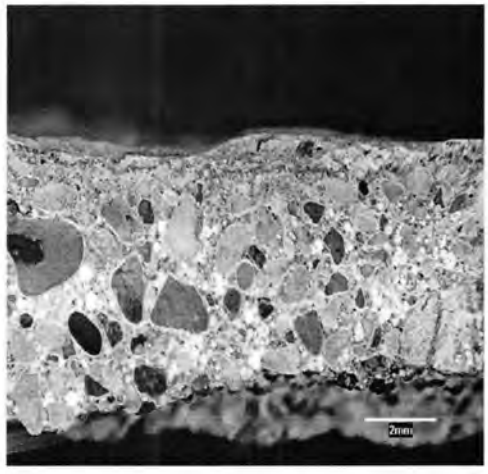

Figure 21. $CaCl_2$ with CI at 25x magnification

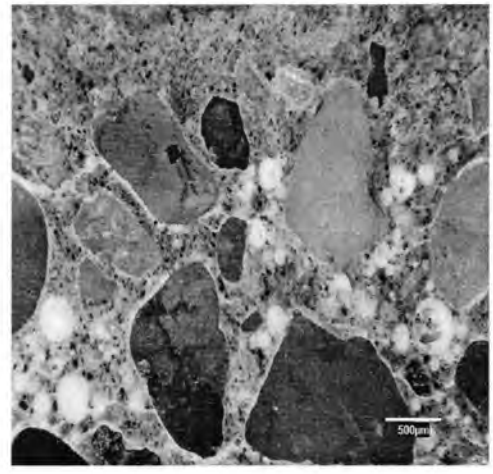

Figure 22. $CaCl_2$ with CI at 8x magnification

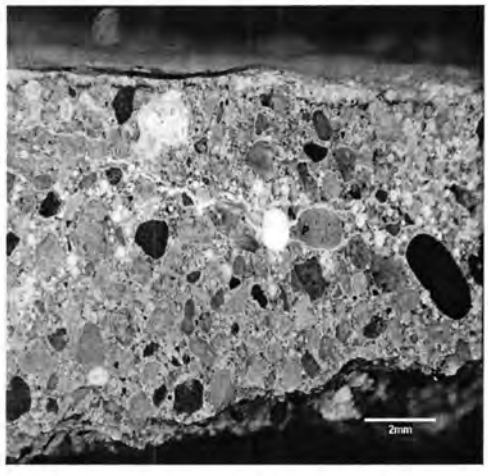

Figure 23. $CaCl_2$ at 8x magnification

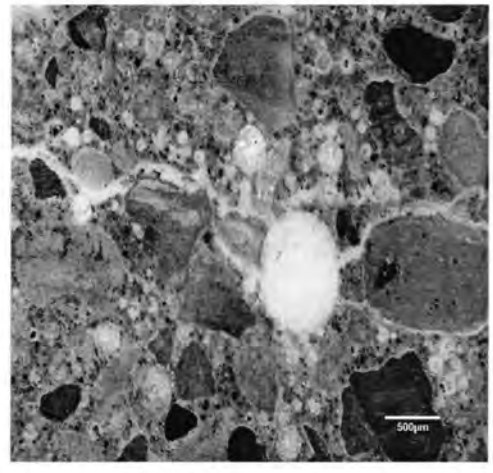

Figure 24. $CaCl_2$ at 25x magnification

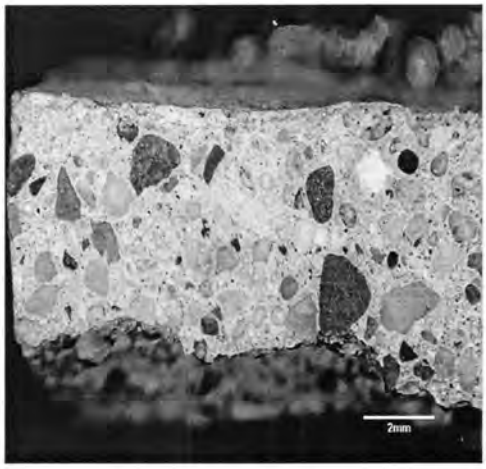

Figure 25. K Acetate at 8x magnification

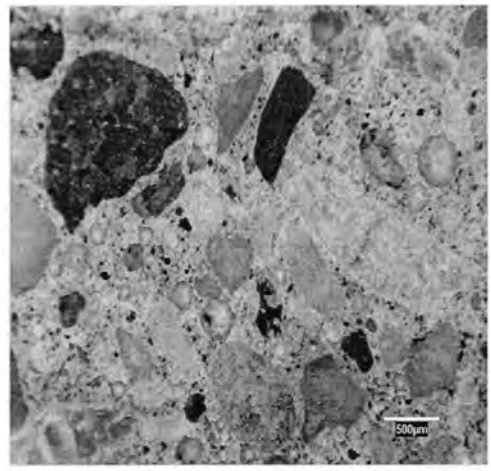

Figure 26. K Acetate at 25x magnification

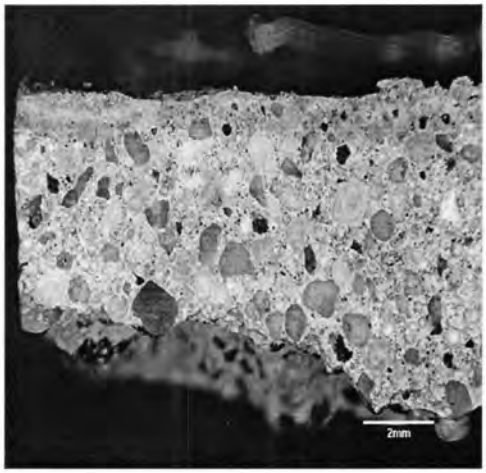

Figure 27. Geomelt at 25x magnification

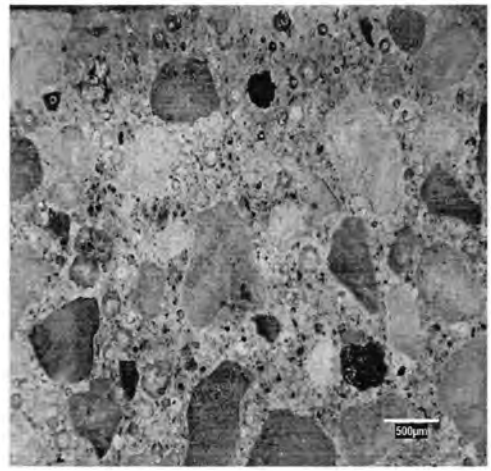

Figure 28. Geomelt at 25x magnification

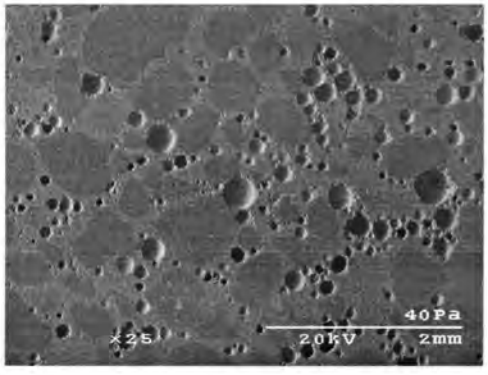

Figure 29. NaCl at 25x magnification

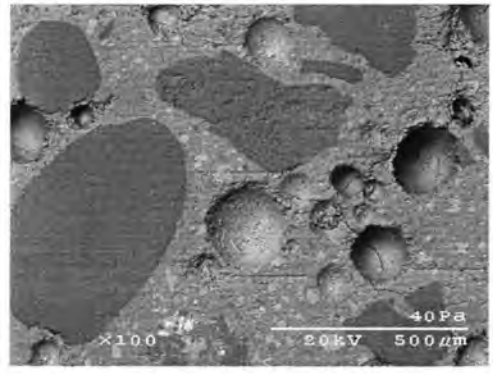

Figure 30. NaCl at 100x magnification

4.2.4 $CaCl_2$

Significant amount of precipitates appear in both large and small air voids as well as along

crack surfaces in the $CaCl_2$ without inhibitor treated sample shown in Figures 23 and 24. In Figure 24, the widespread presence of precipitate is clearly visible throughout the air void system at the top of the figure and throughout the interconnecting regions. Figure 33a shows an SEM image taken at 25x resolution of the region shown in Figure 24. Figure 33a shows zones of significant paste structural alteration. One such zone occurs at the paste-aggregate interface around the large fine aggregate particle at the middle, right side of the figure. This aggregate is shown in Figure 24 to be surrounded with white precipitate. In SEM imaging, the paste both above and below this aggregate is altered significantly (note: this can be viewed at higher resolution in Figure 33b. The aggregate is at the right side of the image.)

Figures 33c and 33d show images of an area near the top of the sample surface. This area is significantly damaged and filled with precipitate. Cracking is abundant, both parallel to and radiating from fine aggregate particles, and between air voids. An elemental map was made for the region shown in Figure 33d (Figure 36). It shows high concentrations of Cl ions around the rim of the large air void at the left of the image, filling smaller air voids, and along crack and aggregate interfaces.

Figure 35 (Appendix B) is an elemental map of the area shown in Figure 33b. The large air void to the left of center is almost completely filled with precipitate. (This void is the one prominently shown to be filled with bright white material in Figure 24). Also noteworthy in the figure is the pattern of Cl and Ca ion concentrations tracing the aggregate interfaces. Figure 29 (Appendix B) shows an ion concentration plot of the area shown in Figure 33b. Figure 29 indicates the strong presence of Cl and Ca ions in pore spaces. Figure 36 also indicates the presence of concentrated Cl and Ca ions along pore perimeters and crack boundaries.

4.2.5 $CaCl_2$ with corrosion inhibitor

$CaCl_2$ with-inhibitor samples show similar results to the samples exposed to $CaCl_2$ solution without the inhibitor: high levels of cracking with cracks along and radiating from aggregate and void interfaces (Figures 37a-37c). Air voids are completely or nearly filled with bright white precipitate (Figure 22). Elemental mapping at 25x resolution, shown in Figure 38 (Appendix B), reveals elevated Cl concentrations in void spaces and along crack and

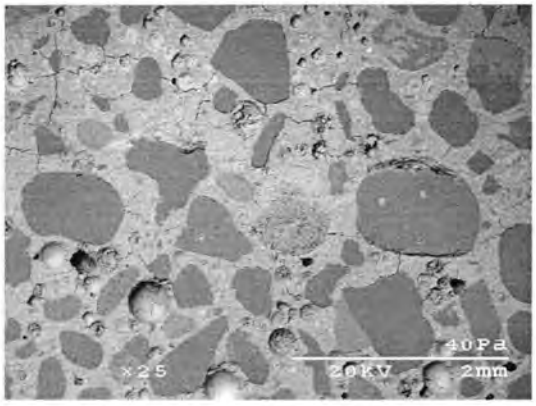

Figure 33a. $CaCl_2$ treated sample at 25x

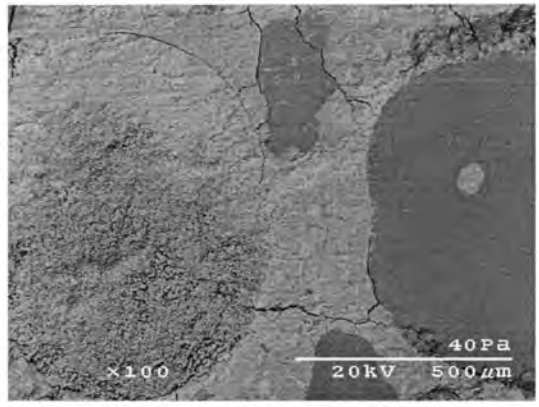

Figure 33b. $CaCl_2$ treated sample at 100x

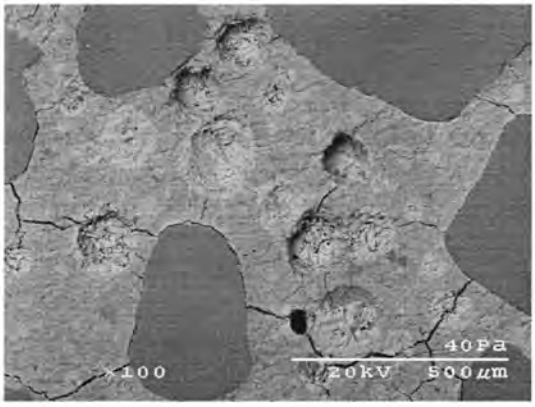

Figure 33c. $CaCl_2$ treated sample at 100x

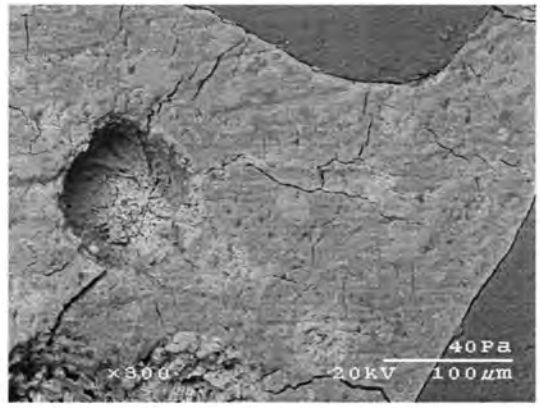

Figure 33d. $CaCl_2$ treated sample at 300x

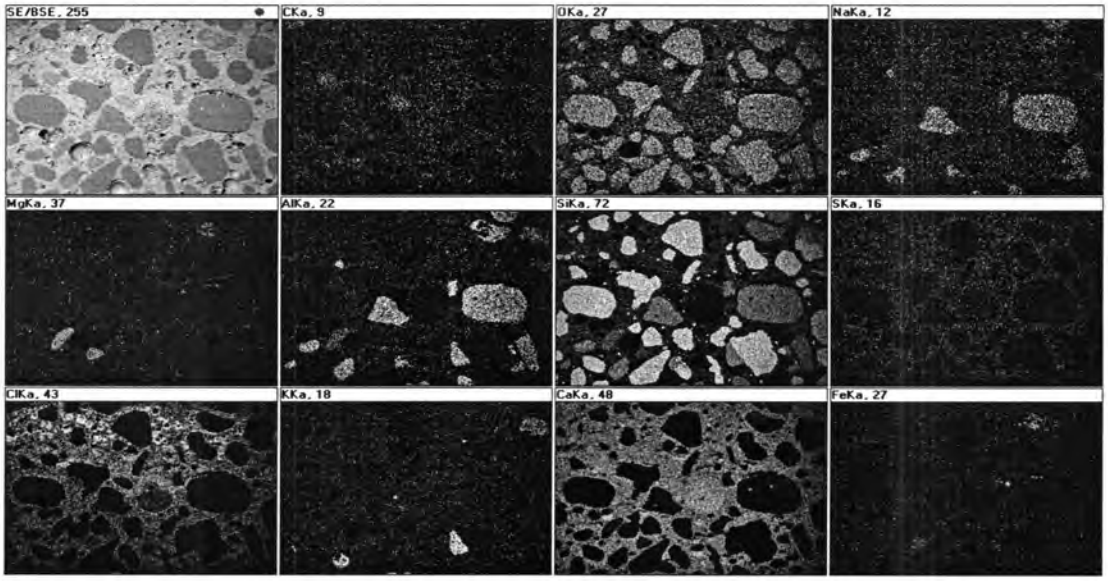

Figure 34. SEM elemental map of $CaCl_2$ at 25x magnification; same region as Figure 33a

aggregate interfaces corresponding to precipitate areas in Figure 22. Ion concentration plots, Figures 39 and 40 (Appendix B), also show elevated Cl and Ca levels.

4.2.6 Potassium Acetate

The K Acetate sample shown in Figures 25 and 26 exhibits no visible signs of deterioration: no cracking is visible and the voids appear free of precipitate. Elemental maps taken at 25x and 200x resolution (not available for publication) indicate no significant presence of precipitates deposited in concrete void spaces.

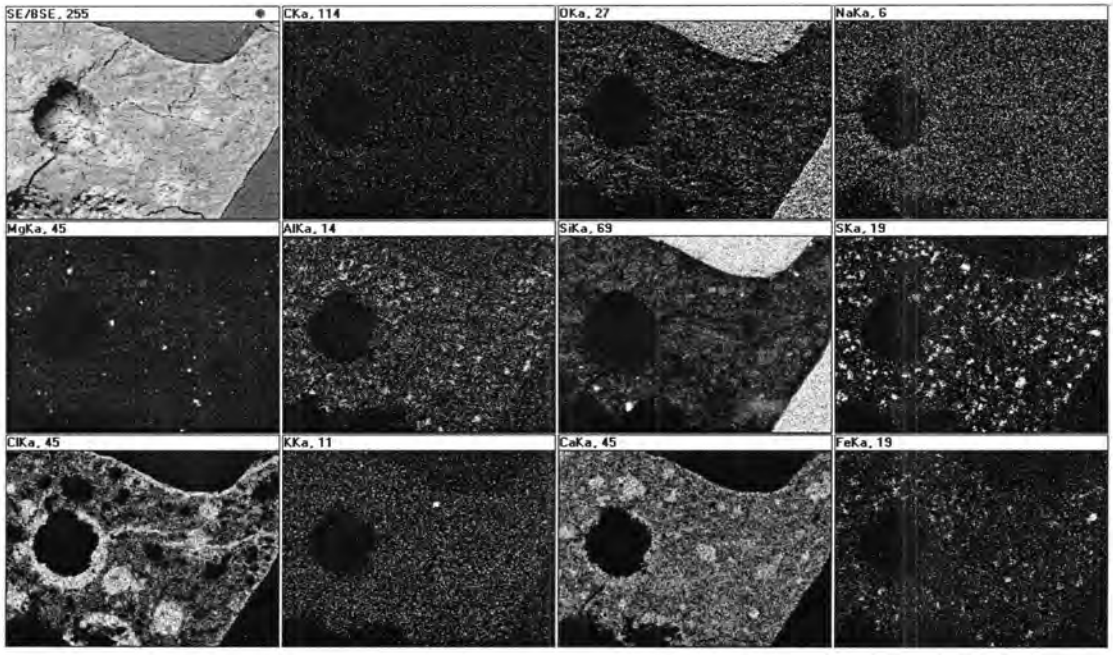

Figure 36. SEM elemental map of $CaCl_2$ treated samples at 300x magnification. Note high Cl and Ca concentrations around pore perimeters and along microcrack interfaces.

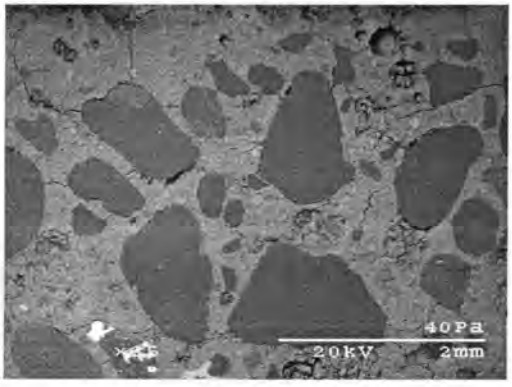

Figure 37a. $CaCl_2$ with CI at 25x magnification

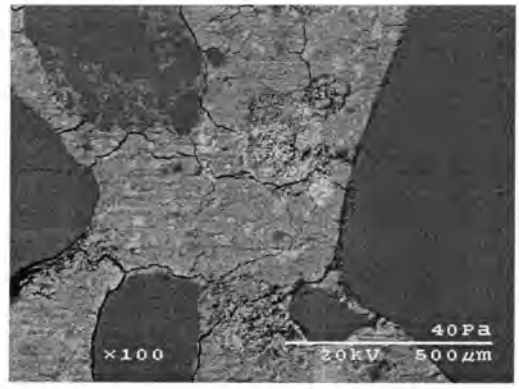

Figure 37b. $CaCl_2$ with CI at 100x magnification

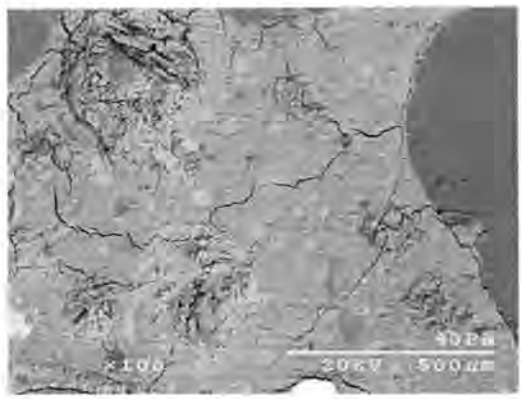

Figure 37c. $CaCl_2$ with CI at 100 x magnification

4.2.7 Geomelt

The Geomelt sample showed little or no damage, as observed in the images of Figures 27 and 28. SEM images shown by Figures 42a and 42b reveal void spaces free from significant precipitate levels. The elemental map shown in Figure 43 likewise does not reveal significant deposits of ions that may have been introduced by Geomelt exposure. Of particular interest is Figure 42c, which shows at 300x resolution small, internestled dark areas throughout the paste matrix.

4.3 Results from XRD Analysis of Concrete

Results are shown in for each chemical in Figures 44-51 (Appendix D) with 20 cycle and 60 cycle sample diffractograms juxtaposed for comparison of chemical alteration with additional exposure. Reporting of results and analysis of the effects of the various deicing chemicals will focus on changes that occurred between 20 and 60 cycles of deicer exposure and on the specific minerals where change occurred.

4.3.1 Distilled water

(See Figure 44, Appendix D.) Concrete in distilled water was studied to identify the locations of principal XRD peaks associated with typical concrete constituents. The samples contained the expected concrete phases: quartz, calcite, portlandite, and feldspathic minerals from the fine aggregate.

4.3.2 NaCl

(See Figure 45, Appendix D.) No new peaks were detected in the 60-cycle sample versus the 20-cycle sample. Halite was detected in minor amounts for both samples and coincides with the white precipitate observed on wet-dry and freeze-thaw precipitates (Tables

4 and 6).

4.3.3 $CaCl_2$

(See Figure 46, Appendix D.) Newly formed peaks were identified at 8.375Å (10.554° 2θ) and at 3.85Å (23.082° 2θ). These peaks were found to match the two most intense peaks for a Calcium Aluminum Chloride Sulfate Hydrate mineral – $Ca_8Al_4O_{12}$-Cl_2SO_4•$24H_2O$ (see Figure 47, Appendix D, for a detailed diffractogram for this mineral). Mineral 19-203 is identified here only as a possible match for observed peak intensities.

Also noted in $CaCl_2$ without inhibitor samples was a decreased peak intensity of portlandite ($Ca(OH)_2$) peaks at 27.804Å (3.206° 2θ) and 50.053Å (1.8208° 2θ).

4.3.4 $CaCl_2$ with inhibitor

As with the diffractogram from $CaCl_2$ without corrosion inhibitor, new peaks at 8.319Å (10.624° 2θ) and 4.161Å (21.337° 2θ) were formed in the 60-cycle sample versus the 20-cycle sample (Figure 49, Appendix D). A detailed diffractogram for $Ca_8Al_4O_{12}$-Cl_2SO_4•$24H_2O$ (19-203) is shown in Figure 48, Appendix D. Ettringite and/or thaumasite peaks were identified in the 60-cycle sample at 9.551Å and 5.502Å.

4.3.5 Potassium acetate

No new significant new peak intensities were detected in 60-cycle diffractogram (Figure 50, Appendix D.)

4.3.6 Geomelt

No significant new peak intensities were detected in the 60-cycle diffractogram (Figure 51, Appendix D.) A small peak was detected at 9.711Å (9.099° 2θ) in the 60-cycle sample that may be indicative of ettringite formation.

4.4 Results and Discussion of SEM Analysis of Concrete

4.4.1 Preliminary photographic analysis

In both $CaCl_2$-exposed samples in Figures 21-24, white streaks radiate from precipitate-filled pores. These white lines follow crack and aggregate interface boundaries. Some of these cracks may have occurred during polishing cutting of the samples as they were prepared for analysis. The presence of these patterns suggests that as salts were deposited in the void spaces, mineral growth pressures caused sub-horizontal cracking in the cement paste, propagating along aggregate interfaces. Salts subsequently deposited on the crack

surfaces. As these samples were never frozen, the cracks cannot be attributed to ice crystallization pressures. Nor are they shrinkage cracks because of their orientation: parallel to the concrete surface rather than perpendicular.

4.4.2 NaCl

The elemental map of Figure 52 (Appendix B) may show slight concentrations of Na and Cl ions precipitating on pore surfaces. If indeed these concentrations of Na and Cl are elevated, these deposits are probably indicative of the halite crystal development observed in XRD (see Figure 45, Appendix D). The cause of the minor cracks seen in Figure 30 is uncertain, as the voids themselves are not filled with precipitate. Significant hydraulic and osmotic pressures are unlikely to develop because of the proximity of the large air voids. Furthermore, the samples were never frozen and thermodynamic instability capable of sufficient pressure to cause cracking is similarly unlikely. The cracks may result from tensile stresses associated with shrinkage, or they could be affiliated with sample preparation.

4.4.3 $CaCl_2$

Figure 24 displays a large white pore filled with white precipitate. Figure 35 (Appendix B) presents an elemental map of this region and indicates elevated levels of Cl and Ca ions, possibly with secondary elements present, filling this pore. The elemental intensity data of Figure 35 (Appendix B) thus suggests that the precipitate filling these air voids may be $CaCl_2$ or a more complex salt.

The images shown in Figures 33c and 33d reveal significant alteration to the concrete. Figure 36 is an elemental map made of the region shown in Figure 33d. Ca ions are associated with Cl ions, particularly in the filled air voids and around the rim of the larger air void. Other elements such as Al, K, Na, Fe, and S may also be associated with the precipitate(s), but such conclusions are not certain from Figure 36. The alteration of the paste above and below aggregate particles shown in Figure 33b, coupled with the significant cracking visible in Figures 24, 33a, 33c, and 33d, suggests that significant damage was done to the concrete by exposure to $CaCl_2$ solution.

Figure 35 (Appendix B) lends further credence to the assertion that Ca and Cl are the principal constituents of the precipitate, which may be dominated by crystalline $CaCl_2$. These images and elemental maps conclusively demonstrate that concrete was damaged by

exposure to $CaCl_2$ without corrosion inhibitor. SEM analysis suggests deterioration is due to the presence of salt precipitates and may result from crystal growth pressures and/or mineralogical change (see XRD analysis below). Deterioration appears to be both physical (crystal growth pressures) and chemical (alteration of paste, particularly at aggregate interfaces). Precipitates dominated by Cl and Ca ions are shown filling all or sections of air voids, as well as aggregate and crack interfaces. The principal mineral phase of this precipitate is probably crystalline $CaCl_2$, although more complex assemblages may be formed. Additional identification of the mineral phases present in the precipitate requires alternative testing procedures.

4.4.4 $CaCl_2$ with corrosion inhibitor

According to the results of ion penetration testing (Figure 17 and Table 6), the permeability of Cl^- ions in $CaCl_2$ with the corrosion inhibitor versus plain $CaCl_2$ were approximately equal. The corrosion inhibitor did not appear to retard Cl^- ion ingress. Microscale visual deterioration in the sample exposed to $CaCl_2$ with a corrosion inhibitor is indistinguishable from that caused by $CaCl_2$ without a corrosion inhibitor. Both samples show significant cracking, and both reveal Ca and Cl deposition in pores and along crack interfaces. The sub-horizontal cracking both exhibit near the sample surface (Figures 21-24) is probably caused by crystal growth pressures as the lack of freezing [probably] prohibits development of hydraulic, osmotic, and thermodynamic pressures strong enough to cause such damage. Figures 37b and 37c show pores and cracks filled with precipitate. Ion concentration plots in Figures 39 and 40 (Appendix B) further indicate that this precipitate is mostly crystalline $CaCl_2$.

4.4.5 Potassium acetate

According to the elemental mapping results (figures unavailable for publishing), potassium concentrations in the concrete matrix were higher than those found in samples exposed to other deicers. However, this elevated concentration level was not associated with any visible deterioration (although it may lead to possible alkali-silica reaction problems), nor did K Acetate-exposed samples exhibit damage in other tests.. Based on these observations, K Acetate appears benign on a basis of mineral precipitation and crystal growth, and in causing chemical alteration. It does contribute large concentrations of K^+

ions to depths greater than 1.2 inches within concrete samples, however (Figure 18 and Table 8).

4.4.6 Geomelt

The image in Figure 42c (Appendix B) at 300x magnification reveals an assemblage of internestled dark areas not observed in any other samples. While the identity of the internestled, dark regions is unclear, they may be areas of low mass density and therefore may reveal the cause of Geomelt-exposed samples' consistent weight loss noted previously. If these dark regions are, in fact, the result of mass leaching, they illustrate the deleterious effects of such reactions. Although macroscopically (Figures 27, 28), this sample looked undamaged, the consistent weight loss demonstrated by Geomelt-exposed samples in wet-dry and freeze-thaw cycling indicates there is considerable damage being done to the paste integrity. Thus, macroscopic deterioration is only an issue of time. The dark regions shown in Figure 42c (Appendix B) may provide insight into the cause of Geomelt-exposed samples' weight loss. However, until the cause of these areas is determined, no solid conjectures can be made.

4.5 XRD Analysis of Concrete Samples

4.5.1 Distilled water

Sampling depth (3/16") was too shallow to encounter much, if any, coarse aggregate, so carbonate minerals were not expected in the diffractograms. Note also that although albite and anorthite are identified in Figure 44, (Appendix D), the actual mineral phases may differ slightly. Feldspathic minerals typically involve solid solution intermediate phases, e.g. like that between albite and anorthite. With such intermediate phases present, peak intensities are unlikely to exactly match the laboratory end-member phase studies that are used to produce the powder diffraction data file. Thus, XRD techniques are not ideal for determining exact compositions of solid solutions.

4.5.2 NaCl

NaCl exposure caused little if any chemical alteration to concrete components. The presence of halite (Figure 45, Appendix D) appears to have had a minimal effect on other mineral phases and was not associated with damage in wet-dry or freeze-thaw testing.

4.5.3 $CaCl_2$

Two new peaks were observed in the 60-cycle diffractogram at 8.375Å (10.554° 2θ) and at 3.85Å (23.082° 2θ) (Figure 47, Appendix D). The rarity of discrete end-member phases in PCC materials makes positive identification of these peaks difficult. These newly formed peaks at 8.375Å and 3.85Å do indicate some kind of mineral alteration is occurring, and that these peaks match so closely to $Ca_8Al_4O_{12}Cl_2SO_4 \bullet 24H_2O$ suggests that the mineral(s) being formed are of similar mineralogy.

The decreased peak intensity of Portlandite in the $CaCl_2$ without inhibitor samples may result from random sampling differences between 20 and 60-cycle samples, or it may correspond to $Ca(OH)_2$ leeching that has been identified in previous studies (Chatterji, 1978; Hoffmann, 1984; Heukamp, 2001).

4.5.4 $CaCl_2$ with corrosion inhibitor

Peak intensities at 8.319Å (10.624° 2θ) and 4.161Å (21.337° 2θ) were observed in the 60-cycle diffractogram (Figure 48, Appendix D). Although not an exact match to the peaks found in Figure 47 (Appendix D), they are also a close match for a Calcium Aluminum Chloride Sulfate Hydrate mineral – $Ca_8Al_4O_{12}Cl_2SO_4 \bullet 24H_2O$ (19-203). That these peaks occur in the 60-cycle sample but not at the 20-cycle sample again suggests that mineral alteration is taking place and that there is some kind of reaction between $CaCl_2$ deicing solution and concrete constituents.

Peaks corresponding to ettringite and/or thaumasite minerals were identified in the 60-cycle sample only (9.551Å and 5.502Å). This suggest the occurrence of secondary ettringite or thaumasite formation. These phases were also identified in trace amounts in the 60-cycle Geomelt-exposed samples (Figure 51, Appendix D), and may have been present in $CaCl_2$ without inhibitor 60-cycle sample (Figure 46, Appendix D) as well. This formation is believed to be typical and not necessarily indicative of chemical alteration due to contact with deicers.

4.5.5 Potassium Acetate

According to Figure 50, Appendix D, the sample exposed to K Acetate solution did not experience any significant chemical alteration. K Acetate appears non-reactive with PCC material. It may contribute to alkali-silica reaction susceptibility by introducing large amounts of K^+ ions into concrete, however (see ion penetration testing results above).

4.5.6 Geomelt

The small amount of ettringite detected in the Geomelt sample (Figure 51, Appendix D) is probably due to normal concrete aging and is not necessarily an indication of chemical interaction between concrete and deicer. According to XRD data, Geomelt does not appear to interact chemically with PCC materials. Relative peak intensities between 20-cycle and 60-cycle diffractograms do not indicate that excessive leaching of $Ca(OH)_2$ occurred.

However, this is not evidence that such leaching did not occur: XRD testing was designed only for qualitative identification, not for qualitative concentration comparisons.

CHAPTER 5. CONCLUSIONS

The experiments and observations performed in this study were designed to ascertain the relative destructiveness of five deicing compounds to Portland cement materials. The five compounds used in the research produced varying degrees of damage to the Portland cement concretes and pastes, ranging from extensive damage with loss of considerable sample integrity to no visible damage at all.

1. The two $CaCl_2$ solutions were shown to be extremely damaging to PCC materials in freeze-thaw conditions. This research suggests exposure to $CaCl_2$ in freeze-thaw conditions produces more damage than wet-dry exposure because of the growth of needle-like crystals (the identity of these crystals was never determined) in freezing temperatures. These crystals may be $CaCl_2$ precipitates, or they may be products formed from $CaCl_2$ and concrete constituents. XRD data for the two 60-cycle $CaCl_2$ diffractograms indicate the presence of new pairs of diffraction peaks at 8.375Å (10.554° 2θ) and 3.85Å (23.082° 2θ), and at 8.319Å (10.624° 2θ) and 4.161Å (21.337° 2θ), respectively, that may correspond to new hydrate mineral formation.

The use of a corrosion inhibitor in $CaCl_2$ deicing solution slowed the development of large needle-like crystals in freeze-thaw samples and delayed damage to the concrete and paste samples. However, the corrosion inhibitor might not affect ultimate damage and therefore should not be counted on to mitigate ultimate $CaCl_2$ damage.

2. The NaCl deicing solution did not readily damage PCC materials. No significant strength loss was recorded for the samples in NaCl deicer under either wet-dry or freeze-thaw exposure environments. The observed halite precipitation in wet-dry testing could ultimately lead to deterioration, but its rate of deposition is slow even at high NaCl solution concentrations.

3. The K Acetate deicer appears to be non-damaging overall to PCC materials. Concrete and paste samples did not show significant weight or strength changes in either wet-dry or freeze-thaw conditions when exposed to the K Acetate deicing solution. SEM and XRD analysis detected no significant chemical reactions or precipitate formation.

4. Exposure to the Geomelt solution caused minor weight loss to samples in both

wet-dry and freeze-thaw conditions. The weight loss experienced was greater in the wet-dry cycling than in the freeze-thaw cycling. Leaching, which is believed to account for this weight loss, therefore appears to be temperature-dependent, with higher temperatures causing increased leaching. What minerals were being leached out of the Geomelt-exposed PCC materials is uncertain; XRD data did not display significant drops in peak intensities corresponding to a specific mineral. In conclusion, Geomelt deicing solution appears to mildly damage PCC materials, causing variable mass loss through leaching processes.

5. Chloride, sodium, and potassium ions were found to penetrate to large depths in wet-dry concrete samples. Chloride and potassium ions were present in elevated numbers – greater than or equal to four times the concentrations in the control sample at depths exceeding 1.2 inches. Sodium concentrations were elevated to just over 0.8 inches depth. If these ions are typically present in such quantities at these depths in concrete, they may increase the amount of deterioration in concrete interiors through chemical reaction and precipitation

5.1 Recommendations and Suggestions for Further Research

* The data generated by this study suggest that NaCl and K Acetate deicing compounds can be applied to PCC materials without causing much damage. Given the relative cost of the two materials, employment of K Acetate might be restricted to select usage. Geomelt deicing solution causes some mass loss through leaching, but in dilute solutions, this problem should be mitigated. $CaCl_2$, with or without the addition of a corrosion inhibitor, causes considerable damage to PCC materials, especially in freeze-thaw, and its use as a deicer in winter environments is not recommended.

* This study established an observational experimental program designed to determine the relative damage to PCC materials from exposure to different deicing solutions. The observations (weight loss, scaling, compressive strength) or analyses (SEM and XRD) of these experiments have provided insight to damage mechanisms of the deicers. Quantitative evaluation and identification of mineral precipitates and crystals are needed in further study.

* Extreme benefit could be gained by conducting long-term observational field studies on the performance of pavements subjected to deicing chemicals. Such studies are vital to accurately determine the validity of laboratory results such as those obtained in this

study.

* As mentioned in the introduction, differences in concrete constituents and mixing and emplacement procedures can significantly alter the behavior of PCC materials. The experiments performed in this study were designed to minimize the influence of such variables, but additional research to address performance alterations with curing and finishing techniques, and with concrete design and ingredient differences, would be helpful. Many studies have addressed these issues, but the increasing use of admixtures and blended cements, as well as new deicing chemicals, maintains the need for continued research about the effects of material variation. As transportation demands in northern climates continue to increase, the use of highway deicers will also increase. As new deicers become commercially available, there will be an increasing demand for research and evaluation of these products and their effects on transportation infrastructure.

REFERENCES CITED

1. Beaudoin, James J. and MacInnis, Cameron. "The Mechanism of Frost Damage in Hardened Cement Paste." Cement and Concrete Research 4 (1974): 139-147.

2. Brown, P.W. and Doerr, April. "Chemical Changes in Concrete Due to the Ingress of Aggressive Species." Cement and Concrete Research 30 (2000): 411-418.

3. Cantor, T.R. and Kneeter, C.P. "Influence of Salt on the Freeze-Thaw Deterioration of Concrete." Materials Performance (May, 1977): 28-32.

4. Chatterji, S. "Mechanism of $CaCl_2$ Attack on Portland Cement Concrete." Cement and Concrete Research 8 (1978): 461-468.

5. Chatterji, S. "Aspects of Freezing Process in Porous Material-Water System; Part 1. Freezing and the Properties of Water and Ice." Cement and Concrete Research 29 (1999): 627-630.

6. Chatterji, S. "Aspects of Freezing Process in Porous Material-Water System; Part 2. Freezing Properties of Frozen Porous Materials." Cement and Concrete Research 29 (1999): 781-784.

7. Cody, Robert D. et al. "Experimental Deterioration of Highway Concrete by Chloride Deicing Salts." Environmental and Engineering Geoscience Vol. II, No. 4, (1996): 575-588.

8. Cordon, William A. Freezing and Thawing of Concrete – Mechanisms and Control. Detroit and Ames, Ia: American Concrete Institute and Iowa State University, 1966. 5-41.

9. Hansson, C.M. et al. "Corrosion Inhibitors in Concrete – Part I: The Principles." Cement and Concrete Research 28 (1998): 1775-1781.

10. Hoffmann, Dirk W. "Changes in Structure and Chemistry of Cement Mortars Stressed by a Sodium Chloride Solution." Cement and Concrete Research 14 (1984): 49-56.

11. Heukamp, F.H. et al. "Mechanical Properties of Calcium-Leached Cement Pastes Triaxial Stress States and the Influence of the Pore Pressures." Cement and Concrete Research 31 (2001): 767-774.

12. Jang, Ji-Won et al. "Cl^-, SO_4^{2-}, and PO_4^{3-} Distribution in Concrete Slabs Ponded by Corrosion-Inhibitor-Added Deicing Salts." Advanced Cement Based Materials 8 (1998): 101-107.

13. Kurdowski, W. et al. "Corrosion of Tobermorite in Strong Chloride Solutions."

Mechanisms of Chemical Degradation of Cement-Based Systems. Edited by K.L. Scrivener and J.F. Young. London: E & FN Spon, 1997. 114-121.

14. Litvan, G.G. "Frost Action in Cement in the Presence of De-Icers." Cement and Concrete Research 6 (1976): 351-356.

15. Mammoliti, L. et al. "Corrosion Inhibitors in Concrete; Part II: Effect on Chloride Threshold Values for Corrosion of Steel in Synthetic Pore Solutions." Cement and Concrete Research 29 (1999): 1583-1589.

16. Mehta, P.K., Concrete: Structure, Properties, and Methods. Englewood Cliffs, NJ: Prentice Hall, 1993. 29-30.

17. Minsk, L. D. Snow and Ice Control Manual for Transportation Facilities. New York: McGraw-Hill, 1998. 44-50, 244-261.

18. Morris, W. and Vazquez, M. "A Migrating Corrosion Inhibitor Evaluated in Concrete Containing Various Contents of Admixed Chlorides." Cement and Concrete Research 32 (2002): 259-267.

19. Mu, Ru et al. "Interaction Between Loading, Freeze-Thaw Cycles, and Chloride Salt Attack of Concrete With and Without Steel Fiber Reinforcement." Cement and Concrete Research 32 (2002): 1061-1066.

20. Naffa, S. Ould, et al. "Detection of Chemical Damage in Concrete Using Ultrasound." Ultrasonics 40 (2002): 247-251.

21. Ost, Borje and Monfore, G.E. "Penetration of Chloride into Concrete." Journal of the Portland Cement Association Research and Development Laboratories Vol. 8, No. 1 (1966): 46-52.

22. Pigeon, M. and Pleau, R. Durability of Concrete in Cold Climates. London: E & FN Spon, 1995. 1-57.

23. Piltner, R. et al. "Stress Analysis of Expansive Reactions in Concrete" Cement and Concrete Research 30 (2000): 843-848.

24. Powers, T.C. "A Working Hypothesis for Further Studies of Frost Resistance of Concrete." Proceedings of the American Concrete Institute Vol. 41, No. 4 (1945): 245-272.

25. Powers, T.C. "Void Spacing as a Basis for Producing Air-Entrained Concrete." PCA Research Bulletin 49a Portland Cement Association, Chicago, 1954.

26. Santagat, M.C. and Collepardi, M. "The Effect of CMA Deicers on Concrete

Properties." Cement and Concrete Research 30 (2000): 1389-1394.

27. Scherer, George W. "Crystallization in Pores." Cement and Concrete Research 29 (1999): 1347-1358.

28. Setzer, M.J. "Action of Frost and Deicing Chemicals – Basic Phenomena and Testing." Freeze-Thaw Durability of Concrete. Edited by J. Marchand, M. Pigeon, and M. Setzer. London: E & FN Spon, 1997. 3-21.

29. Trepanier, S.M. et al. "Corrosion Inhibitors in Concrete; Part III. Effect on Time to Chloride-Induced Corrosion Initiation and Subsequent Corrosion Rates of Steel in Mortar." Cement and Concrete Research 31 (2001): 713-718.

30. Tritthart, J. "Transport of a Surface-Applied Corrosion Inhibitor in Cement Paste and Concrete." (Article in Press) Cement and Concrete Research

APPENDIX A. SUPPLEMENTS TO MATERIALS AND METHODS

Geomelt Composition.
(Note: source: Grain Processing Corporation.)

Component Groups:	% By Wt.
Dissolved Solids	74.84
Ash	22.81
Crude Protein	19.44
Nitrogen Compounds (as N)	3.11
Alpha-Amino Nitrogen Compounds	0.41
Individual Compounds:	
Sucrose	13.13
Raffinose	3.96
Invert	0.020
Betaine	8.95
Potassium	8.85
Sodium	1.98
Calcium	0.04
Chloride	1.83
Nitrate	0.70
Sulfate	2.1
Pyrrolidone Carboxylic Acid	6.29
Tyrosine	0.28
Serine	0.05
Isoleucine and/or Proline	0.47
Leucine and/or Methionine	0.25
Glutamic Acid	0.88
Aspartic Acid	0.89
Threonine	0.015
Alanine	0.16
Valine	0.12
Glycine	0.06

PASTE MIX DESIGN:

Mix design calculations were based on a total volume of 0.097 ft^3 intended to fill fifteen eight-inch cubic samples (material safety factor of 1.4). Designed air content was 6%.

Constituent:	**Amount:**	
Cement	3.82 kg	
Water	1.53 kg	
AEA	1.9 mL	(AEA = Air-entraining agent)

Procedures for Mixing Paste Samples:

1. Added air-entraining agent to two-thirds of total mixing water and mixed for thirty seconds.
2. With mixer off, added first cement, then the remaining mix water.
3. Started mixer and mixed for three minutes.
4. Turned off mixer and allowed paste to sit for two minutes; scraped cement clumps off mixing drum sides and the mixing arm itself.
5. Mixed for a final two minutes (summary: 3-2-2 mixing).
6. Scooped paste into molds, filling entire mold volume in one layer.
7. Rodded each mold twenty-five times.
8. Vibrated for thirty seconds.
9. Scraped excess material off mold surfaces and smoothed surfaces with flat bladed spatula.
10. Paste molds were covered and placed in laboratory room (~ 21°C) for twenty-four hours, then transferred to curing room (RH>100%, T ~ 19°C) for an additional six days of curing.
11. After seven days total curing, samples were placed in designated chemical/environment exposure condition.

CONCRETE MIX DESIGN

Material	DOT, lb/ft^3	Wt., lb/kg	Abs., %	MC, %	Moisture Correction, kg	Corrected Batch, kg (C2-C8)	Corrected Batch, kg (C1, C9-C12)
Coarse Aggregate	80	42.32 / 19.20	4.25	0.13	-0.79	18.41	16.57
Fine Aggregate	63	35.33 / 15.12	0.71	1.29	+0.09	15.21	13.69
H_2O	14	7.41 / 3.36				4.06	3.65
Cement	29	15.34 / 6.96				6.96	6.26
Air-Entraining Agent	.75oz / 100 lb cement	0.115oz / 3.40 mL				3.40 mL	3.06 mL

Table 3: Concrete Mix Designs for Concrete Samples.

Notes: 1. Batch designs for C1 and C9-C12 are 0.9 (90%) the material used in batches C2-C8.

2. DOT = Iowa Department of Transportation recommended mix design.
3. Abs. = absorption; MC = moisture content.
4. Calculations are based on a total design volume of 0.529 ft^3.
5. Designed air content was 6%.

Table 4: Coarse Aggregate Blending for Concrete Samples.

Aggregate Size	IaDOT Recommended Percentage	Blended Wt., kg (C2-C8)	Blended Wt., kg (C1, C9-C12)
1"	2.5	0.460	0.414
3/4"	7.5	1.381	1.243
1/2"	40.0	7.364	6.628
3/8"	25.0	4.603	4.143
#4 Sieve	25.0	4.603	4.143

Procedures for Mixing Concrete Samples:

1. Mixed coarse aggregate with approximately one-third of total mixing water and [all] air-entraining agent for thirty seconds.
2. With mixer running, added fine aggregate and mixed an additional thirty seconds.
3. Turned off mixer and added cement then turned on mixer and added remaining water.
4. Once remainder of water was added, mixed for an additional three minutes.
5. Turned mixer off for three minutes.
6. Turned on mixer for a final two minutes of mixing (summary: 3-3-2).
7. Filled molds in two layers (~ 2 in height of each layer in 4 in^3 molds), while rodding twenty-five times with addition of each layer.
8. Once concrete was emplaced and molds were filled, the surface was smoothed off using a flat, bladed spatula.
9. Concrete molds were covered and placed in laboratory room (~ 21°C) for twenty-four hours, then transferred to curing room (RH>100%, T ~ 19°C) for an additional six days of curing.
10. After seven days total curing, samples were placed in designated chemical/environment exposure condition.

CHEMICAL ANALYSIS TEST PROCEDURES FOR IPT

Quantification of ion concentration was performed by the Soil and Plant Analysis Laboratory at Iowa State University. Powdered samples were obtained from concrete specimens using a drill press with depth intervals of 3/16 inches. Samples were obtained over seven intervals, or 1.31 inches (33.3 mm) of total depth from the concrete surfaces. Sample preparation involved a water extraction, described as follows:

* 10 grams of cement powder were mixed with 0.025 grams of charcoal
* Added 25 mL distilled water
* Solution was agitated for 15 minutes

Analyses of K^+ and Na^+ concentrations utilized atomic cation absorption techniques. Chloride concentrations were obtained via the Mercury (II) Thiocyanate Method. (See Appendix for test description.)

Mercury (II) Thiocyanate Test Procedure:

SOURCE: *Recent Chemical Soil Test Procedures for the North Central Region*; Missouri Agricultural Experiment Station; SB 1001; Revised: January, 1998. The following description is taken directly from this text. Authors: Gelderman, R.H., Denning, J.L., and Goos, R.J.

The Mercury (II) Thiocyanate Method is a modification of the procedure of Adriano and Doner (10) for Cl^- determination and uses an extraction procedure similar to that suggested by Bolton (9). In this colorimetric method, Cl^- displaces thiocyanate which, in the presence of ferric iron, forms a highly colored ferric thiocyanate complex:

$$2\ Cl^- + Hg(SCN)_2 + 2\ Fe^{3+} \rightarrow HgCl_2 + 2\ Fe\ (SCN)^{2+}$$

The resulting solution's color is stable and proportional to the original chloride ion concentration.

The procedure is very sensitive and has a detection limit of approximately 1μg Cl^-g^{-1} soil. Nitrate, sulfide, cyanide, thiocyanate, bromide, and iodide can cause interferences, but are usually not present in sufficient amounts to be a problem. Similar procedures have been modified for use with auto-analyzers.

Equipment

1. Standard NCR-13, 10g scoop
2. Spectrophotometer
3. Shaker
4. 50 mL Erlenmeyer flasks, filter funnels, or tubes

Reagents

1. Extracting solution (0.01M $Ca(NO_3)_2 \bullet 4\ H_2O$). Weigh 4.72 g into a 2 L volumetric flask. Bring to volume with distilled water.

2. Saturated Mercury (II) Thiocyanate [$Hg(SCN)_2$] Solution, 0.075 percent: Add approximately 0.75 g $Hg(SCN)_2$ to 1 L of distilled water and stir overnight. Filter through Whatman No. 42 paper. It is important that this solution be saturated because it may then be stored for long periods of time.

3. Ferric Nitrate Solution: Dissolve 20.2 g Fe $(NO_3)_3 \bullet 9\ H_2O$ (Ferric (III) nitrate nonahydrate) in approximately 500 mL of distilled water and add concentrated nitric acid (HNO_3) until the solution is almost colorless (20 to 30 mL). Make up to 1 L with distilled water. Excess HNO_3 is unimportant as long as there is enough to prevent darkening of stored solution.

4. Charcoal washed in 0.01M Ca $(NO_3)_2$ and dried.

5. Chloride Standard Stock Solution (1,000 ppm Cl^-): Dissolve 0.2103 g reagent-grade KCl in approximately 50 mL of extracting solution. Bring up to 100 mL.

6. Chloride Standard Intermediate Solution (100 ppm): Dilute 10 mL of stock solution to 100 mL with extracting solution.

7. Chloride Standard Working Solutions: Dilute 0.5, 1.0, 2.0, 3.0, 4.0, 5.0, and 10.0 mL of 100 ppm standard solution to 100 mL of 100 ppm standard solution to 100 mL with extracting solution. This is equivalent to 0.5, 1.0, 2.0, 4.0, 5.0, and 10.0 ppm Cl^-.

Procedure

1. Scoop 10 g of crushed soil into a 50 mL Erlenmeyer flask. Do duplicate or triplicate analyses. Include a blank.

2. Add approximately 25 mg washed charcoal (dried).

3. Add 25 mL extracting solution.

4. Shake for 15 minutes at 180 or more excursions per minute (epm) and filter immediately following shaking using Whatman No. 42 filter paper or equivalent.

5. Transfer a 10 mL aliquot to a 50 mL beaker.

6. Add 4 mL each of the thiocyanate and the ferric nitrate solutions. Swirl to mix.

7. Allow 10 minutes for color development and read at 460 nm. Set 100 percent transmittancy with extracting solution.

8. Prepare a standard curve by pipetting a 10 mL aliquot of each of the working standards and proceeding as with the soil extracts. Plot transmittance or absorbance against concentration of the working standards.

9. Determine chloride concentration in the extract from the meter reading and standard curve. Subtract the chloride in the blank and convert to ppm in soil by multiplying by a dilution factor of 2.5.

APPENDIX B. SUPPLEMENTARY FIGURES

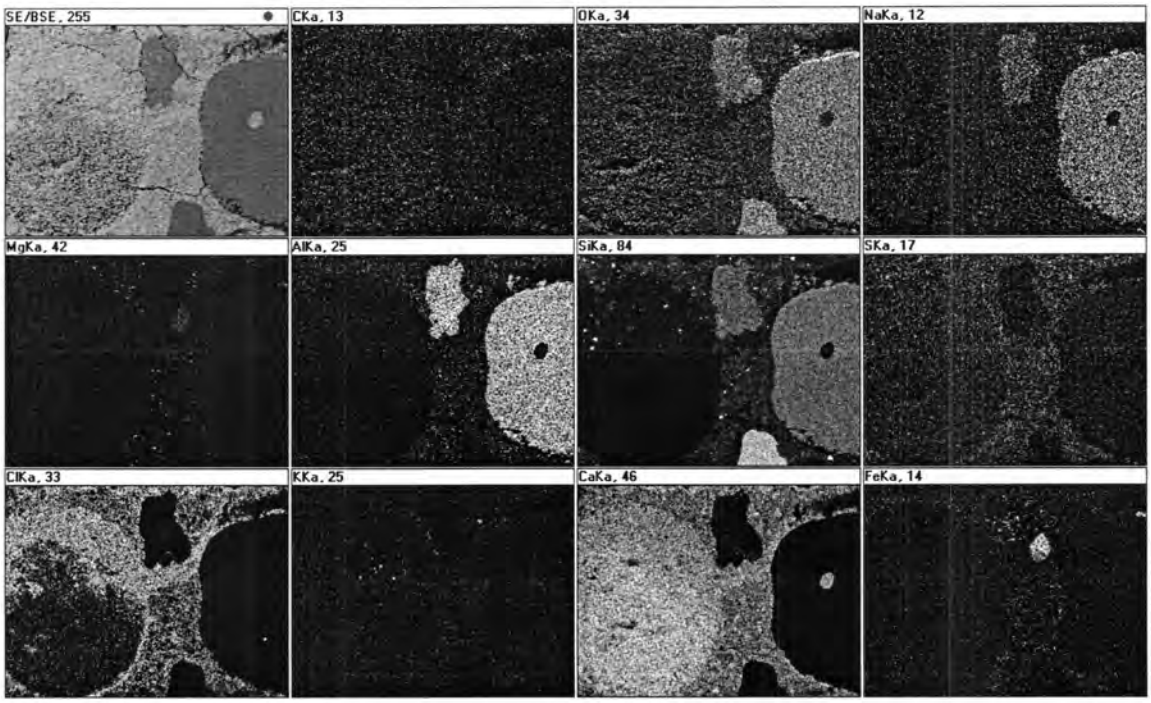

Figure 35. SEM elemental map of $CaCl_2$ treated sample at 100x magnification.

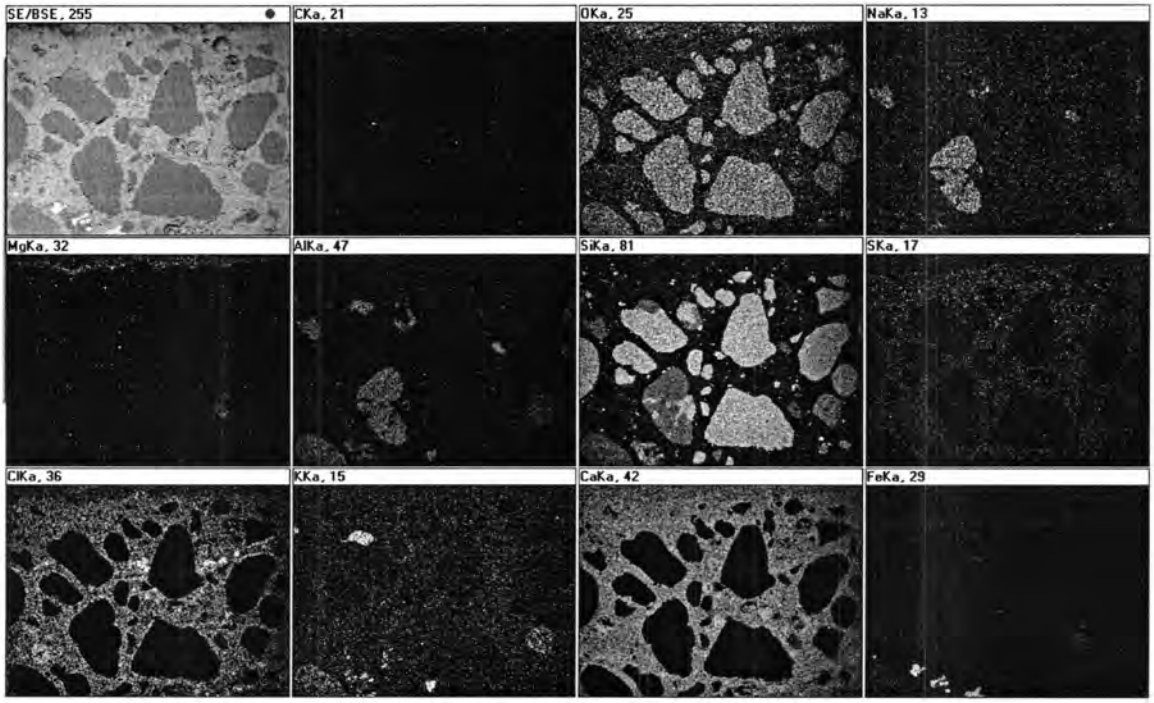

Figure 38. SEM elemental map of $CaCl_2$ with CI treated sample at 25x magnification

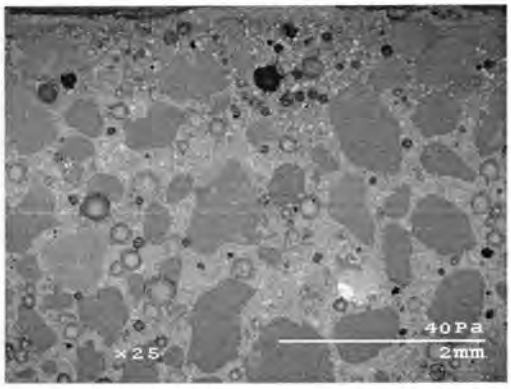

Figure 42a. Geomelt sample at 25x magnification

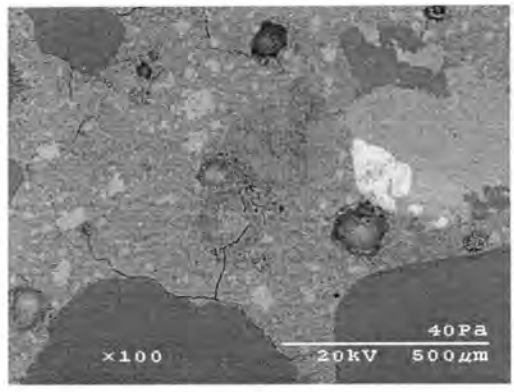

Figure 42b. Geomelt sample at 100x magnification

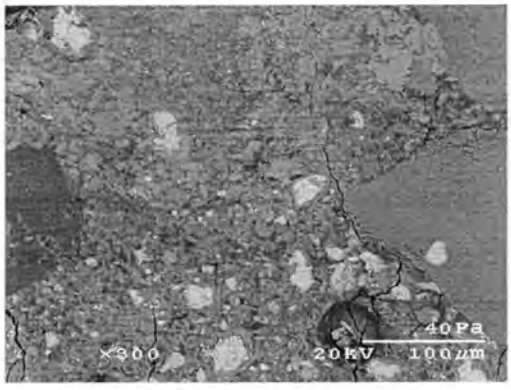

Figure 42c Geomelt sample lat at 300x magnification

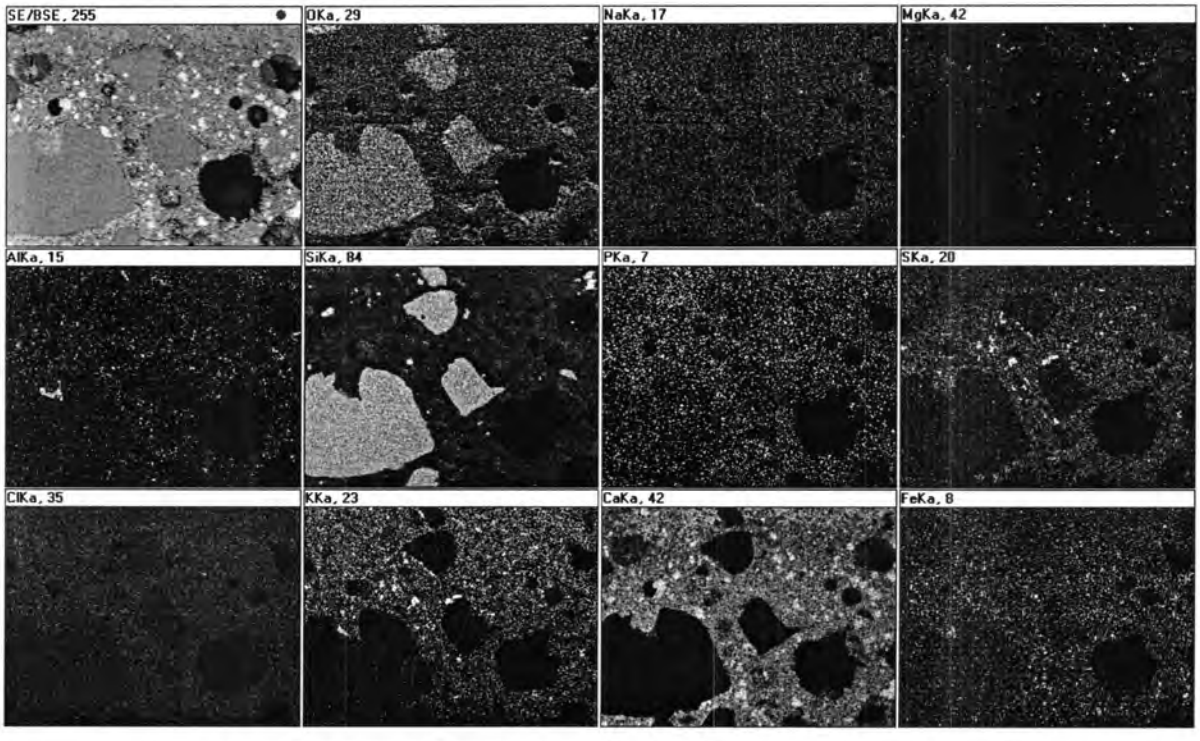

Figure 43. SEM elemental map of Geomelt treated sample at 100x magnification

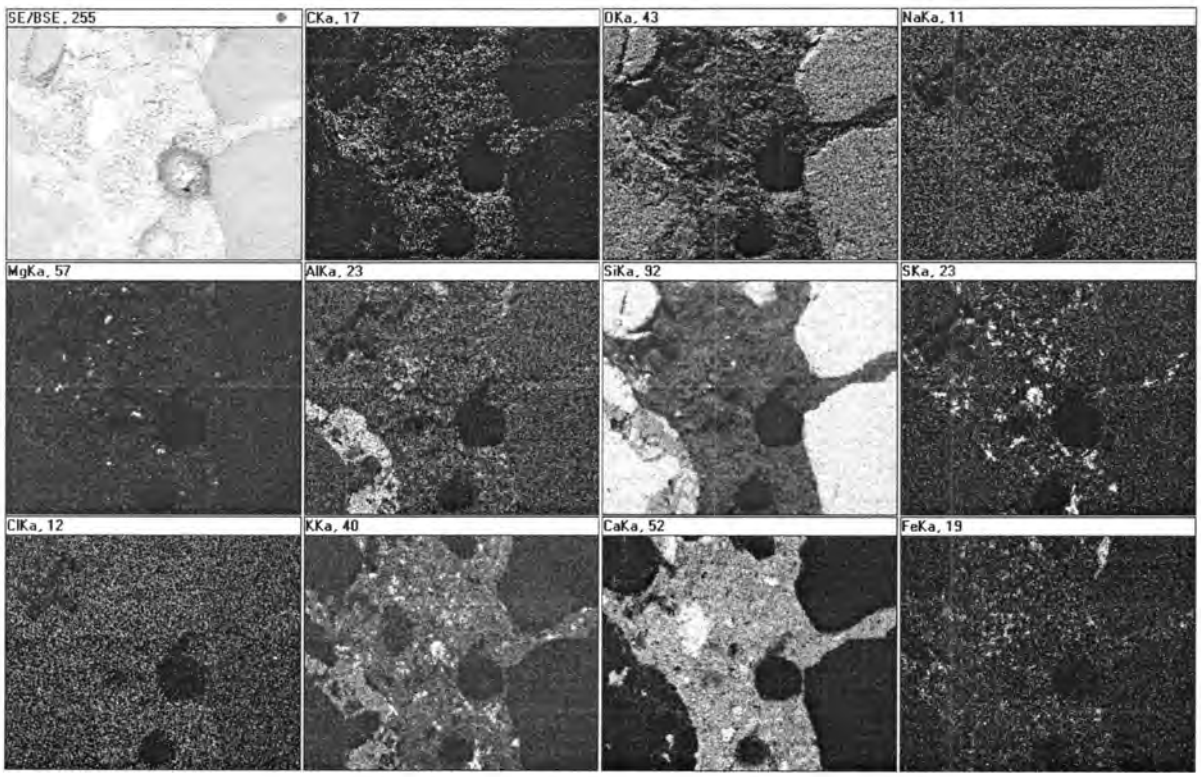

Figure 10. SEM elemental map of NaCl at 25x

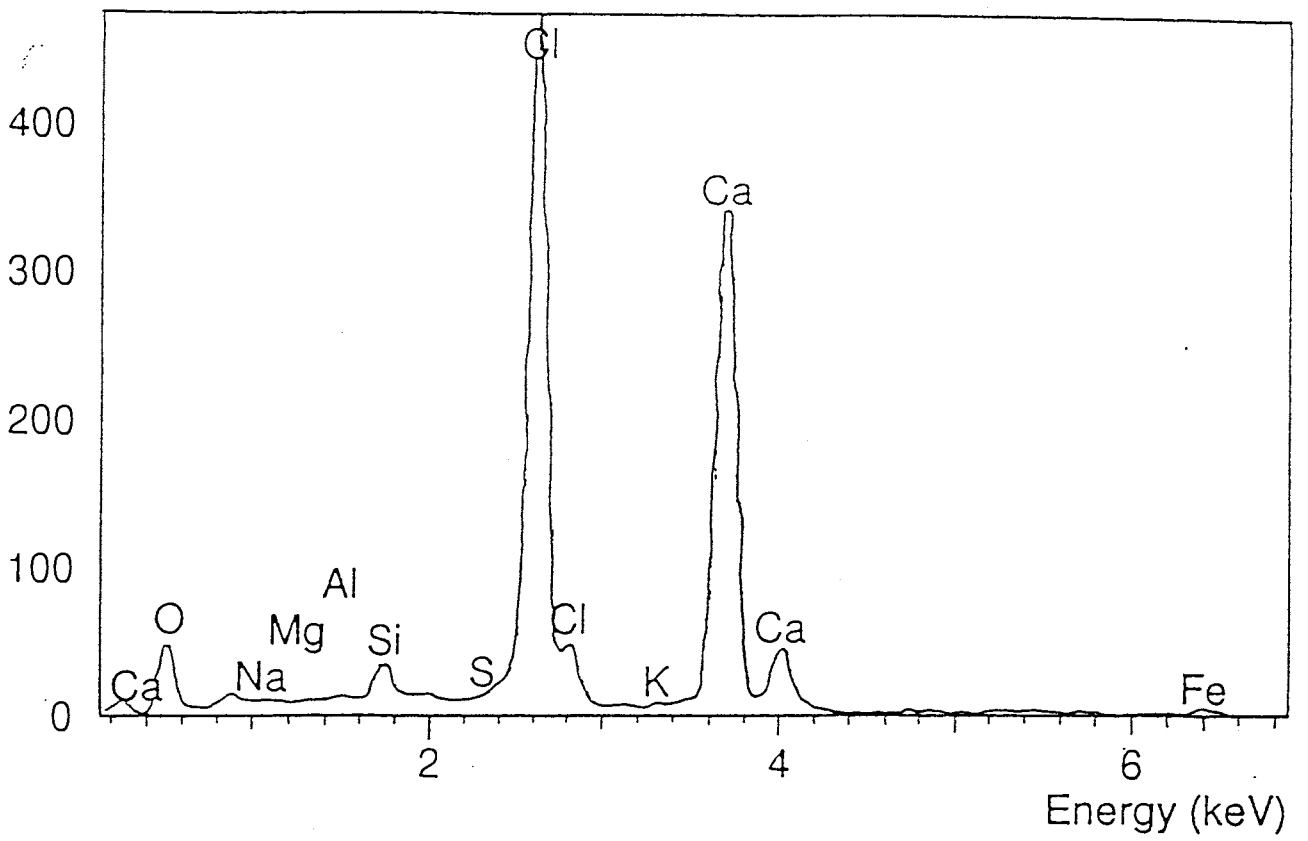

Figure 29. Ion concentration plot of the $CaCl_2$-exposed sample at 100x magnification.

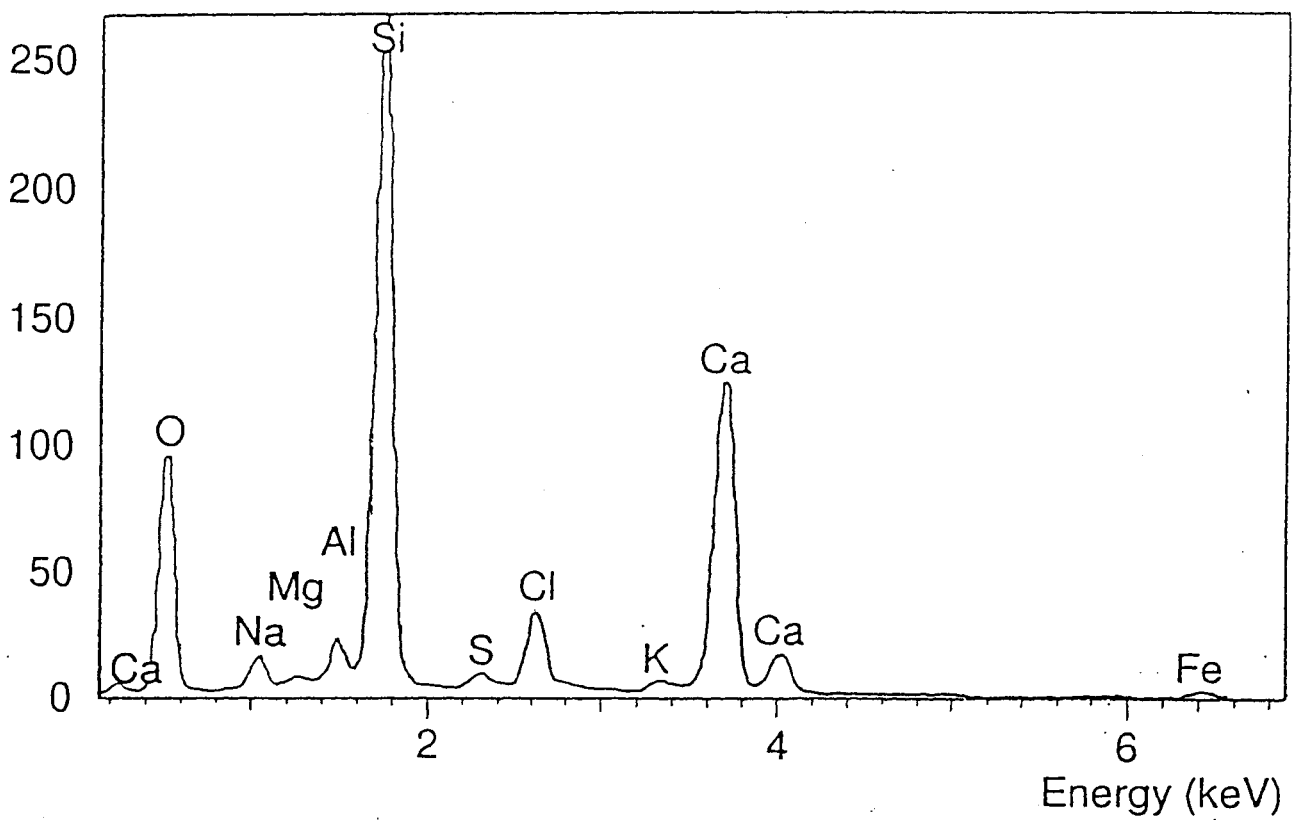

Figure 31. Ion concentration plot of the NaCl-exposed sample at 25x magnification.

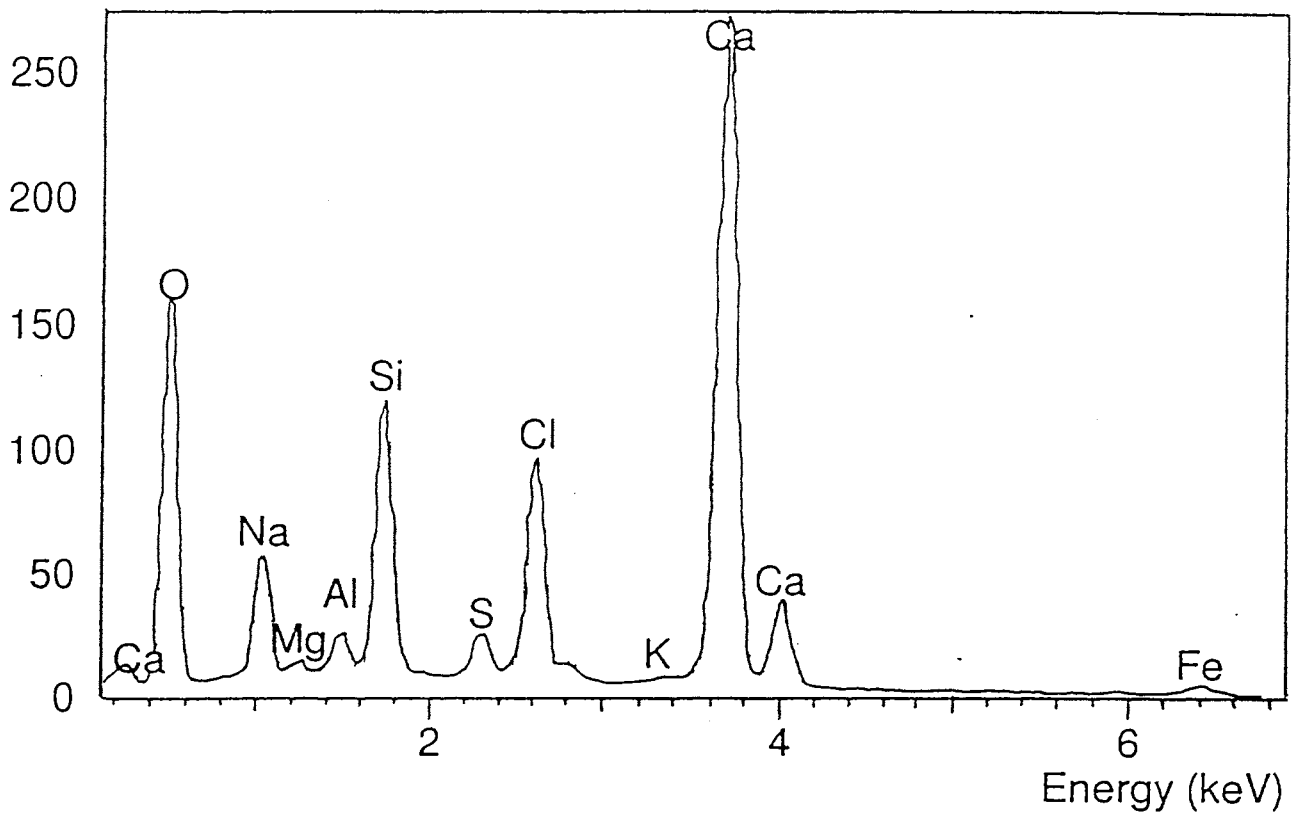

Figure 32. Ion concentration plot of the NaCl-exposed sample at 100x magnification.

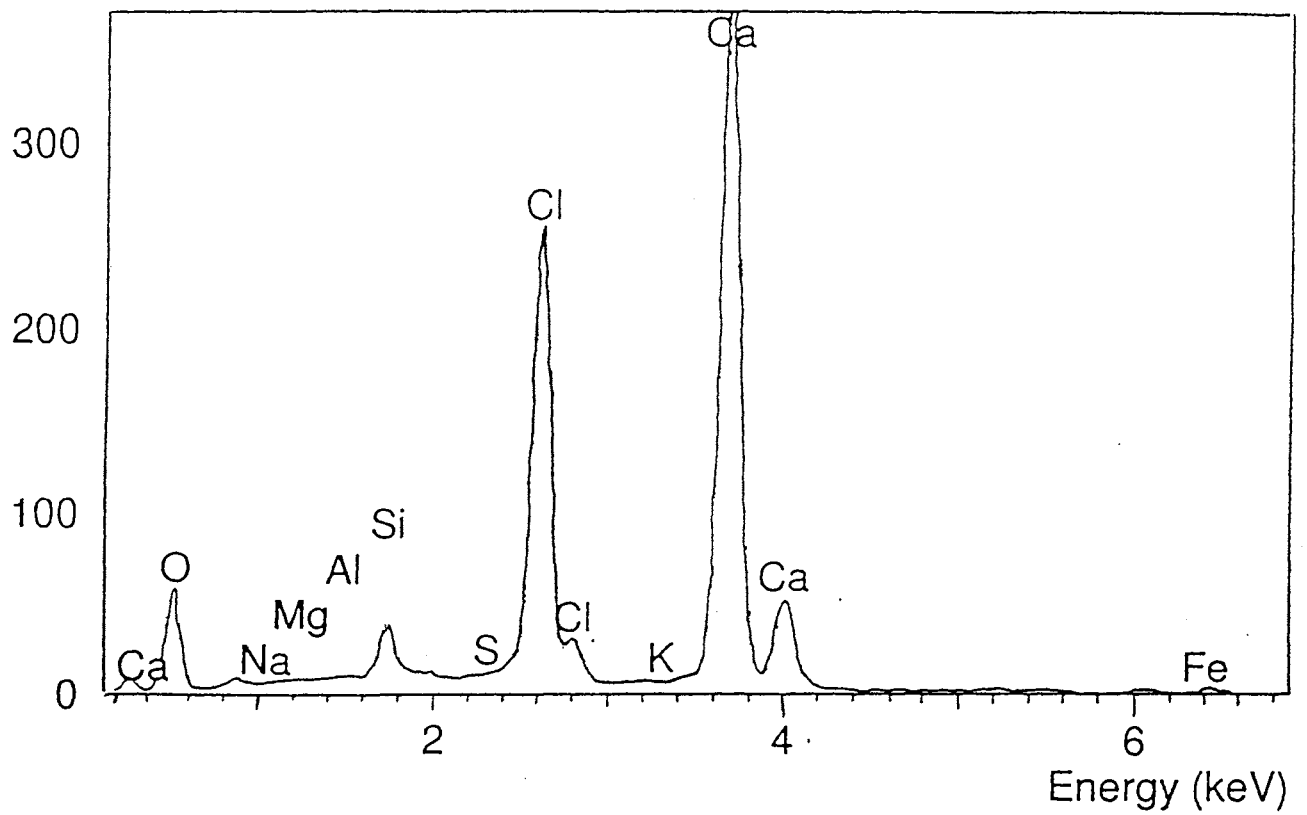

Figure 39. Ion concentration plot of the $CaCl_2$ with CI-exposed sample at 100x magnification.

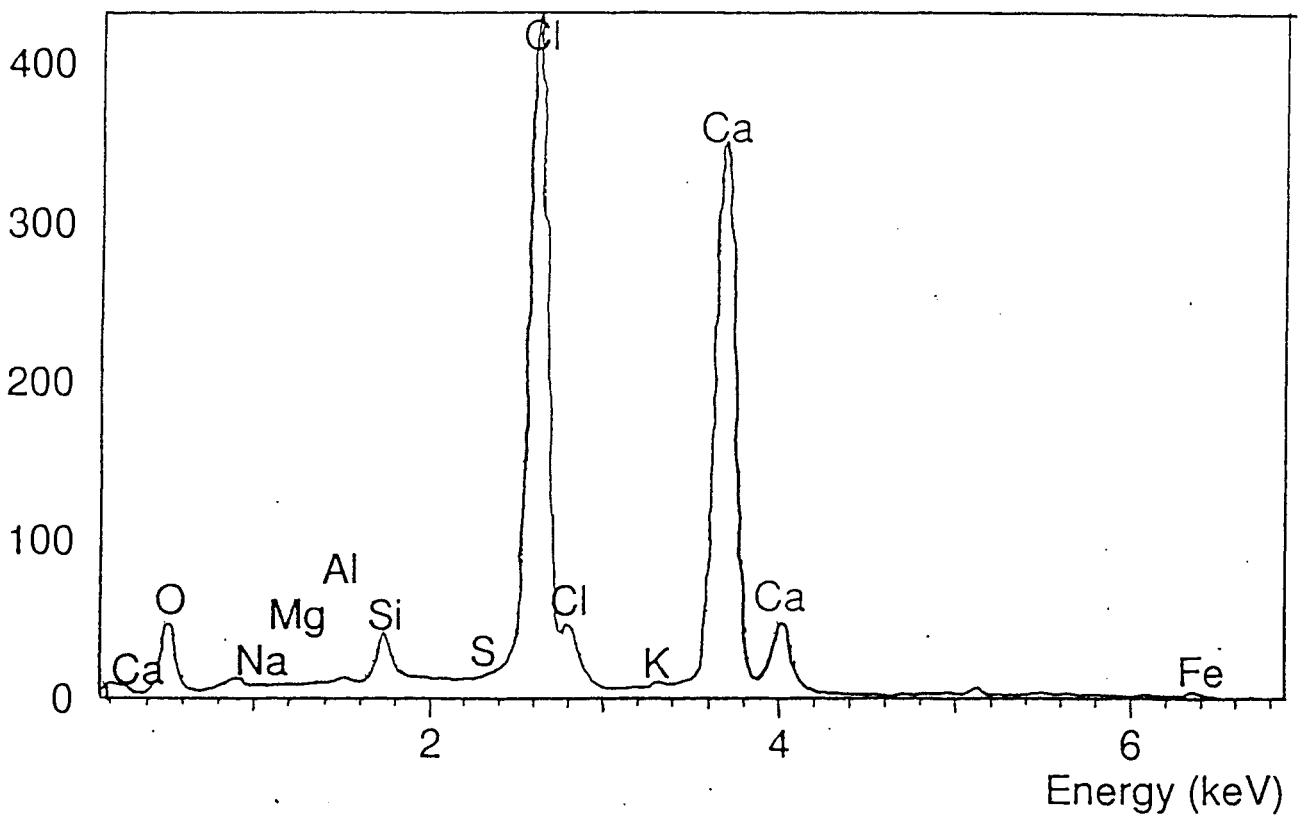

Figure 40. Ion concentration plot of the $CaCl_2$ with CI-exposed sample at 300x magnification.

APPENDIX C. PHYSICAL DETERIORATION DATA

Table C-a-1. Paste Sample Weights of Wet/Dry Distilled Water Samples

(Note: all weights in grams. Negative weight change = weight gain.)

Cycle #	0	10	%Change	20	%Change	30	%Change	40	%Change	50	%Change	60	%Change	130	%Change
2-1	263.74	264.94	-0.45	265.21	-0.56	264.93	-0.45	265.57	-0.69						
2-2	263.22	264.45	-0.47	264.90	-0.64										
2-3	263.44	264.59	-0.44	264.71	-0.48	264.55	-0.42	264.85	-0.54						
2-4	264.35	265.45	-0.42	265.87	-0.57	265.51	-0.44	266.09	-0.66						
2-5	264.41	265.74	-0.50	265.65	-0.47	265.73	-0.50	266.12	-0.65						
2-6	264.47	265.81	-0.51	266.05	-0.60										
2-7	262.19	263.30	-0.42	263.33	-0.43										
2-8	264.58	265.77	-0.45	265.98	-0.53										
2-9	264.00	264.86	-0.33	265.01	-0.38	264.98	-0.37	265.41	-0.53	265.27	-0.48	265.41	-0.53		
2-10	261.00	261.35	-0.13	261.86	-0.33	261.72	-0.28	261.94	-0.36	262.36	-0.52	262.24	-0.48		
2-11	260.80	261.75	-0.36	261.74	-0.36	261.56	-0.29	261.94	-0.44	262.08	-0.49	262.25	-0.56		
2-12	264.32	265.04	-0.27	265.62	-0.49	265.22	-0.34	265.77	-0.55	265.87	-0.59	265.91	-0.60		
2-13	262.95	263.55	-0.23	263.93	-0.37	264.08	-0.43	264.51	-0.59	264.46	-0.57	264.40	-0.55	264.52	-0.60
2-14	264.23	265.10	-0.33	265.23	-0.38	265.62	-0.53	266.13	-0.72	265.94	-0.65	265.98	-0.66	266.05	-0.69
2-15	264.08	264.97	-0.34	265.23	-0.44	265.25	-0.44	265.89	-0.69	265.61	-0.58	265.76	-0.64	265.96	-0.71
	0		**-0.38**		**-0.47**		**-0.41**		**-0.58**		**-0.55**		**-0.57**		**-0.67**

Paste Sample Weights of Wet/Dry CaCl2 w/o Samples

(Note: all weights in grams. Negative weight change = weight gain.)

Cycle #	0	10	%Change	20	%Change	31	%Change	40	%Change	50	%Change	60	%Change	130	%Change
4-1	264.27	259.25	1.94	258.28	2.27										
4-2	262.75	258.52	1.61	257.79	1.89										
4-3	263.13	258.52	1.78	257.71	2.06										
4-4	263.43	259.10	1.64	258.37	1.92										
4-5	263.81	258.60	2.01	257.89	2.24	257.40	2.43	257.31	2.46						
4-6	263.92	259.24	1.77	258.36	2.11	257.54	2.42	257.47	2.44						
4-7	262.47	257.41	1.97	256.19	2.39	255.33	2.72	255.34	2.72						
4-8	264.42	259.32	1.93	258.40	2.28	257.66	2.56	257.00	2.81						
4-9	263.47	258.94	1.75	258.12	2.03	257.61	2.22	256.97	2.47	256.20	2.76	256.87	2.51		
4-10	264.73	260.12	1.74	259.53	1.96	259.24	2.07	259.18	2.10	258.84	2.22	259.35	2.03		
4-11	262.36	257.55	1.87	256.42	2.26	255.83	2.49	255.33	2.68	254.99	2.81	255.22	2.72		
4-12	267.37	262.18	1.94	261.46	2.21	260.76	2.47	260.26	2.66	259.87	2.81	259.91	2.79		
4-13	263.91	258.82	1.97	258.56	2.03	258.33	2.11	258.40	2.09	258.48	2.06	258.47	2.06	261.10	1.06
4-14	266.62	261.83	1.80	261.17	2.04	260.42	2.33	260.38	2.34	259.41	2.70	259.79	2.56	259.92	2.51
4-15	263.09	258.64	1.72	257.79	2.01	257.19	2.24	256.57	2.48	256.44	2.53	256.85	2.37	258.19	1.86
	0		**1.83**		**2.11**		**2.37**		**2.48**		**2.56**		**2.43**		**1.81**

Paste Sample Weights of Wet/Dry NaCl Samples

(Note: all weights in grams. Negative weight change = weight gain.)

Cycle #	0	10	%Change	20	%Change	30	%Change	41	%Change	50	%Change	60	%Change	130	%Change
6-1	261.46	262.56	-0.42	262.64	-0.45										
6-2	263.59	264.83	-0.47	264.98	-0.53										
6-3	260.40	261.97	-0.60	262.20	-0.69										
6-4	262.52	263.73	-0.46	263.89	-0.52										
6-5	260.12	261.65	-0.59	261.82	-0.65	262.07	-0.75	262.24	-0.82						
6-6	260.15	261.76	-0.62	261.95	-0.69	262.26	-0.81	262.46	-0.89						
6-7	261.68	262.78	-0.42	262.90	-0.47	263.18	-0.57	263.25	-0.60						
6-8	260.99	262.31	-0.51	262.54	-0.59	262.80	-0.69	262.96	-0.75						
6-9	261.37	262.81	-0.55	263.05	-0.64	263.33	-0.75	263.41	-0.78	263.57	-0.84	263.64	-0.87		
6-10	263.18	264.68	-0.57	264.89	-0.65	265.14	-0.74	265.26	-0.79	265.43	-0.85	265.51	-0.89		
6-11	260.87	262.03	-0.44	262.26	-0.53	262.51	-0.63	262.64	-0.68	262.85	-0.76	262.92	-0.79		
6-12	258.89	260.26	-0.53	260.57	-0.65	260.74	-0.71	260.88	-0.77	261.07	-0.84	261.08	-0.85		
6-13	261.71	263.02	-0.50	263.34	-0.62	263.55	-0.70	263.71	-0.76	263.90	-0.84	263.95	-0.86	264.88	-1.21
6-14	260.77	262.07	-0.50	262.18	-0.54	262.39	-0.62	262.59	-0.70	262.59	-0.70	262.74	-0.76	263.52	-1.05
6-15	261.62	263.15	-0.58	263.40	-0.68	263.62	-0.76	263.75	-0.81	263.95	-0.89	264.01	-0.91	264.84	-1.23
	0		**-0.52**		**-0.59**		**-0.70**		**-0.76**		**-0.82**		**-0.84**		**-1.17**

Paste Sample Weights of Wet/Dry CaCl2 w/ Samples

(Note: all weights in grams. Negative weight change = weight gain.)

Cycle #	0	11	%Change	20	%Change	30	%Change	40	%Change	50	%Change	61	%Change	130	%Change
8b-1	263.79	259.27	1.71	258.74	1.91	259.57	1.60	260.83	1.12						
8b-2	264.36	260.35	1.52	259.61	1.80	260.12	1.60	261.05	1.25						
8b-3	266.66	261.25	2.03	260.24	2.41	260.22	2.42	261.18	2.06						
8b-4	263.66	258.35	2.01	257.41	2.37	257.74	2.25	258.30	2.03						
8b-5	262.62	257.72	1.87	257.38	2.00	257.70	1.87	258.37	1.62	258.46	1.58	258.39	1.61		
8b-6	263.16	257.70	2.07	256.98	2.35	256.72	2.45	257.25	2.25	257.24	2.25	257.29	2.23		
8b-7	263.86	259.24	1.75	258.46	2.05	259.05	1.82	259.67	1.59	260.21	1.38	260.13	1.41		
8b-8	264.39	259.75	1.75	258.94	2.06	259.32	1.92	260.08	1.63	259.99	1.66	259.92	1.69		
8b-9	263.34	259.08	1.62	257.82	2.10	258.55	1.82	259.91	1.30	260.35	1.14	260.12	1.22	264.42	-0.41
8b-10	264.33	260.39	1.49	259.19	1.94										
8b-11	263.98	258.33	2.14	257.95	2.28	258.26	2.17	259.18	1.82	259.42	1.73	259.63	1.65	263.72	0.10
8b-12	264.42	259.61	1.82	259.20	1.97										
8b-13	263.40	256.68	2.55	258.09	2.02										
8b-14	262.61	258.02	1.75	257.36	2.00										
8b-15	266.37	260.88	2.06	260.17	2.33	259.98	2.40	260.49	2.21	260.38	2.25	260.30	2.28	263.17	1.20
	0		**1.88**		**2.11**		**2.03**		**1.72**		**1.71**		**1.73**		**0.30**

Paste Sample Weights of Wet/Dry Potassium Acetate Samples

(Note: all weights in grams. Negative weight change = weight gain.)

Cycle #	0	10	%Change	20	%Change	30	%Change	40	%Change	50	%Change	60	%Change	130	%Change
10-1	262.76	263.39	-0.24	263.11	-0.13										
10-2	260.75	259.33	0.54	258.50	0.86										
10-3	263.40	263.70	-0.11	263.26	0.05										
10-4	265.27	264.72	0.21	264.37	0.34										
10-5	262.01	262.27	-0.10	262.07	-0.02	261.54	0.18	261.38	0.24	259.77	0.85				
10-6	262.72	261.98	0.28	261.50	0.46	260.71	0.77	260.50	0.85						
10-7	270.64	271.24	-0.22	271.37	-0.27	271.08	-0.16	271.22	-0.21						
10-8	269.55	270.57	-0.38	270.63	-0.40	270.36	-0.30	270.37	-0.30						
10-9	262.14	261.60	0.21	261.08	0.40	260.42	0.66	260.33	0.69	259.95	0.84	259.90	0.85		
10-10	263.26	262.37	0.34	261.61	0.63	260.73	0.96	260.46	1.06	260.06	1.22	259.91	1.27		
10-11	269.83	270.32	-0.18	270.31	-0.18	269.95	-0.04	269.90	-0.03	269.61	0.08	269.60	0.09		
10-12	261.29	260.03	0.48	259.38	0.73	258.43	1.09	258.05	1.24	257.41	1.48	257.12	1.60		
10-13	262.24	260.80	0.55	259.91	0.89	259.02	1.23	258.84	1.30	258.37	1.48	258.22	1.53	258.74	1.33
10-14	262.30	260.03	0.87	259.16	1.20	258.21	1.56	257.88	1.69	257.36	1.88	257.13	1.97	257.45	1.85
10-15	263.00	262.43	0.22	261.83	0.44	260.85	0.82	260.46	0.97			259.49	1.33	260.79	0.84
	0		**0.16**		**0.33**		**0.61**		**0.68**		**1.12**		**1.24**		**1.34**

Paste Sample Weights of Wet/Dry Geomelt Samples

(Note: all weights in grams. Negative weight change = weight gain.)

Cycle #	0	10	%Change	20	%Change	30	%Change	40	%Change	49	%Change	60	%Change	130	%Change
12-1	268.03	262.16	2.19	261.09	2.59										
12-2	267.51	261.71	2.17	260.71	2.54										
12-3	266.24	260.70	2.08	259.78	2.43										
12-4	265.25	259.15	2.30	258.13	2.68										
12-5	265.23	259.21	2.27	258.28	2.62	257.26	3.00	257.01	3.10	257.05	3.08	256.83	3.17	256.35	3.35
12-6	267.13	261.63	2.06	260.68	2.41	259.53	2.85	259.31	2.93	259.01	3.04	258.83	3.11		
12-7	265.48	259.48	2.26	258.47	2.64	257.33	3.07	257.12	3.15	256.76	3.28	256.51	3.38	256.17	3.51
12-8	265.04	259.25	2.18	258.13	2.61	257.05	3.01	256.73	3.14						
12-9	265.48	259.71	2.17	258.68	2.56	257.48	3.01	257.34	3.07	257.18	3.13	257.01	3.19		
12-10	265.35	259.60	2.17	258.57	2.56	257.54	2.94	257.30	3.03	257.10	3.11	256.96	3.16	256.57	3.31
12-11	268.69	262.86	2.17	261.72	2.59	260.60	3.01	260.29	3.13						
12-12	265.80	259.83	2.25	258.91	2.59	257.94	2.96	257.69	3.05	257.53	3.11	257.29	3.20		
12-13	266.09	260.11	2.25	259.21	2.59	258.27	2.94	257.99	3.04						
12-14	264.96	259.28	2.14	258.16	2.57	257.08	2.97	256.77	3.09						
12-15	266.70	260.93	2.16	259.93	2.54	258.93	2.91	258.70	3.00	258.50	3.07	258.29	3.15		
	0		**2.19**		**2.57**		**2.97**		**3.07**		**3.12**		**3.19**		**3.39**

Table C-a-2. **Paste wet-dry compressive strength data.**

Dist. H2O	20	40	60	130
2-1				
2-2	62.0			
2-3		70.9		
2-4		67.0		
2-5		75.2		
2-6	58.9			
2-7	64.7			
2-8				
2-9				
2-10			69.0	
2-11			68.2	
2-12			73.2	
2-13				92.6
2-14				73.6
2-15				81.8
Average:	61.9	71.0	71.6	82.7

CaCl2 w/o	20	40	60	130
4-1				
4-2	57.0			
4-3	68.2			
4-4	59.7			
4-5				
4-6		70.9		
4-7		66.6		
4-8		64.7		
4-9				
4-10			60.4	
4-11			61.2	
4-12			62.0	
4-13				58.5
4-14				55.8
4-15				51.5
Average:	61.6	67.4	61.2	55.3

NaCl	20	40	60	130
6-1				
6-2	65.9			
6-3	62.4			
6-4	69.0			
6-5				
6-6		63.5		
6-7		64.7		
6-8		69.4		
6-9				
6-10			64.7	
6-11			66.3	
6-12			62.8	
6-13				69.0
6-14				55.8
6-15				59.7
Average:	65.8	65.9	64.6	61.5

CaCl2 w/	20	41	60	130
8-1				
8-2		60.4		
8-3		65.9		
8-4		61.6		
8-5				
8-6			55.4	
8-7			56.2	
8-8			56.6	
8-9				49.2
8-10				
8-11				48.8
8-12	57.3			
8-13	56.6			
8-14	64.7			
8-15				54.6
Average:	59.5	62.6	56.1	50.9

K.Ace.	20	40	60	130
10-1				
10-2	62.4			
10-3	61.2			
10-4	63.2			
10-5				
10-6		65.1		
10-7		59.7		
10-8		66.3		
10-9				
10-10			65.1	
10-11			66.6	
10-12			69.7	
10-13				63.9
10-14				62.0
10-15				59.7
Average:	62.3	63.7	67.1	61.9

Geomelt	20	40	60	130
12-1				
12-2	69.0			
12-3	67.8			
12-4	65.5			
12-5				68.2
12-6				
12-7				65.9
12-8		62.4		
12-9			68.2	
12-10				77.5
12-11		70.5		
12-12			65.5	
12-13				
12-14		67.8		
12-15			64.3	
Average:	67.4	66.9	66.0	70.5

Table C-a-3. Paste wet-dry scaling data.

Dist. H2O:	24	40	60	130
2-1		0		
2-2	0			
2-3		0		
2-4		0		
2-5		0		
2-6	0			
2-7	0			
2-8	0			
2-9			0	
2-10			0	
2-11			0	
2-12			0	
2-13				0
2-14				0
2-15				0
Average:	0.0	0.0	0.0	0.0

CaCl2 w/o:	20	40	60	130
4-1	1			
4-2	1			
4-3	1			
4-4	1			
4-5		1		
4-6		1		
4-7		1		
4-8		1		
4-9			2	
4-10			2	
4-11			2	
4-12			2	
4-13				3
4-14				3
4-15				4
Average:	1.0	1.0	2.0	3.3

NaCl:	20	41	60	130
6-1	0			
6-2	0			
6-3	0			
6-4	0			
6-5		0		
6-6		0		
6-7		0		
6-8		0		
6-9			0	
6-10			0	
6-11			0	
6-12			0	
6-13				0
6-14				0
6-15				0
Average:	0.0	0.0	0.0	0.0

CaCl2 w/:	20	41	62	130
8-1		2		
8-2		2		
8-3		1		
8-4		2		
8-5			2	
8-6			2	
8-7			2	
8-8			2	
8-9				3
8-10	1			
8-11				2
8-12	2			
8-13	1			
8-14	1			
8-15				2
Average:	1.3	1.8	2.0	2.3

K. Ace:	20	40	60	130
10-1	0			
10-2	0			
10-3	0			
10-4	0			
10-5		0		
10-6		0		
10-7		0		
10-8		0		
10-9			1	
10-10			1	
10-11			1	
10-12			1	
10-13				1
10-14				1
10-15				1
Average:	0.0	0.0	1	1

Geomelt:	20	41	62	130
12-1	1			
12-2	1			
12-3	1			
12-4	1			
12-5				1
12-6			1	
12-7				1
12-8		1		
12-9			1	
12-10				1
12-11		1		
12-12			1	
12-13		1		
12-14		1		
12-15			1	
Average:	1.0	1.0	1.0	1.0

Table C-b-1. Paste Sample Weights of Freeze/Thaw Distilled Water Samples

(Note: all weights in grams. Negative weight change = weight gain.)

Cycle #	0	5	%Change	10	%Change	20	%Change	25	%Change	30	%Change	36	%Change	40	%Change
1-1	259.80	259.82	-0.01	260.27	-0.18	260.62	-0.32								
1-2	257.94	258.13	-0.07	258.78	-0.33	259.30	-0.53								
1-3	257.97	257.90	0.03	258.48	-0.20	258.72	-0.29								
1-4	258.65	258.60	0.02	259.30	-0.25	259.42	-0.30								
1-5	257.85	257.59	0.10	258.30	-0.17	258.74	-0.35	258.77	-0.36	259.30	-0.56	259.07	-0.47	259.38	-0.59
1-6	258.74	258.72	0.01	259.60	-0.33	259.98	-0.48	260.06	-0.51	260.47	-0.67	260.35	-0.62	260.41	-0.65
1-7	258.71	258.56	0.06	258.99	-0.11	259.30	-0.23	259.60	-0.34	260.08	-0.53	260.00	-0.50	260.20	-0.58
1-8	258.24	258.25	0.00	259.05	-0.31	259.45	-0.47	259.68	-0.56	260.05	-0.70	259.96	-0.67	260.16	-0.74
1-9	257.66	257.55	0.04	258.36	-0.27	258.55	-0.35	258.63	-0.38	258.87	-0.47	258.85	-0.46	258.98	-0.51
1-10	257.46	257.44	0.01	258.19	-0.28	258.41	-0.37	258.51	-0.41	258.90	-0.56	258.73	-0.49	258.82	-0.53
1-11	257.84	257.96	-0.05	258.68	-0.33	259.01	-0.45	259.15	-0.51	259.40	-0.61	259.30	-0.57	259.50	-0.64
1-12	258.43	258.41	0.01	258.90	-0.18	259.31	-0.34	259.49	-0.41	260.03	-0.62	260.10	-0.65	260.23	-0.70
1-13	258.32	257.95	0.14	258.59	-0.10	259.07	-0.29	259.24	-0.36	259.55	-0.48	259.49	-0.45	259.87	-0.60
1-14	258.01	258.13	-0.05	258.94	-0.36	259.15	-0.44	259.31	-0.50	259.52	-0.59	259.46	-0.56	259.68	-0.65
1-15	257.69	257.74	-0.02	258.32	-0.24	258.70	-0.39	258.76	-0.42	258.93	-0.48	259.05	-0.53	259.27	-0.61
	0		**0.01**		**-0.24**		**-0.37**		**-0.43**		**-0.57**		**-0.54**		**-0.62**

Cycle #	45	%Change	50	%Change	55	%Change	60	%Change
1-1								
1-2								
1-3								
1-4								
1-5								
1-6								
1-7								
1-8								
1-9	258.63	-0.38	258.71	-0.41	258.51	-0.33	258.92	-0.49
1-10	258.52	-0.41	258.43	-0.38	258.46	-0.39	258.74	-0.50
1-11	259.10	-0.49	259.06	-0.47	258.82	-0.38	258.94	-0.43
1-12	259.72	-0.50	259.67	-0.48	259.68	-0.48	260.03	-0.62
1-13	259.49	-0.45	259.29	-0.38	258.90	-0.22	259.11	-0.31
1-14	259.39	-0.53	259.17	-0.45	259.01	-0.39	259.33	-0.51
1-15	259.01	-0.51	258.98	-0.50	258.89	-0.47	259.19	-0.58
		-0.47		**-0.44**		**-0.38**		**-0.49**

Paste Sample Weights of Freeze/Thaw CaCl2 w/o Samples

(Note: all weights in grams. Negative weight change = weight gain.)

Cycle #	1	6	%Change	10	%Change	15	%Change	20	%Change	25	%Change	31	%Change	35	%Change
3-1	258.59	257.72	0.34	258.44	0.06	260.06	-0.57	262.38	-1.47						
3-2	256.65	255.50	0.45	255.68	0.38	256.74	-0.04	258.60	-0.76						
3-3	257.05	256.23	0.32	256.21	0.33	257.67	-0.24	260.17	-1.21						
3-4	255.57	254.48	0.43	255.35	0.09	256.89	-0.52	258.94	-1.32						
3-5	257.96	257.46	0.19	258.38	-0.16	260.16	-0.85	262.81	-1.88	264.13	-2.39	267.08	-3.54	239.21	7.27
3-6	257.68	257.43	0.10	256.51	0.45	257.29	0.15	259.24	-0.61	260.22	-0.99	252.76	1.91	243.79	5.39
3-7	257.55	256.75	0.31	257.08	0.18	258.03	-0.19	259.79	-0.87	261.15	-1.40	261.85	-1.67	254.24	1.29
3-8	258.83	257.56	0.49	257.61	0.47	258.27	0.22	259.65	-0.32	260.94	-0.82	261.91	-1.19	247.14	4.52
3-9	257.50	257.06	0.17	256.97	0.21	258.42	-0.36	260.78	-1.27	262.10	-1.79	265.19	-2.99	241.70	6.14
3-10	257.96	256.85	0.43	257.20	0.29	258.44	-0.19	260.46	-0.97	261.83	-1.50	265.00	-2.73	242.57	5.97
3-11	259.29	258.63	0.25	258.82	0.18	259.93	-0.25	262.06	-1.07	263.39	-1.58	265.51	-2.40	244.64	5.65
3-12	257.42	256.68	0.29	256.49	0.36	257.50	-0.03	259.75	-0.91	261.07	-1.42	262.60	-2.01	241.80	6.07
3-13	258.74	258.09	0.25	258.45	0.11	260.29	-0.60	262.64	-1.51	264.86	-2.37	265.76	-2.71	243.52	5.88
3-14	255.72	254.58	0.45	254.71	0.39	256.06	-0.13	258.40	-1.05	259.92	-1.64	263.92	-3.21	239.90	6.19
3-15	255.61	254.87	0.29	255.56	0.02	256.68	-0.42	257.91	-0.90	258.32	-1.06	258.90	-1.29	243.07	4.91
	0		**0.32**		**0.22**		**-0.27**		**-1.07**		**-1.54**		**-1.98**		**5.39**

Cycle #	40	%Change	46	%Change	50	%Change	55	%Change	60	%Change
3-1										
3-2										
3-3										
3-4										
3-5	239.81	7.04								
3-6	240.83	6.54								
3-7	245.72	4.59								
3-8	246.24	4.86								
3-9	239.78	6.88	239.13	7.13	237.63	7.72	235.79	8.43	235.78	8.43
3-10	241.02	6.57	238.23	7.65	237.44	7.95	237.23	8.04	237.36	7.99
3-11	243.86	5.95	241.90	6.71	242.12	6.62	240.19	7.37	240.33	7.31
3-12	241.64	6.13	240.74	6.48	239.31	7.04	238.77	7.24	238.83	7.22
3-13	242.30	6.35	240.14	7.19	239.29	7.52	238.27	7.91	238.13	7.97
3-14	240.58	5.92	237.83	7.00	237.18	7.25	235.51	7.90	235.89	7.75
3-15	243.25	4.84	241.07	5.69	239.38	6.35	237.86	6.94	238.49	6.70
		5.97		**6.83**		**7.21**		**7.69**		**7.62**

Paste Sample Weights of Freeze/Thaw NaCl Samples

(Note: all weights in grams. Negative weight change = weight gain.)

Cycle #	0	9	%Change	15	%Change	19	%Change	24	%Change	30	%Change	38	%Change	40	%Change
5-1	256.37	257.94	-0.61	258.40	-0.79	258.55	-0.85								
5-2	256.33	257.74	-0.55	258.26	-0.75	258.18	-0.72								
5-3	253.07	254.51	-0.57	254.99	-0.76	255.07	-0.79								
5-4	255.03	256.46	-0.56	256.92	-0.74	256.86	-0.72								
5-5	255.30	256.77	-0.58	257.15	-0.72	256.97	-0.65	257.28	-0.78	257.32	-0.79	257.62	-0.91	257.83	-0.99
5-6	254.51	255.89	-0.54	256.44	-0.76	256.35	-0.72	256.78	-0.89	256.74	-0.88	257.12	-1.03	257.31	-1.10
5-7	255.27	256.57	-0.51	256.97	-0.67	256.79	-0.60	257.10	-0.72	257.22	-0.76	257.55	-0.89	257.71	-0.96
5-8	255.01	256.43	-0.56	256.93	-0.75	256.78	-0.69	257.11	-0.82	257.21	-0.86	257.55	-1.00	257.69	-1.05
5-9	255.76	256.84	-0.42	257.24	-0.58	256.98	-0.48	256.98	-0.48	257.14	-0.54	257.45	-0.66	257.67	-0.75
5-10	256.14	257.59	-0.57	257.95	-0.71	257.65	-0.59	257.95	-0.71	258.10	-0.77	258.45	-0.90	258.59	-0.96
5-11	253.68	255.20	-0.60	255.79	-0.83	255.72	-0.80	256.04	-0.93	255.93	-0.89	256.20	-0.99	256.37	-1.06
5-12	253.77	255.24	-0.58	255.76	-0.78	255.69	-0.76	256.03	-0.89	256.09	-0.91	256.46	-1.06	256.67	-1.14
5-13	256.04	257.45	-0.55	257.82	-0.70	257.77	-0.68	258.06	-0.79	258.18	-0.84	258.40	-0.92	258.57	-0.99
5-14	254.64	256.27	-0.64	256.76	-0.83	256.77	-0.84	257.09	-0.96	257.23	-1.02	257.60	-1.16	257.77	-1.23
5-15	255.08	256.66	-0.62	257.03	-0.76	256.70	-0.64	256.89	-0.71	257.00	-0.75	257.30	-0.87	257.48	-0.94
	0		**-0.56**		**-0.74**		**-0.70**		**-0.79**		**-0.82**		**-0.94**		**-1.01**

Cycle #	44	%Change	55	%Change	60	%Change
5-1						
5-2						
5-3						
5-4						
5-5						
5-6						
5-7						
5-8						
5-9	257.84	-0.81	257.89	-0.83	257.83	-0.81
5-10	258.75	-1.02	258.51	-0.93	258.31	-0.85
5-11	256.52	-1.12	256.83	-1.24	256.46	-1.10
5-12	256.79	-1.19	257.06	-1.30	256.99	-1.27
5-13	258.74	-1.05	258.97	-1.14	258.86	-1.10
5-14	257.98	-1.31	257.63	-1.17	256.02	-0.54
5-15	257.64	-1.00	257.70	-1.03	257.38	-0.90
		-1.07		**-1.09**		**-0.94**

Paste Sample Weights of Freeze/Thaw CaCl2 w/ Samples

(Note: all weights in grams. Negative weight change = weight gain.)

Cycle #	0	5	%Change	11	%Change	15	%Change	20	%Change	26	%Change	30	%Change	35	%Change
7-1	253.71	254.89	-0.47	255.18	-0.58	255.32	-0.63	253.60	0.04						
7-2	254.54	255.74	-0.47	256.04	-0.59	255.84	-0.51	255.72	-0.46						
7-3	256.17	257.22	-0.41	257.47	-0.51	257.59	-0.55	255.87	0.12						
7-4	253.56	254.75	-0.47	255.17	-0.63	254.68	-0.44	253.41	0.06						
7-5	254.01	255.45	-0.57	256.06	-0.81	255.29	-0.50	253.75	0.10	254.03	-0.01	251.33	1.06	252.06	0.77
7-6	253.56	254.60	-0.41	254.68	-0.44	254.87	-0.52	254.54	-0.39	253.48	0.03	251.67	0.75	252.62	0.37
7-7	252.07	253.19	-0.44	253.73	-0.66	253.26	-0.47	252.71	-0.25	252.13	-0.02	251.37	0.28	252.43	-0.14
7-8	252.03	253.22	-0.47	253.69	-0.66	253.71	-0.67	251.38	0.26	251.45	0.23	249.34	1.07	250.04	0.79
7-9	254.08	255.59	-0.59	255.89	-0.71	254.54	-0.18	253.96	0.05	253.61	0.18	251.76	0.91	252.49	0.63
7-10	254.65	255.94	-0.51	256.33	-0.66	256.03	-0.54	254.36	0.11	253.84	0.32	252.30	0.92	253.25	0.55
7-11	250.25	251.33	-0.43	251.64	-0.56	251.52	-0.51	249.67	0.23	248.01	0.90	247.82	0.97	248.26	0.80
7-12	255.48	256.62	-0.45	257.02	-0.60	256.89	-0.55	255.52	-0.02	255.49	0.00	254.36	0.44	255.02	0.18
7-13	254.71	256.11	-0.55	256.67	-0.77	256.65	-0.76	256.32	-0.63	256.70	-0.78	254.92	-0.08	255.21	-0.20
7-14	251.75	252.98	-0.49	253.46	-0.68	253.39	-0.65	252.55	-0.32	252.69	-0.37	251.22	0.21	251.33	0.17
7-15															
	0		**-0.48**		**-0.63**		**-0.54**		**-0.08**		**0.05**		**0.65**		**0.39**

Cycle #	40	%Change	50	%Change	55	%Change	61	%Change
7-1								
7-2								
7-3								
7-4								
7-5	252.75	0.50						
7-6	253.45	0.04						
7-7	252.95	-0.35						
7-8	250.32	0.68						
7-9	253.55	0.21	255.80	-0.68	256.37	-0.90	244.03	3.96
7-10	253.37	0.50	255.49	-0.33	256.97	-0.91	252.91	0.68
7-11	248.90	0.54	250.14	0.04	250.9	-0.26	248.40	0.74
7-12	255.21	0.11	257.38	-0.74	258.42	-1.15	256.30	-0.32
7-13	255.69	-0.38	256.48	-0.69	257.06	-0.92	253.06	0.65
7-14	252.31	-0.22	253.04	-0.51	253.96	-0.88	243.02	3.47
7-15								
		0.16		**-0.49**		**-0.84**		**1.53**

Paste Sample Weights of Freeze/Thaw Potassium Acetate Samples

(Note: all weights in grams. Negative weight change = weight gain.)

Cycle #	0	5	%Change	10	%Change	15	%Change	21	%Change	27	%Change	30	%Change	35	%Change
9-1	253.28	252.27	0.40	252.53	0.30	253.00	0.11	253.16	0.05						
9-2	254.75	253.74	0.40	254.07	0.27	254.41	0.13	254.61	0.05						
9-3	255.64	254.43	0.47	254.80	0.33	255.41	0.09	255.61	0.01						
9-4	252.65	251.70	0.38	251.90	0.30	252.38	0.11	252.55	0.04						
9-5	253.55	252.17	0.54	252.64	0.36	253.21	0.13	253.44	0.04	253.53	0.01	253.58	-0.01	253.67	-0.05
9-6	254.64	253.96	0.27	254.21	0.17	254.83	-0.07	255.05	-0.16	255.04	-0.16	255.20	-0.22	255.28	-0.25
9-7	255.01	254.37	0.25	254.51	0.20	254.93	0.03	255.14	-0.05	255.28	-0.11	255.24	-0.09	255.30	-0.11
9-8	255.90	255.06	0.33	255.33	0.22	255.99	-0.04	256.15	-0.10	256.28	-0.15	256.32	-0.16	256.36	-0.18
9-9	252.22	251.30	0.36	251.53	0.27	251.99	0.09	252.33	-0.04	252.31	-0.04	252.39	-0.07	252.42	-0.08
9-10	250.86	250.23	0.25	250.57	0.12	250.96	-0.04	251.20	-0.14	251.24	-0.15	251.34	-0.19	251.47	-0.24
9-11	253.14	252.47	0.26	252.61	0.21	253.12	0.01	253.42	-0.11	253.38	-0.09	253.47	-0.13	253.52	-0.15
9-12	253.65	252.87	0.31	253.23	0.17	253.66	0.00	253.84	-0.07	253.94	-0.11	254.01	-0.14	254.11	-0.18
9-13	254.00	253.33	0.26	253.62	0.15	254.08	-0.03	254.24	-0.09	254.43	-0.17	254.42	-0.17	254.47	-0.19
9-14	254.30	253.19	0.44	253.61	0.27	254.24	0.02	254.46	-0.06	254.51	-0.08	254.58	-0.11	254.72	-0.17
9-15	253.03	251.65	0.55	252.11	0.36	252.77	0.10	252.95	0.03	253.09	-0.02	253.12	-0.04	253.38	-0.14
	0		**0.36**		**0.25**		**0.04**		**-0.04**		**-0.10**		**-0.12**		**-0.16**

Cycle #	41	%Change	51	%Change	56	%Change	62	%Change
9-1								
9-2								
9-3								
9-4								
9-5	253.99	-0.17						
9-6	255.29	-0.26						
9-7	255.67	-0.26						
9-8	256.65	-0.29						
9-9	252.84	-0.25	252.69	-0.19	252.67	-0.18	252.75	-0.21
9-10	251.82	-0.38	251.68	-0.33	251.69	-0.33	251.79	-0.37
9-11	253.92	-0.31	253.77	-0.25	253.73	-0.23	253.85	-0.28
9-12	254.39	-0.29	253.98	-0.13	253.77	-0.05	253.79	-0.06
9-13	254.74	-0.29	254.60	-0.24	254.51	-0.20	254.66	-0.26
9-14	255.01	-0.28	254.53	-0.09	254.86	-0.22	255.10	-0.31
9-15	253.66	-0.25	253.32	-0.11	253.45	-0.17	253.58	-0.22
		-0.28		**-0.19**		**-0.20**		**-0.24**

Paste Sample Weights of Freeze/Thaw Geomelt Samples

(Note: all weights in grams. Negative weight change = weight gain.)

Cycle #	0	5	%Change	11	%Change	21	%Change	26	%Change	32	%Change	35	%Change	40	%Change
11-1	251.67	249.15	1.00	248.73	1.17	247.67	1.59								
11-2	249.01	245.99	1.21	245.64	1.35	244.66	1.75								
11-3	248.19	245.37	1.14	245.21	1.20	244.30	1.57								
11-4	251.74	248.73	1.20	248.45	1.31	247.36	1.74								
11-5	248.63	245.83	1.13	245.42	1.29	244.55	1.64	244.28	1.75	244.27	1.75	244.30	1.74	244.55	1.64
11-6	251.43	248.41	1.20	247.83	1.43	246.72	1.87	246.38	2.01	246.38	2.01	246.45	1.98	246.72	1.87
11-7	249.88	247.02	1.14	246.51	1.35	245.42	1.78	245.11	1.91	245.06	1.93	245.11	1.91	245.39	1.80
11-8	251.36	248.32	1.21	247.79	1.42	246.71	1.85	246.45	1.95	246.41	1.97	246.50	1.93	246.70	1.85
11-9	252.29	249.57	1.08	249.14	1.25	248.19	1.63	247.97	1.71	247.85	1.76	247.96	1.72	248.12	1.65
11-10	249.70	246.78	1.17	246.22	1.39	245.32	1.75	245.02	1.87	244.91	1.92	244.98	1.89	245.25	1.78
11-11	250.28	247.35	1.17	246.92	1.34	245.64	1.85	245.41	1.95	245.22	2.02	245.31	1.99	245.56	1.89
11-12	249.70	246.90	1.12	246.29	1.37	245.18	1.81	244.94	1.91	244.87	1.93	244.91	1.92	245.20	1.80
11-13	252.03	249.60	0.96	249.08	1.17	247.95	1.62	247.68	1.73	247.63	1.75	247.69	1.72	248.00	1.60
11-14	248.58	245.65	1.18	245.10	1.40	244.16	1.78	243.85	1.90	243.76	1.94	243.86	1.90	244.05	1.82
11-15	251.97	249.28	1.07	248.66	1.31	247.51	1.77	247.28	1.86	247.21	1.89	247.31	1.85	247.48	1.78
	0		**1.13**		**1.32**		**1.73**		**1.87**		**1.90**		**1.87**		**1.77**

Cycle #	45	%Change	50	%Change	55	%Change	60	%Change
11-1								
11-2								
11-3								
11-4								
11-5								
11-6								
11-7								
11-8								
11-9	248.86	1.36	249.55	1.09	249.66	1.04	249.36	1.16
11-10	246.40	1.32	246.76	1.18	247.23	0.99	246.91	1.12
11-11	246.23	1.62	246.58	1.48	247.06	1.29	247.18	1.24
11-12	245.98	1.49	246.47	1.29	247.19	1.01	247.07	1.05
11-13	248.78	1.29	249.22	1.11	249.57	0.98	249.22	1.11
11-14	244.41	1.68	244.74	1.54	245.08	1.41	245.12	1.39
11-15	248.31	1.45	248.44	1.40	249.12	1.13	249.20	1.10
		1.46		**1.30**		**1.12**		**1.17**

Table C-b-2. Paste freeze-thaw compressive strength data.

Dist. H2O	20	40	60
1-1			
1-2	54.2		
1-3	55.0		
1-4	60.8		
1-5			
1-6		67.0	
1-7		63.5	
1-8		63.9	
1-9			
1-10			63.9
1-11			58.1
1-12			63.9
Average:	56.7	64.8	62.0
(Mpa)			

CaCl2 w/o	20	40	60
3-1			
3-2	43.8		
3-3	31.8		
3-4	46.9		
3-5			
3-6		26.7	
3-7		35.6	
3-8		38.4	
3-9			
3-10			18.2
3-11			22.9
3-12			19.0
Average:	45.4	37.0	20.0

NaCl	20	40	60
5-1			
5-2	57.3		
5-3	55.4		
5-4	58.5		
5-5			
5-6		61.6	
5-7		60.1	
5-8		57.7	
5-9			
5-10			57.0
5-11			62.8
5-12			63.5
Average:	57.1	59.8	61.1

CaCl2 w/	20	40	61
7-1			
7-2	48.0		
7-3	54.2		
7-4	51.1		
7-5			
7-6		45.3	
7-7		39.9	
7-8		No Data	
7-9			
7-10			30.6
7-11			30.6
7-12			27.9
Average:	51.1	42.6	29.7

K. Ace.	20	41	62
9-1			
9-2	61.6		
9-3	58.1		
9-4	56.2		
9-5			
9-6		63.2	
9-7		62.8	
9-8		66.6	
9-9			
9-10			55.4
9-11			57.3
9-12			60.1
9-13			
9-14			
9-15			
Average:	58.6	64.2	57.6

Geomelt	21	40	60
11-1			
11-2	53.1		
11-3	56.6		
11-4	56.2		
11-5			
11-6		61.6	
11-7		60.8	
11-8		57.7	
11-9			
11-10			61.2
11-11			60.4
11-12			56.6
11-13			
11-14			
11-15			
Average:	55.3	60.0	59.4

Table C-b-3. Paste freeze-thaw scaling data.

Dist. H2O:	24	40	60
1-1	0		
1-2	0		
1-3	0		
1-4	0		
1-5		1	
1-6		1	
1-7		1	
1-8		1	
1-9			1
1-10			1
1-11			1
1-12			1
Average:	0.0	1.0	1.0

CaCl2 w/o:	20	40	60
3-1	2		
3-2	2		
3-3	2		
3-4	2		
3-5		4	
3-6		4	
3-7		4	
3-8		4	
3-9			5
3-10			5
3-11			5
3-12			5
Average:	2.0	4.0	5.0

NaCl:	20	41	60
5-1	1		
5-2	1		
5-3	1		
5-4	1		
5-5		2	
5-6		1	
5-7		2	
5-8		1	
5-9			
5-10			2
5-11			2
5-12			1
Average:	1.0	1.5	1.7

CaCl2 w/:	20	41	62
7-1	1		
7-2	1		
7-3	1		
7-4	2		
7-5		3	
7-6		3	
7-7		4	
7-8		4	
7-9			5
7-10			5
7-11			4
7-12			4
Average:	1.3	3.5	4.5

K. Ace:	20	40	60
9-1	0		
9-2	0		
9-3	0		
9-4	0		
9-5		0	
9-6		0	
9-7		0	
9-8		0	
9-9			0
9-10			0
9-11			0
9-12			1
Average:	0.0	0.0	0.25

Geomelt:	20	41	60
11-1	1		
11-2	1		
11-3	1		
11-4	1		
11-5		1	
11-6		1	
11-7		1	
11-8		1	
11-9			1
11-10			1
11-11			1
11-12			1
Average:	1.0	1.0	1.0

Table C-c-1. Concrete Sample Weights of Wet/Dry Distilled Water Samples.

(Note: all weights in grams. Negative weight change = weight gain.)

Cycle #	0	10	%Change	20	%Change	30	%Change	40	%Change	50	%Change	60	%Change
2-1	2350.07	2353.02	-0.13	2353.02	-0.13								
2-2	2337.75	2340.29	-0.11	2340.24	-0.11								
2-3	2390.51	2393.20	-0.11	2393.45	-0.12								
2-4	2367.53	2368.84	-0.06	2368.58	-0.04								
2-5	2240.57	2239.97	0.03	2239.10	0.07	2237.23	0.15	2234.61	0.27				
2-6	2349.28	2349.23	0.00	2348.88	0.02	2347.62	0.07	2346.05	0.14				
2-7	2328.66	2331.63	-0.13	2330.94	-0.10	2329.10	-0.02	2327.99	0.03				
2-8	2385.38	2386.75	-0.06	2387.23	-0.08	2385.16	0.01	2382.67	0.11				
2-9	2219.33	2219.67	-0.02	2219.11	0.01	2217.29	0.09	2215.16	0.19	2214.03	0.24	2214.17	0.23
2-10	2377.59	2379.84	-0.09	2380.13	-0.11	2378.75	-0.05	2377.21	0.02	2376.74	0.04	2376.91	0.03
2-11	2210.40	2211.72	-0.06	2211.23	-0.04	2209.27	0.05	2207.09	0.15	2206.36	0.18	2207.08	0.15
2-12	2213.50	2213.83	-0.01	2213.48	0.00	2210.92	0.12	2208.53	0.22	2206.83	0.30	2206.92	0.30
2-13	2243.45	2243.04	0.02	2242.18	0.06	2240.51	0.13	2238.34	0.23	2236.88	0.29	2236.86	0.29
2-14	2214.58	2213.12	0.07	2212.58	0.09	2210.85	0.17	2208.88	0.26	2207.91	0.30	2208.14	0.29
	0		**-0.05**		**-0.03**		**0.07**		**0.16**		**0.23**		**0.22**

Concrete Sample Weights of Wet/Dry CaCl2 w/o Samples.

(Note: all weights in grams. Negative weight change = weight gain.)

Cycle #	0	20	%Change	30	%Change	40	%Change	50	%Change	61	%Change
4-1	2371.65	2381.86	-0.43								
4-2	2371.97	2395.74	-1.00								
4-3	2382.08	2395.24	-0.55								
4-4	2225.18	2237.78	-0.57								
4-5	2264.08	2280.15	-0.71	2286.77	-1.00	2290.78	-1.18				
4-6	2379.15	2401.63	-0.94	2410.37	-1.31	2415.39	-1.52				
4-7	2249.45	2264.53	-0.67	2272.07	-1.01	2276.55	-1.20				
4-8	2374.43	2393.58	-0.81	2399.6	-1.06	2404.16	-1.25				
4-9	2392.31	2400.56	-0.34	2407.07	-0.62	2410.68	-0.77	2411.88	-0.82	2412.46	-0.84
4-10	2389.64	2406.21	-0.69	2414.92	-1.06	2420.23	-1.28	2422.72	-1.38	2425.09	-1.48
4-11	2270.76	2291.62	-0.92	2298.88	-1.24	2304.06	-1.47	2304.14	-1.47	2305.53	-1.53
4-12	2371.65	2382.24	-0.45	2391.33	-0.83	2396.20	-1.04	2398.29	-1.12	2399.73	-1.18
	0		**-0.67**		**-1.02**		**-1.21**		**-1.20**		**-1.26**

Concrete Sample Weights of Wet/Dry NaCl Samples.

(Note: all weights in grams. Negative weight change = weight gain.)

Cycle #	0	10	%Change	21	%Change	30	%Change	41	%Change	52	%Change	60	%Change
6-1	2365.20	2368.45	-0.14	2367.20	-0.08								
6-2	2394.68	2397.51	-0.12	2395.44	-0.03								
6-3	2249.57	2250.02	-0.02	2248.94	0.03								
6-4	2269.95	2273.62	-0.16	2271.84	-0.08								
6-5	2439.47	2440.97	-0.06	2438.40	0.04	2437.82	0.07	2436.72	0.11	2437.33	0.09	2435.84	0.15
6-6	2387.36	2389.76	-0.10	2387.27	0.00	2386.87	0.02	2386.02	0.06				
6-7	2384.43	2385.47	-0.04	2383.95	0.02	2383.87	0.02	2383.28	0.05				
6-8	2385.41	2388.78	-0.14	2386.35	-0.04	2385.21	0.01	2384.06	0.06				
6-9	2355.51	2363.47	-0.34	2361.76	-0.27	2361.56	-0.26	2360.48	-0.21				
6-10	2421.63	2425.05	-0.14	2423.21	-0.07	2422.94	-0.05	2421.72	0.00	2422.35	-0.03	*2438.69*	*-0.70*
6-11	2257.02	2261.60	-0.20	2259.58	-0.11	2259.35	-0.10	2258.41	-0.06	2259.04	-0.09	2257.30	-0.01
6-12	2263.39	2266.30	-0.13	2264.36	-0.04	2264.21	-0.04	2263.39	0.00	2263.20	0.01	2262.30	0.05
	0		**-0.13**		**-0.05**		**-0.04**		**0.00**		**-0.01**		**0.18**

Accidentally compressed 6-10 prematurely; cracking w/ additional adsorption.

Concrete Sample Weights of Wet/Dry CaCl2 w/ Samples.

(Note: all weights in grams. Negative weight change = weight gain.)

Cycle #	0	7	%Change	10	%Change	15	%Change	20	%Change	25	%Change
7-1	2408.17	2413.15	-0.21	2421.29	-0.54	2429.38	-0.88	2436.53	-1.18		
7-2	2415.78	2417.25	-0.06	2426.11	-0.43	2435.25	-0.81	2443.01	-1.13		
7-3	2260.28	2258.80	0.07	2268.43	-0.36	2276.34	-0.71	2283.25	-1.02		
7-4	2389.89	2393.97	-0.17	2402.49	-0.53	2410.22	-0.85	2414.94	-1.05		
7-5	2362.04	2364.31	-0.10	2374.95	-0.55	2383.32	-0.90	2390.45	-1.20	2398.24	-1.53
7-6	2420.97	2423.87	-0.12	2434.10	-0.54	2442.73	-0.90	2447.74	-1.11	2455.33	-1.42
7-7	2247.06	2250.85	-0.17	2258.83	-0.52	2276.19	-1.30	2272.18	-1.12	2279.57	-1.45
7-8	2233.54	2236.89	-0.15	2244.52	-0.49	2251.59	-0.81	2257.70	-1.08	2263.41	-1.34
7-9	2265.21	2270.00	-0.21	2277.87	-0.56	2284.70	-0.86	2290.59	-1.12	2297.20	-1.41
7-10	2405.72	2408.80	-0.13	2416.93	-0.47	2425.16	-0.81	2431.00	-1.05	2436.87	-1.29
7-11	2417.42	2422.39	-0.21	2430.35	-0.53	2437.39	-0.83	2444.41	-1.12	2451.45	-1.41
7-12	2384.00	2387.13	-0.13	2396.68	-0.53	2403.89	-0.83	2410.83	-1.13	2418.89	-1.46
	0		**-0.13**		**-0.50**		**-0.87**		**-1.11**		**-1.41**

Cycle #	32	%Change	35	%Change	40	%Change	50	%Change	62	%Change
7-1										
7-2										
7-3										
7-4										
7-5	2406.03	-1.86	2408.72	-1.98	2411.25	-2.08				
7-6	2463.09	-1.74	2465.22	-1.83	2468.26	-1.95				
7-7	2287.25	-1.79	2289.70	-1.90	2292.82	-2.04				
7-8	2270.03	-1.63	2272.30	-1.74	2275.17	-1.86				
7-9	2304.75	-1.75	2306.59	-1.83	2309.00	-1.93	2312.54	-2.09	2318.72	-2.36
7-10	2442.92	-1.55	2445.26	-1.64	2447.16	-1.72	2449.27	-1.81	2453.90	-2.00
7-11	2458.00	-1.68	2460.33	-1.78	2462.78	-1.88	2465.57	-1.99	2470.06	-2.18
7-12	2426.70	-1.79	2428.71	-1.88	2431.80	-2.01	2436.64	-2.21	2441.79	-2.42
		-1.72		**-1.82**		**-1.93**		**-2.02**		**-2.24**

Concrete Sample Weights of Wet/Dry Potassium Acetate Samples.

(Note: all weights in grams. Negative weight change = weight gain.)

Cycle #	0	10	%Change	21	%Change	30	%Change	40	%Change	52	%Change	60	%Change
10-1	2394.92	2392.12	0.12	2391.46	0.14								
10-2	2390.19	2388.31	0.08	2387.78	0.10								
10-3	2383.44	2381.64	0.08	2380.84	0.11								
10-4	2386.15	2385.20	0.04	2385.16	0.04								
10-5	2391.18	2386.80	0.18	2386.92	0.18	2387.58	0.15	2391.10	0.00				
10-6	2391.48	2389.29	0.09	2387.98	0.15	2388.28	0.13	2391.18	0.01				
10-7	2218.14	2216.53	0.07	2216.22	0.09	2217.35	0.04	2220.63	-0.11				
10-8	2372.80	2370.29	0.11	2369.84	0.12	2371.16	0.07	2374.50	-0.07				
10-9	2264.73	2262.92	0.08	2262.41	0.10	2262.89	0.08	2265.73	-0.04	2267.92	-0.14	2269.08	-0.19
10-10	2230.69	2230.00	0.03	2229.75	0.04	2230.35	0.02	2233.15	-0.11	2235.10	-0.20	2236.00	-0.24
10-11	2235.46	2234.41	0.05	2233.75	0.08	2234.23	0.06	2237.21	-0.08	2239.56	-0.18	2241.09	-0.25
10-12	2359.77	2359.68	0.00	2359.67	0.00	2360.72	-0.04	2363.81	-0.17	2365.74	-0.25	2366.46	-0.28
	0		**0.08**		**0.10**		**0.06**		**-0.07**		**-0.19**		**-0.24**

Concrete Sample Weights of Wet/Dry Geomelt Samples.

(Note: all weights in grams. Negative weight change = weight gain.)

Cycle #	0	10	%Change	22	%Change	30	%Change	40	%Change	50	%Change	60	%Change
12-1	2257.61	2224.18	1.48	2218.29	1.74								
12-2	2378.34	2343.60	1.46	2337.50	1.72								
12-3	2377.14	2345.69	1.32	2339.25	1.59								
12-4	2403.94	2371.52	1.35	2365.32	1.61								
12-5	2393.17	2357.34	1.50	2351.25	1.75	2344.39	2.04	2342.55	2.12				
12-6	2360.53	2326.88	1.43	2320.03	1.72	2313.76	1.98	2311.77	2.07				
12-7	2381.68	2349.28	1.36	2343.10	1.62	2336.67	1.89	2334.99	1.96				
12-8	2227.18	2194.78	1.45	2189.53	1.69	2183.26	1.97	2181.95	2.03				
12-9	2252.40	2221.21	1.38	2215.45	1.64	2209.46	1.91	2208.24	1.96	2207.46	2.00	2206.51	2.04
12-10	2367.29	2334.81	1.37	2328.43	1.64	2322.67	1.88	2321.31	1.94	2319.66	2.01	2319.10	2.04
12-11	2394.55	2361.76	1.37	2355.37	1.64	2349.05	1.90	2347.89	1.95	2347.07	1.98	2346.62	2.00
12-12	2243.72	2213.18	1.36	2207.48	1.62	2201.59	1.88	2200.17	1.94	2199.10	1.99	2198.34	2.02
	0		**1.40**		**1.66**		**1.93**		**2.00**		**1.99**		**2.02**

Table C-c-2. Concrete wet-dry compressive strength data.

Dist. H2O	20	40	60
2-1			
2-2	26.6		
2-3	20.9		
2-4	27.3		
2-5			
2-6		29.7	
2-7		29.4	
2-8		28.8	
2-9			
2-10			29.4
2-11			28.1
2-12			31.0
Average:	27.0	29.3	29.5
(Mpa)			

CaCl2 w/o	20	40	61
4-1			
4-2	27.4		
4-3	28.3		
4-4	26.2		
4-5			
4-6		24.7	
4-7		25.6	
4-8		27.6	
4-9			
4-10			27.3
4-11			28.1
4-12			27.6
Average:	27.3	26.0	27.7

NaCl	21	41	60
6-1			
6-2	26.3		
6-3	31.1		
6-4	29.0		
6-5			32.2
6-6			
6-7		29.8	
6-8		31.8	
6-9		29.5	
6-10			
6-11			26.9
6-12			26.5
Average:	28.8	30.4	28.5

CaCl2 w/	20	40	60
7-1			
7-2	21.9		
7-3	25.7		
7-4	26.9		
7-5			
7-6		27.2	
7-7		23.1	
7-8		25.0	
7-9			
7-10			27.2
7-11			28.5
7-12			27.1
Average:	24.8	25.1	27.6

K. Ace.	20	40	60
10-1			
10-2	26.2		
10-3	27.1		
10-4	25.8		
10-5			
10-6		25.9	
10-7		27.0	
10-8		27.5	
10-9			
10-10			26.8
10-11			25.6
10-12			29.3
Average:	26.4	26.8	27.2

Geomelt	20	40	60
12-1			
12-2	29.7		
12-3	30.5		
12-4	29.1		
12-5			
12-6		33.3	
12-7		24.7	
12-8		32.1	
12-9			
12-10			30.7
12-11			30.1
12-12			28.1
Average:	29.8	30.0	29.6

Table C-c-3. Concrete wet-dry scaling data.

H2O	20	40	60
2-1	0		
2-2	0		
2-3	0		
2-4	0		
2-5		0	
2-6		0	
2-7		0	
2-8		0	
2-9			0
2-10			0
2-11			0
2-12			0
Average:	0.0	0.0	0.0

CaCl2 w/o:	21	40	61
4-1	0		
4-2	1		
4-3	0		
4-4	1		
4-5		2	
4-6		2	
4-7		2	
4-8		2	
4-9			3
4-10			3
4-11			3
4-12			3
Average:	0.5	2.0	3.0

NaCl:	21	41	60
6-1	0		
6-2	0		
6-3	0		
6-4	0		
6-5			0
6-6		0	
6-7		0	
6-8		0	
6-9		0	
6-10			0
6-11			0
6-12			0
Average:	0.0	0.0	0.0

CaCl2 w/:	20	40	62
7-1	1		
7-2	1		
7-3	1		
7-4	1		
7-5		1	
7-6		1	
7-7		1	
7-8		1	
7-9			2
7-10			2
7-11			1
7-12			2
Average:	1.0	1.0	1.8

K. Ace:	21	40	60
10-1	0		
10-2	0		
10-3	0		
10-4	0		
10-5		0	
10-6		0	
10-7		0	
10-8		0	
10-9			0
10-10			0
10-11			0
10-12			0
Average:	0.0	0.0	0.0

Geomelt:	22	41	62
12-1	1		
12-2	1		
12-3	1		
12-4	1		
12-5		1	
12-6		1	
12-7		1	
12-8		1	
12-9			1
12-10			1
12-11			1
12-12			1
Average:	1.0	1.0	1.0

Table C-d-1. Concrete Sample Weights of Freeze/Thaw Distilled Water Samples.

(Note: all weights in grams. Negative weight change = weight gain.)

Cycle #	0	5	%Change	10	%Change	15	%Change	21	%Change	31	%Change
1-1	2234.29	2240.14	-0.26	2242.35	-0.36	2243.27	-0.40	2243.61	-0.42		
1-2	2187.34	2193.43	-0.28	2195.41	-0.37	2198.05	-0.49	2198.26	-0.50		
1-3	2340.57	2345.61	-0.22	2348.33	-0.33	2350.40	-0.42	2350.35	-0.42		
1-4	2324.07	2330.49	-0.28	2332.25	-0.35	2335.70	-0.50	2336.08	-0.52		
1-5	2355.68	2362.34	-0.28	2364.12	-0.36	2367.04	-0.48	2367.55	-0.50	2370.40	-0.62
1-6	2346.27	2354.01	-0.33	2355.92	-0.41	2357.98	-0.50	2358.70	-0.53	2362.22	-0.68
1-7	2365.14	2373.33	-0.35	2376.01	-0.46	2375.93	-0.46	2377.78	-0.53	2381.11	-0.68
1-8	2353.38	2360.87	-0.32	2362.99	-0.41	2366.11	-0.54	2365.82	-0.53	2368.86	-0.66
1-9	2348.38	2357.04	-0.37	2359.64	-0.48	2362.78	-0.61	2362.91	-0.62	2365.99	-0.75
1-10	2212.71	2218.37	-0.26	2221.59	-0.40	2224.34	-0.53	2224.07	-0.51	2227.09	-0.65
1-11	2358.86	2363.78	-0.21	2366.45	-0.32	2369.14	-0.44	2369.13	-0.44	2371.88	-0.55
1-12	2211.60	2217.76	-0.28	2219.07	-0.34	2221.71	-0.46	2221.93	-0.47	2224.10	-0.57
	0		**-0.29**		**-0.38**		**-0.49**		**-0.50**		**-0.64**

Cycle #	37	%Change	40	%Change	45	%Change	50	%Change	57	%Change	60	%Change
1-1												
1-2												
1-3												
1-4												
1-5	2371.98	-0.69	2371.88	-0.69								
1-6	2364.21	-0.76	2363.75	-0.75								
1-7	2382.55	-0.74	2382.39	-0.73								
1-8	2370.06	-0.71	2369.75	-0.70								
1-9	2367.12	-0.80	2367.09	-0.80	2367.70	-0.82	2368.08	-0.84	2369.77	-0.91	2371.35	-0.98
1-10	2227.58	-0.67	2227.85	-0.68	2228.60	-0.72	2228.62	-0.72	2230.60	-0.81	2232.03	-0.87
1-11	2373.32	-0.61	2372.95	-0.60	2373.35	-0.61	2373.68	-0.63	2375.46	-0.70	2376.87	-0.76
1-12	2225.44	-0.63	2225.60	-0.63	2226.12	-0.66	2226.60	-0.68	2228.73	-0.77	2229.68	-0.82
		-0.70		**-0.70**		**-0.70**		**-0.72**		**-0.80**		**-0.86**

Concrete Sample Weights of Freeze/Thaw CaCl2 w/o Samples.

(Note: all weights in grams. Negative weight change = weight gain.)

Cycle #	0	10	%Change	20	%Change	32	%Change	41	%Change	50	%Change
3-1	2374.02	2384.57	-0.44	2355.06	0.80	2363.45	0.45	2326.81	1.99		
3-2	2360.65	2377.35	-0.71	2371.64	-0.47	2369.94	-0.39	2271.96	3.76		
3-3	2239.52	2248.74	-0.41	2242.66	-0.14						
3-4	2257.21	2272.26	-0.67	2276.69	-0.86	2281.26	-1.07	2194.88	2.76	2166.64	4.01
3-5	2219.40	2225.51	-0.28	2219.51	0.00	2209.50	0.45	2174.37	2.03	2168.43	2.30
3-6	2253.31	2259.09	-0.26	2254.68	-0.06						
3-7	2389.60	2401.93	-0.52	2396.22	-0.28	2380.60	0.38	2358.03	1.32	2353.11	1.53
3-8	2381.69	2392.97	-0.47	2389.44	-0.33	2381.23	0.02	2318.58	2.65	2277.17	4.39
3-10	2364.06	2376.69	-0.53	2346.67	0.74						
3-11	2382.49	2394.83	-0.52	2380.20	0.10	2389.19	-0.28	2333.00	2.08		
3-12	2281.39	2299.58	-0.80	2273.45	0.35	2272.56	0.39	2165.07	5.10		
3-13	2381.66	2393.01	-0.48	2381.27	0.02						
	0		**-0.51**		**-0.01**		**-0.01**		**2.71**		**3.06**

Cycle #	61	%Change
3-1		
3-2		
3-3		
3-4	2089.29	7.44
3-5	2143.27	3.43
3-6		
3-7	2323.83	2.75
3-8	2245.21	5.73
3-10		
3-11		
3-12		
3-13		
		4.84

Concrete Sample Weights of Freeze/Thaw NaCl Samples.

(Note: all weights in grams. Negative weight change = weight gain.)

Cycle #	0	6	%Change	10	%Change	15	%Change	20	%Change	30	%Change
5-1	2380.04	2404.76	-1.04	2415.64	-1.50	2414.04	-1.43	2418.60	-1.62		
5-2	2346.59	2372.06	-1.09	2381.72	-1.50	2380.60	-1.45	2385.28	-1.65		
5-3	2336.60	2362.57	-1.11	2373.11	-1.56	2372.71	-1.55	2375.39	-1.66		
5-4	2210.62	2234.39	-1.08	2243.79	-1.50	2243.15	-1.47	2247.48	-1.67		
5-5	2365.05	2390.06	-1.06	2399.54	-1.46	2398.77	-1.43	2403.37	-1.62	2406.15	-1.74
5-6	2230.10	2256.72	-1.19	2263.15	-1.48	2263.46	-1.50	2268.16	-1.71	2270.53	-1.81
5-7	2335.48	2262.72	3.12	2369.26	-1.45	2369.18	-1.44	2373.76	-1.64	2375.32	-1.71
5-8	2337.35	2358.32	-0.90	2271.29	2.83	2271.48	2.82	2275.35	2.65	2276.75	2.59
5-9	2382.86	2408.64	-1.08	2418.45	-1.49	2418.38	-1.49	2420.83	-1.59	2422.16	-1.65
5-10	2340.62	2365.73	-1.07	2375.91	-1.51	2377.69	-1.58	2380.94	-1.72	2384.45	-1.87
5-11	2231.43	2254.83	-1.05	2263.26	-1.43	2263.74	-1.45	2266.58	-1.58	2270.26	-1.74
5-12	2335.72	2358.80	-0.99	2369.98	-1.47	2370.76	-1.50	2373.86	-1.63	2376.02	-1.73
	0		**-0.71**		**-1.13**		**-1.12**		**-1.29**		**-1.21**

Cycle #	35	%Change	41	%Change	45	%Change	50	%Change	55	%Change	61	%Change
5-1												
5-2												
5-3												
5-4												
5-5	2409.03	-1.86	2409.09	-1.86								
5-6	2270.98	-1.83	2271.66	-1.86								
5-7	2377.62	-1.80	2378.16	-1.83								
5-8	2279.28	2.48	2278.48	2.52								
5-9	2424.47	-1.75	2425.64	-1.80	2423.12	-1.69	2422.69	-1.67	2422.53	-1.66	2422.88	-1.68
5-10	2386.62	-1.97	2387.16	-1.99	2384.06	-1.86	2383.67	-1.84	2383.13	-1.82	2383.08	-1.81
5-11	2272.43	-1.84	2273.39	-1.88	2270.34	-1.74	2270.53	-1.75	2269.77	-1.72	2270.21	-1.74
5-12	2379.94	-1.89	2379.24	-1.86	2376.60	-1.75	2376.66	-1.75	2376.28	-1.74	2377.04	-1.77
		-1.31		**-1.32**		**-1.76**		**-1.75**		**-1.73**		**-1.75**

Concrete Sample Weights of Freeze/Thaw CaCl2 w/ Samples.

(Note: all weights in grams. Negative weight change = weight gain.)

Cycle #	0	6	%Change	11	%Change	20	%Change	31	%Change	40	%Change	45	%Change
8-1	2384.75	2382.22	0.11	2389.80	-0.21	2400.89	-0.68						
8-2	2395.72	2393.45	0.09	2400.63	-0.20	2410.63	-0.62						
8-3	2388.10	2386.52	0.07	2396.06	-0.33	2407.33	-0.81						
8-4	2226.00	2222.50	0.16	2229.46	-0.16	2238.81	-0.58						
8-5	2258.80	2256.83	0.09	2264.83	-0.27	2274.33	-0.69	2287.05	-1.25	2293.95	-1.56		
8-6	2371.37	2369.04	0.10	2377.92	-0.28	2388.60	-0.73	2403.50	-1.35	2410.74	-1.66		
8-7	2369.70	2371.06	-0.06	2378.66	-0.38	2389.83	-0.85	2404.59	-1.47	2412.23	-1.79		
8-8	2267.80	2267.71	0.00	2276.19	-0.37	2288.09	-0.89	2303.05	-1.55	2309.35	-1.83		
8-9	2415.30	2415.11	0.01	2421.76	-0.27	2433.15	-0.74	2449.00	-1.40	2455.34	-1.66	2451.81	-1.51
8-10	2245.25	2245.32	0.00	2251.31	-0.27	2260.26	-0.67	2273.21	-1.25	2280.06	-1.55	2279.17	-1.51
8-11	2389.73	2388.17	0.07	2394.61	-0.20	2407.22	-0.73	2421.11	-1.31	2425.14	-1.48	2400.78	-0.46
8-12	2402.03	2403.30	-0.05	2411.79	-0.41	2423.89	-0.91	2437.05	-1.46	2439.72	-1.57	2420.02	-0.75
	0		**0.05**		**-0.28**		**-0.74**		**-1.38**		**-1.64**		**-1.06**

Cycle #	50	%Change	55	%Change	61	%Change
8-1						
8-2						
8-3						
8-4						
8-5						
8-6						
8-7						
8-8						
8-9	2423.08	-0.32	2358.25	2.36	2222.32	7.99
8-10	2248.11	-0.13	2183.85	2.73	2123.28	5.43
8-11	2358.58	1.30	2320.56	2.89	2200.60	7.91
8-12	2376.23	1.07	2297.95	4.33	2157.96	10.16
		0.48		**3.08**		**7.87**

Concrete Sample Weights of Freeze/Thaw Potassium Acetate Samples.

(Note: all weights in grams. Negative weight change = weight gain.)

Cycle #	0	5	%Change	11	%Change	15	%Change	20	%Change	25	%Change	30	%Change
9-1	2411.62	2428.39	-0.70	2436.89	-1.05	2439.14	-1.14	2443.86	-1.34				
9-2	2360.65	2374.49	-0.59	2382.08	-0.91	2384.96	-1.03	2387.33	-1.13				
9-3	2365.90	2381.31	-0.65	2389.08	-0.98	2392.41	-1.12	2395.99	-1.27				
9-4	2387.07	2401.19	-0.59	2407.98	-0.88	2411.55	-1.03	2414.65	-1.16				
9-5	2369.55	2385.90	-0.69	2392.11	-0.95	2396.98	-1.16	2400.81	-1.32	2403.67	-1.44	2407.89	-1.62
9-6	2384.10	2396.59	-0.52	2405.71	-0.91	2409.38	-1.06	2412.95	-1.21	2415.21	-1.30	2419.67	-1.49
9-7	2383.52	2401.18	-0.74	2409.72	-1.10	2413.21	-1.25	2416.49	-1.38	2417.91	-1.44	2422.85	-1.65
9-8	2247.08	2261.76	-0.65	2268.35	-0.95	2272.23	-1.12	2274.69	-1.23	2277.33	-1.35	2282.36	-1.57
9-9	2237.32	2250.80	-0.60	2258.62	-0.95	2262.16	-1.11	2265.74	-1.27	2267.44	-1.35	2272.31	-1.56
9-10	2250.46	2264.13	-0.61	2272.16	-0.96	2275.82	-1.13	2277.92	-1.22	2280.04	-1.31	2284.28	-1.50
9-11	2253.28	2268.53	-0.68	2276.28	-1.02	2280.04	-1.19	2282.76	-1.31	2284.04	-1.37	2288.24	-1.55
9-12	2366.87	2381.45	-0.62	2389.72	-0.97	2392.77	-1.09	2396.30	-1.24	2399.31	-1.37	2403.54	-1.55
	0		**-0.64**		**-0.97**		**-1.12**		**-1.26**		**-1.37**		**-1.56**

Cycle #	35	%Change	41	%Change	46	%Change	50	%Change	55	%Change	60	%Change
9-1												
9-2												
9-3												
9-4												
9-5	2408.90	-1.66	2407.98	-1.62								
9-6	2420.94	-1.55	2417.50	-1.40								
9-7	2422.85	-1.65	2420.71	-1.56								
9-8	2282.72	-1.59	2279.96	-1.46								
9-9	2271.93	-1.55	2271.25	-1.52	2267.40	-1.34	2266.88	-1.32	2267.65	-1.36	2268.81	-1.41
9-10	2285.32	-1.55	2282.26	-1.41	2279.86	-1.31	2279.13	-1.27	2279.60	-1.29	2281.52	-1.38
9-11	2288.71	-1.57	2287.65	-1.53	2283.27	-1.33	2282.27	-1.29	2282.70	-1.31	2284.86	-1.40
9-12	2404.26	-1.58	2400.28	-1.41	2398.50	-1.34	2398.19	-1.32	2398.48	-1.34	2401.10	-1.45
		-1.59		**-1.49**		**-1.33**		**-1.30**		**-1.32**		**-1.41**

Concrete Sample Weights of Freeze/Thaw Geomelt Samples.

(Note: all weights in grams. Negative weight change = weight gain.)

Cycle #	0	5	%Change	10	%Change	15	%Change	23	%Change	25	%Change	31	%Change
11-1	2420.10	2421.88	-0.07	2421.97	-0.08	2421.77	-0.07	2424.82	-0.20				
11-2	2260.23	2259.71	0.02	2261.60	-0.06	2261.63	-0.06	2263.51	-0.15				
11-3	2381.66	2381.76	0.00	2382.85	-0.05	2382.60	-0.04	2384.24	-0.11				
11-4	2401.39	2403.79	-0.10	2405.47	-0.17	2404.49	-0.13	2407.46	-0.25				
11-5	2380.76	2381.99	-0.05	2383.23	-0.10	2382.85	-0.09	2384.53	-0.16	2383.44	-0.11	2384.00	-0.14
11-6	2403.17	2405.17	-0.08	2404.54	-0.06	2404.41	-0.05	2406.72	-0.15	2405.71	-0.11	2406.18	-0.13
11-7	2374.24	2375.25	-0.04	2375.66	-0.06	2374.54	-0.01	2376.78	-0.11	2376.12	-0.08	2375.97	-0.07
11-8	2252.24	2250.02	0.10	2251.40	0.04	2249.66	0.11	2251.82	0.02	2251.14	0.05	2251.08	0.05
11-9	2247.72	2249.81	-0.09	2250.75	-0.13	2250.76	-0.14	2252.55	-0.21	2252.24	-0.20	2252.62	-0.22
11-10	2392.88	2393.50	-0.03	2394.02	-0.05	2394.07	-0.05	2396.25	-0.14	2395.64	-0.12	2395.47	-0.11
11-11	2428.99	2431.82	-0.12	2432.99	-0.16	2433.39	-0.18	2434.22	-0.22	2433.37	-0.18	2432.87	-0.16
11-12	2256.85	2257.38	-0.02	2260.24	-0.15	2258.84	-0.09	2259.93	-0.14	2259.25	-0.11	2259.82	-0.13
	0		**-0.04**		**-0.09**		**-0.07**		**-0.15**		**-0.11**		**-0.11**

Cycle #	42	%Change	51	%Change	56	%Change	60	%Change
11-1								
11-2								
11-3								
11-4								
11-5	2381.97	-0.05						
11-6	2404.39	-0.05						
11-7	2373.99	0.01						
11-8	2249.36	0.13						
11-9	2250.61	-0.13	2252.58	-0.22	2252.18	-0.20	2252.94	-0.23
11-10	2392.68	0.01	2393.75	-0.04	2393.79	-0.04	2394.29	-0.06
11-11	2431.28	-0.09	2429.95	-0.04	2429.80	-0.03	2430.62	-0.07
11-12	2257.33	-0.02	2257.19	-0.02	2257.15	-0.01	2258.01	-0.05
		-0.02		**-0.08**		**-0.07**		**-0.10**

Table C-d-2. Concrete freeze-thaw compressive strength data.

Dist. H2O	21	40	60
1-1			
1-2	22.4		
1-3	23.4		
1-4	22.6		
1-5			
1-6		27.0	
1-7		25.7	
1-8		25.1	
1-9			
1-10			26.6
1-11			26.2
1-12			23.6
1-13			
1-14			
1-15			
Average:	22.8	25.9	25.5
(Mpa)			

CaCl2 w/o	21	42	61
3-1			
3-2		9.2	
3-3	10.4		
3-4			7.0
3-5			
3-6	13.1		
3-7			9.2
3-8			6.8
3-9			
3-10			
3-11		8.3	
3-12		No Data	
3-13	19.4		
3-14			
3-15			
Average:	11.8	8.8	7.7

NaCl	20	41	61
5-1			
5-2	21.3		
5-3	19.8		
5-4	19.5		
5-5			
5-6		22.8	
5-7		23.6	
5-8		22.9	
5-9			
5-10			23.8
5-11			24.6
5-12			24.3
Average:	20.2	23.1	24.2

CaCl2 w/	20	40	60
8-1			
8-2	25.4		
8-3	27.0		
8-4	24.8		
8-5			
8-6		24.6	
8-7		24.6	
8-8		22.5	
8-9			
8-10			9.5
8-11			9.5
8-12			10.1
Average:	25.7	23.9	9.7

K. Ace.	20	40	60
9-1			
9-2	22.3		
9-3	21.5		
9-4	24.3		
9-5			
9-6		22.9	
9-7		23.2	
9-8		23.2	
9-9			
9-10			21.0
9-11			22.1
9-12			20.5
Average:	22.7	23.1	21.2

Geomelt	20	40	60
11-1			
11-2	26.3		
11-3	26.6		
11-4	26.6		
11-5			
11-6		21.9	
11-7		26.3	
11-8		27.3	
11-9			
11-10			25.4
11-11			26.7
11-12			20.9
Average:	26.5	25.2	24.3

Table C-d-3. Concrete freeze-thaw scaling data.

H2O:	21	40	60
1-1	0		
1-2	0		
1-3	0		
1-4	0		
1-5		0	
1-6		0	
1-7		0	
1-8		0	
1-9			0
1-10			0
1-11			0
1-12			0
Average:	0.0	0.0	0.0

CaCl2 w/o:	21	42	61
3-1		4	
3-2		4	
3-3	4		
3-4			5
3-5			5
3-6	3		
3-7			5
3-8			5
3-9			
3-10	3		
3-11		4	
3-12		4	
3-13	4		
Average:	3.5	4.0	5.0

NaCl:	21	41	61
5-1	1		
5-2	1		
5-3	1		
5-4	1		
5-5		1	
5-6		1	
5-7		1	
5-8		1	
5-9			1
5-10			1
5-11			1
5-12			1
Average:	1.0	1.0	1.0

CaCl2 w/:	20	40	61
8-1	1		
8-2	1		
8-3	1		
8-4	1		
8-5		1	
8-6		1	
8-7		2	
8-8		2	
8-9			5
8-10			5
8-11			5
8-12			5
Average:	1.0	1.5	5.0

K. Ace:	20	40	60
9-1	0		
9-2	0		
9-3	0		
9-4	0		
9-5		0	
9-6		0	
9-7		0	
9-8		0	
9-9			0
9-10			0
9-11			0
9-12			0
Average:	0.0	0.0	0.0

Geomelt:	23	41	62
11-1	1		
11-2	1		
11-3	1		
11-4	1		
11-5		1	
11-6		1	
11-7		1	
11-8		1	
11-9			1
11-10			1
11-11			1
11-12			1
Average:	1.0	1.0	1.0

APPENDIX D. X-RAY DIFFRACTION DATA

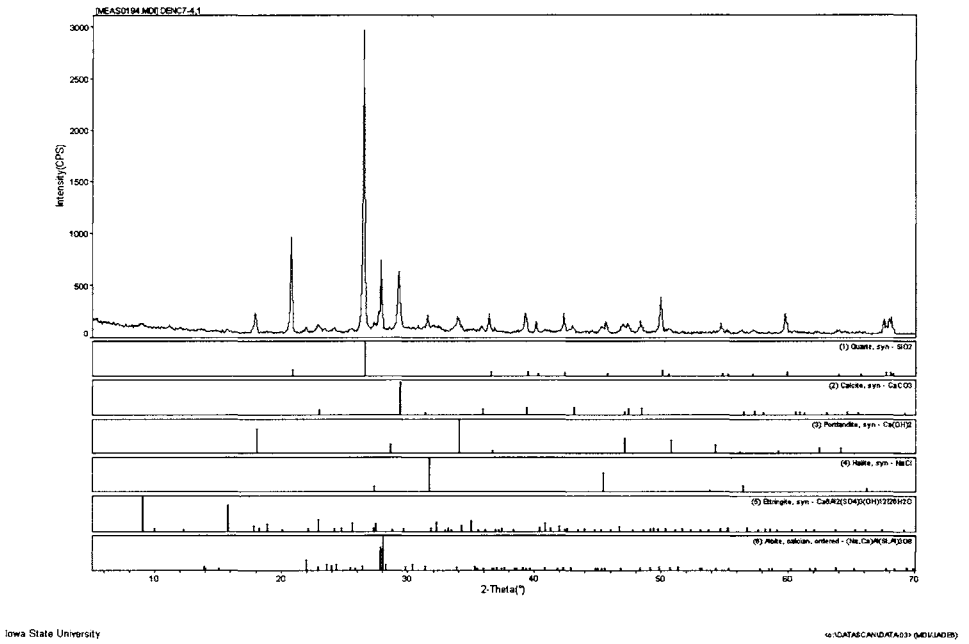

Figure 44. XRD diffractogram of H_2O-exposed sample

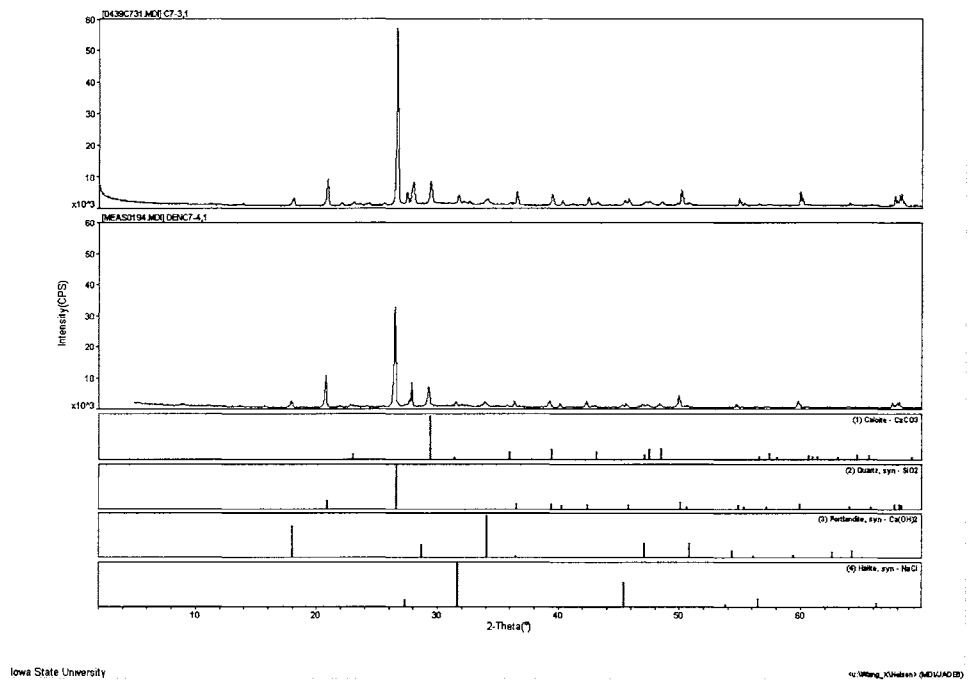

Figure 45. XRD diffractogram of w-d NaCl-exposed samples (20-cycle t top, 60-cycle at bottom)

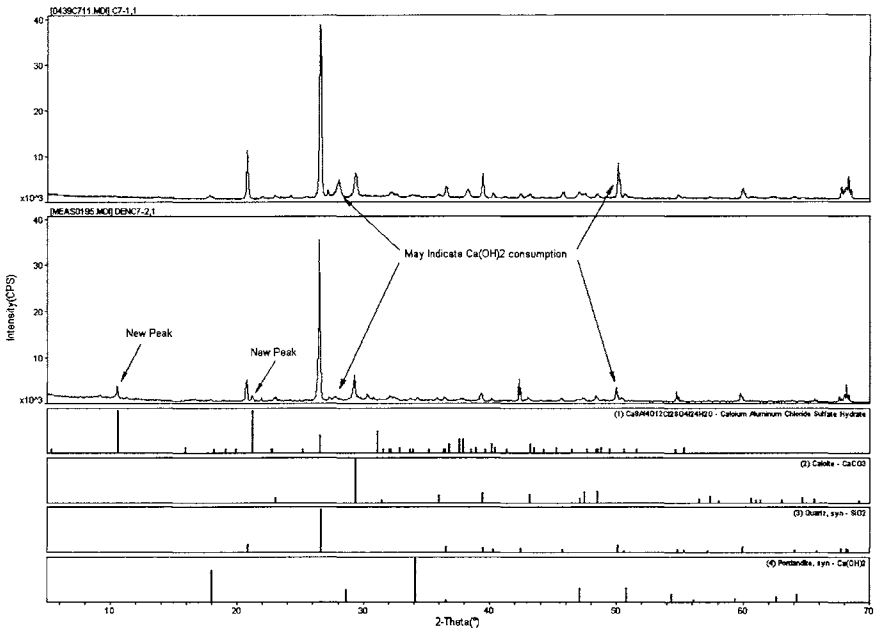

Figure 46. XRD diffractogram of w-d $CaCl_2$-exposed samples (20-cycle at top, 60-cycle at bottom)

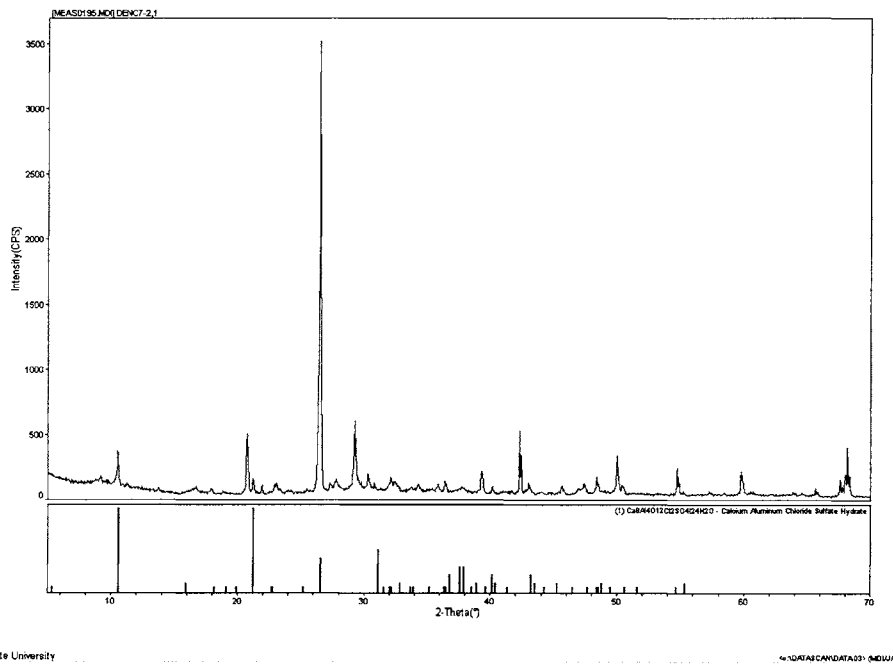

Figure 47. XRD diffractogram of $CaCl_2$-exposed sample at 60-cycles showing possible match with Calcium Aluminum Chloride Sulfate Hydrate mineral

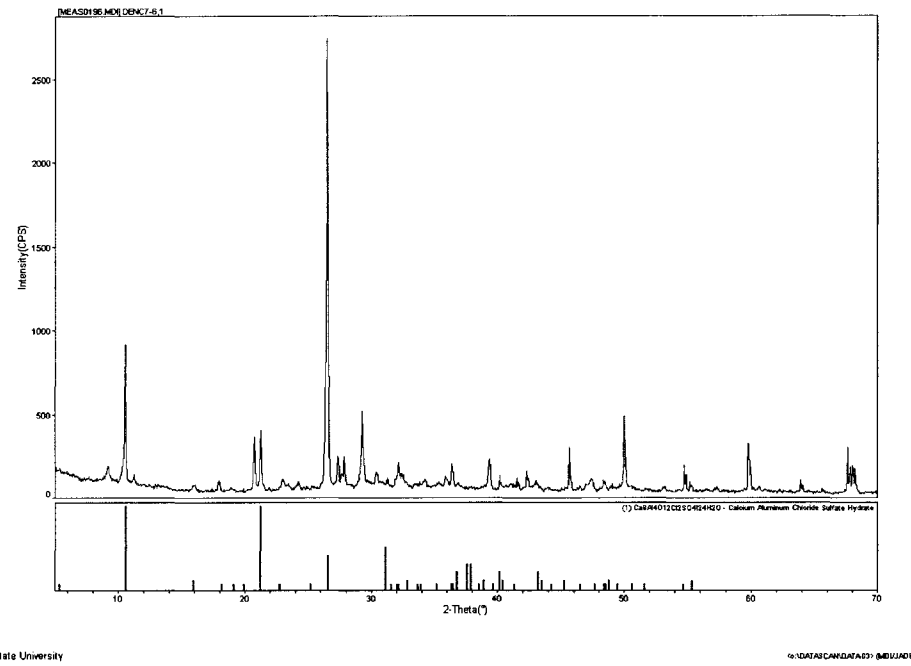

Figure 48. XRD diffractogram of $CaCl_2$ with CI-exposed sample at 60-cycles showing possible match with Calcium Aluminum Chloride Sulfate Hydrate mineral.

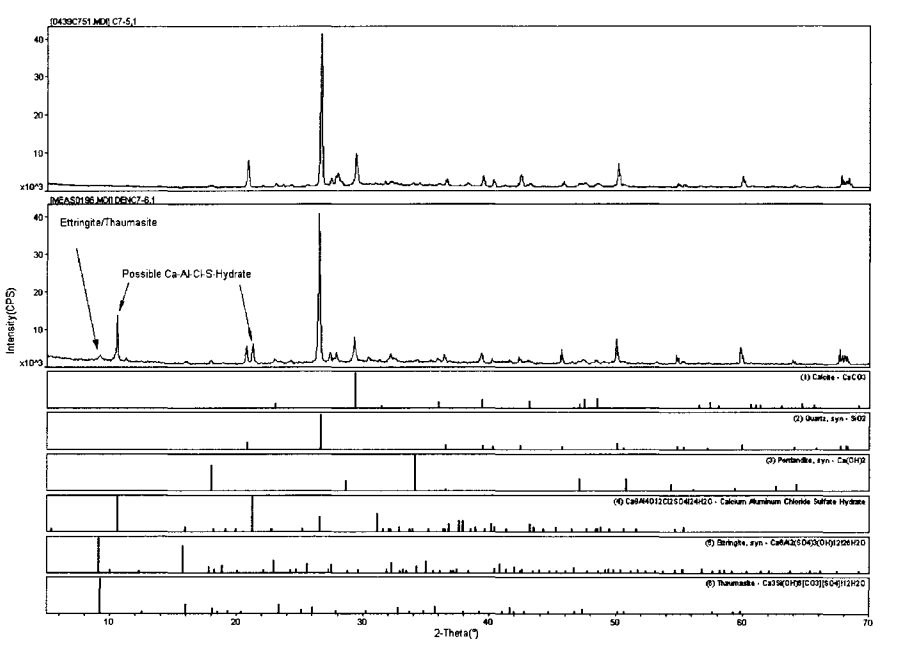

Figure 49. XRD diffractogram of $CaCl_2$ with CI-exposed samples (20-cycles at top, 60-cycles at bottom).

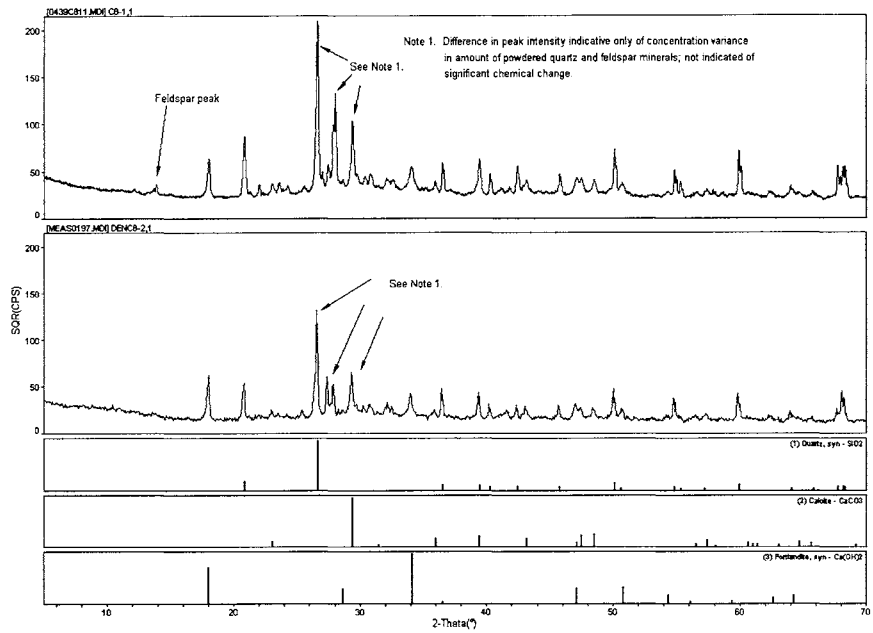

Figure 50. XRD diffractogram of K Acetate-exposed samples (20-cycle at top, 60-cycle at bottom).

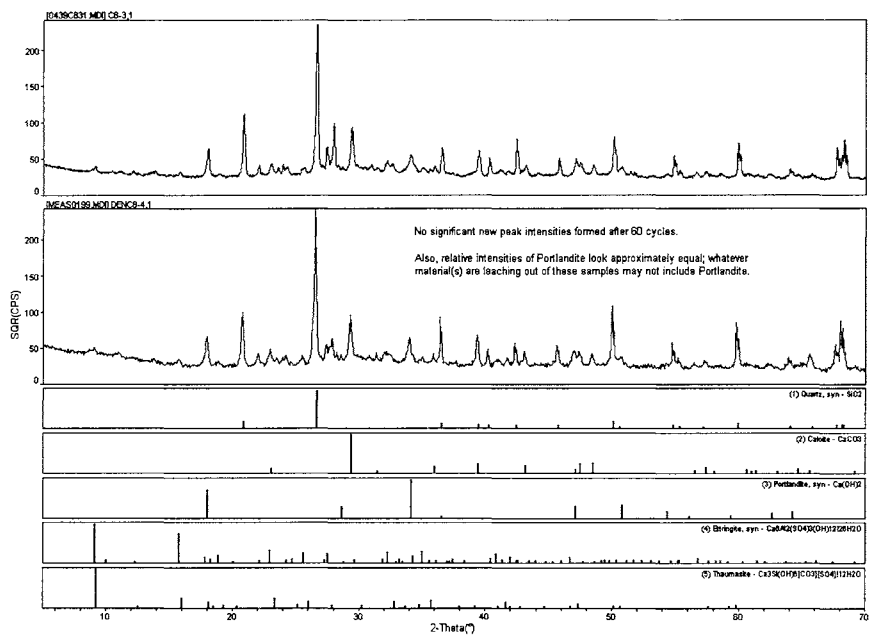

Figure 51. XRD diffractogram of Geomelt-exposed samples (20-cycle at top, 60-cycle at bottom).